NASA CONTRACTOR REPORT

NASA CR-1076

A STUDY OF AIRCRAFT FIRE HAZARDS RELATED TO NATURAL ELECTRICAL PHENOMENA

by Frank L. Kester, Melvin Gerstein, and J. A. Plumer

Prepared by
DYNAMIC SCIENCE
Monrovia, Calif.
for

NATIONAL AERONAUTICS AND SPACE ADMINISTRATION • WASHINGTON, D. C. • JUNE 1968

NASA CR-1076

A STUDY OF AIRCRAFT FIRE HAZARDS RELATED TO

NATURAL ELECTRICAL PHENOMENA

By Frank L. Kester, Melvin Gerstein, and J. A. Plumer

Prepared under Contract No. NASw-1416 by
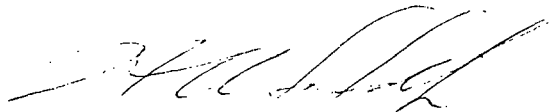DYNAMIC SCIENCE
Monrovia, Calif.

for

NATIONAL AERONAUTICS AND SPACE ADMINISTRATION

FOREWORD

This report was prepared by Dynamic Science on NASA Contract NASW-1416, "A Study of Aircraft Fire Hazards Related to Natural Electrical Phenomena." Contributions were also made by the General Electric High Voltage Laboratory on those sections where lightning simulation was employed. Mr. Irving Pinkel from NASA's Lewis Research Center directed the technical work on the project.

The studies presented in this report began in June 1966, and concluded in July 1967. The research on this program represents a joint effort by the staff of Dynamic Science and the General Electric High Voltage Laboratory. The work was initially directed by Dr. H. Dwight Fisher and later by Mr. Frank L. Kester as Program Manager for Dynamic Science. The Project Manager for the tests performed at the General Electric High Voltage Laboratory, Pittsfield, Massachusetts, was Mr. J. A. Plumer.

This report is the final report and concludes the work on Contract NASW-1416. The Contractor's Report No. is SN-9000. The authors wish to acknowledge the assistance of personnel of both Dynamic Science and General Electric High Voltage Laboratory for their efforts on this program. Personnel from Dynamic Science are Mr. Edward Ewin and Dr. Lawrence Zung. Personnel from General Electric are Messrs. E. R. Uhlig, A. F. Rohlfs, and D. J. Marino.

Harry A. Schmidt
Director of Special Projects

ABSTRACT

The problems of natural electrical phenomena as a fire hazard to aircraft are evaluated. Assessment of the hazard is made over the range of low level electrical discharges, such as static sparks, to high level discharges, such as lightning strikes to aircraft. In addition, some fundamental work is presented on the problem of flame propagation in aircraft fuel vent systems.

This study consists of a laboratory investigation in five parts: (1) a study of the ignition energies and flame propagation rates of kerosene-air and JP-6-air foams, (2) a study of the rate of flame propagation of n-heptane, n-octane, n-nonane, and n-decane in aircraft vent ducts, (3) a study of the damage to aluminum, titanium, and stainless steel aircraft skin materials by lightning strikes, (4) a study of fuel ignition by lightning strikes to aircraft skins, and (5) a study of lightning induced flame propagation in an aircraft vent system.

CONTENTS

LIST OF FIGURES

LIST OF TABLES

INTRODUCTION

The problem of fire hazards in aircraft has been the subject of a number of studies conducted at various times during the history of aircraft development. As a result of these studies, certain design principles and operating practices have evolved with the objective of minimizing these fire hazards. Even though considerable work has been accomplished, voids still exist in the knowledge of the causes and elimination of certain types of fire hazards. The particular problem area toward which this work was directed, involves fire hazards associated with natural electrical phenomena such as lightning and static electricity.

The objective of the work described here was to obtain a better understanding of the mechanism by which these types of fires are caused and propagated in aircraft. Several problem areas were defined. Specifically, these were the ability of lightning to ignite fuel vapors beneath both stainless steel and titanium metal skin and the need for a better means of slowing or stopping the increased flame speeds associated with lightning induced ignition at the vent exit. Additional research is recommended in both of these areas.

The experimental portions of the program involving flame propagation in fuel foams, low energy multiple discharges upon metal surfaces, and flame propagation in fuel ducts were carried out at the laboratories of Dynamic Science, Monrovia, California. The tests involving high energy lightning discharges upon aircraft skin materials and simulated aircraft fuel vent systems were conducted at the General Electric High Voltage Laboratory, Pittsfield, Massachusetts.

FLAMMABILITY OF FUEL FOAMS

Introduction

The production and persistence of flammable mixture zones during the fueling of an air-filled tank depends upon fuel vapor pressure, temperature, flow rate, fuel inlet size and location, and tank dimension (1). Flammable fuel vapor-air mixtures occur when the fuel temperature exceeds the flash point which is a measure of the lean flammability limit. Flammable conditions can also occur at fuel temperatures, below the flash point, if the liquid is dispersed in a foam or mist. Extreme agitation of the fuel in aircraft tanks during rapid fueling operations or rough flight conditions, such as those encountered in storms or in turbulence, can produce foams and mists within the tanks. It is possible, therefore, that ignition and flame propagation could occur under conditions where equilibrium fuel vapor/air mixture ratios would be considered below the lean flammability limit.

In order to investigate the characteristics of ignition and flame propagation through foams of aircraft fuels and air, a series of experiments were conducted in the laboratories of Dynamic Science.

The rate of flame propagation through typical fuel foams was determined. A high and a low volatility fuel were selected to be studied. A few tests were conducted to determine the effect of foam cell size on propagation. A foam with smaller cells was obtained by the addition of a foaming agent to the fuel. 640 turbine fuel and JP-6 were selected as the low and high volatility fuels, respectively. In addition, tests were conducted to determine the critical ignition energy and the spark breakdown potential of a typical fuel foam. For this effort 640 turbine fuel was selected, since it displayed better foaming characters than JP-6 and other fuels and because of its wide spread use in commercial aircraft. 640 turbine fuel is a typical kerosene.

Prior to beginning the tests on foam ignition and propagation a literature survey was conducted to determine the progress made by other investigators in this field. While considerable work was found in the vapor-air, and vapor-mist regime, little work was found specifically oriented toward the ignition and propagation of flame in a hydrocarbon fuel foam.

Literature Discussion

The major zones which can exist within a fuel tank are illustrated below:

Vapor-Air and/or

Mist-Air

Foam

Liquid
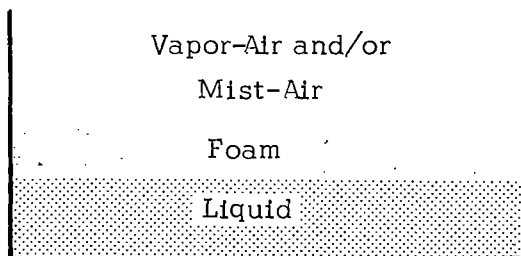
Regions which can contain combustible mixtures are 1) vapor-air, 2) mist-air, and 3) foam. Of these, the vapor-air mixtures have received the most extensive treatment in previous research efforts. Consequently, most assessments of potential fire hazards have been made in terms of conclusions based on vapor-air studies.

However, fuel mist-air systems can also represent a potential fire hazard. For example, Liebman (1) has shown that ignition and flame propagation is possible in a fuel mist-air system. This work was conducted under conditions of simulated fuel loading. His determination of the critical ignition energy for a kerosene-air mist, was 15 millijoules at room temperature. However, the likelihood of generating such mists under either normal and abnormal conditions (severely turbulent conditions or violent vibration due to damage or malfunction of the aircraft) has not received much study.

The study of the flammability of fuel foam has received less attention. Foam generated by the agitation of a liquid fuel consists of air, fuel vapor, and fuel mist as well as the thin liquid fuel walls which comprise the boundaries of the cells which constitute the foam. As foam is a dispersion of a gas in a liquid, most of the volume is a gas with the liquid in thin cell forming sheets called lamellea (2). In general, the gas bubbles are from 0.1 to 10 mm in diameter and have a wall thickness of from 0.3μ to 3.0μ. The gas phase of these bubbles consists of air, vapor of the liquid, and a fine mist of the liquid. This mist, within the individual cells, can contain droplets of liquid up to 10μ in diameter.

Flammability studies of fuel foams have been carried out by A. Bartkowiah, S. Lambiris, and M. G. Zabetahis (3). Their experiments were directed at determining the total pressure and rate of pressure rise in burning kerosene fuel foams. No measurements were conducted on the burning rate. They found the maximum pressures produced by the ignition of kerosene foams were much less than those produced by the ignition of fuel vapor-air mixtures.

Thomas (4) has studied the problem of foam flammability in kerosene. His results can be summarized as the following:

1. An increase of oxygen concentration in the gaseous component of the foam greatly promotes flame propagation;

2. An increase of fuel temperature promotes flame propagation;

3. A decrease of ambient pressure has little effect on flame propagation at low fuel temperatures but promotes it at high fuel temperatures;

4. There is an optimum rate of foam formation at which flame propagating tendency is greatest;

The problem of electrostatic charge buildup in liquid hydrocarbon fuels is well known (5-9), but little is known about the mechanism of charge decay. If this charge buildup is released as an actual spark in a flammable region, ignition could occur provided the discharge is sufficiently energetic.

3

The energy range of spark discharges in fuels can be estimated. Work cited in the literature (5-9) indicates that static spark discharges at potentials from 7000 to 25,000 volts have been measured in fuel systems. Also, a typical fuel in an aircraft tank has a capacitance of about 300 $\mu\mu$f in the bulk. From this information the discharge energy can be calculated. The governing equation for the energy of the discharge is

$$E = \tfrac{1}{2}CV^2$$

E = Energy--Joules

C = Capacitance--Farads

V = Potential--Volts

The numbers noted above, when evaluated in this equation, indicate a discharge energy range of from 7 to 80 millijoules is possible in liquid fuel. As reported by Liebman (1) 15 millijoules can ignite a kerosene-air mist. Other workers (3) (10) have shown 0.3 millijoules can ignite fuel vapor-air mixtures. No work had been done, previous to this study, on the ignition energy of fuel foams.

The production of static electricity has been reported to be associated with the presence of colloidal particles which ionize in the fuel (1). The contaminants are largely organic and represent fuel degradation and oxidation products or residue from treating operations. These products are only partially removed by ultrafiltration and absorption on silica gel or activated clay. Hydrocarbon fuels are most susceptible to static electricity buildup when exposed to elevated temperatures, gamma and ultraviolet radiation, and when they have traces of moisture in them (1). There appears to be a definite relationship between static charge production and electrical conductivity. Hydrocarbons which have an electrical conductivity in the approximate range of 1×10^{-11} to 1×10^{-15} $\text{ohm}^{-1}\text{cm}^{-1}$ have been shown to permit the greatest buildup of static electricity (1). For example, raw kerosene has a conductivity in the range of 1 to 3×10^{-12} $\text{ohm}^{-1}\text{cm}^{-1}$ and JP-6 fuel 3 to 8×10^{-12} $\text{ohm}^{-1}\text{cm}^{-1}$.

Rogers (6) reports that hydrocarbon fuels can be charged to such a degree that visible sparks occur. He found that the static discharges would occur most readily at the surfaces and under conditions of high surface curvature.

Other reports (7) on the triboelectric properties of fluid suggest that electrostatic charges can be built-up whenever there is a motion of a hydrocarbon with respect to a second substance. This second substance could be the surface with which the fuels are in contact. When Rogers (6) pumped fuel through silica gel, a much greater charge buildup occurred. In rapid aircraft fueling operations, passage of the fuel over a high surface area region such as an in-line filter can promote this type of charge buildup.

In summary one can conclude the following:

1.   Most aircraft fuels can be charged with static electricity by rapid agitation or filtration.

2. A charge of sufficient magnitude can be stored in bulk fuel to produce a visible spark with sufficient energy to ignite a combustible vapor-air mixture and probably, a fuel air mist.

3. Although work has been done on foam flammability, no work has been done on the minimum ignition energy required to ignite a fuel foam.

Apparatus

Under laboratory conditions, foams can be generated by (a) rapid stirring and (b) by vibration. In order to simulate aircraft conditions to some degree, the vibrational frequency range associated with aircraft was selected. Obviously, the wave length and amplitude associated with full-scale systems are difficult to simulate in the laboratory and no attempt was made to simulate these quantities in the work reported here.

The apparatus for investigating the properties of foam ignition and combustion, shown in Figure 1, is constructed of stainless steel and has a total volume of 1 cu. ft. It is constructed so that a lucite top viewing window can be installed and is designed to be operated with an air-driven vibrator for mechanical agitation. When operated at 15 psig, the air vibrator produced a vibrational force of 160 pounds at a frequency of 100 cps which is transferred to the test chamber. This produces a linear displacement of about 10^{-5} inches at the surface of the liquid. By this method, a foam 2 to 3 inches thick has been produced. The one drawback is that the surface of the liquid is slightly turbulent during the period of foam formation. Not shown in Figure 1 is an air-driven stirring motor and paddle which was used for mechanical stirring. The stirring technique produces a slightly coarser foam than the shaking method but is capable of producing a foam thickness up to 3 inches. This method had the advantage of maintaining a relatively smooth liquid surface for easier flame studies. Both foam generating methods were employed in this study.

In the testing and calibration of the apparatus, it was found that more reproducible foam conditions were obtained just after turning off the foam generator. Most experiments were started at this point. The rate at which the foam collapses or decays is shown in Figure 2 for 640 turbine fuel. A decay half-life for 640 turbine fuel was found to be the order of 2 seconds. In this time the depth of foam was reduced by one half. This was sufficient time to provide enough foam for the flame propagation and ignition studies. The fuel foam produced by mechanical shaking with the pneumatic vibrator is shown in Figures 3a through 3c. The foam layer shown in Figure 3a is the result of relatively low mechanical agitation. The foam is produced in the central portion of the system and flows to each end where it accumulates prior to its collapse. The foam layer increases as increased energy is put into the system. Figure 3b shows the system being vigorously driven by the pneumatic vibrator. A foam layer, shown in Figure 3c approximately one-inch in depth, is produced by this method and is stable for several seconds after removal of the driving force.
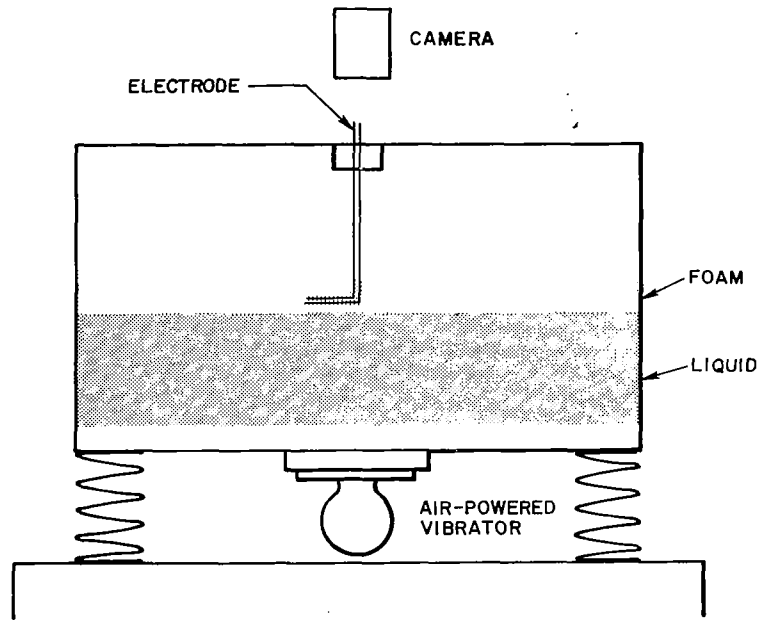
FIGURE 1. Foam Study Apparatus.
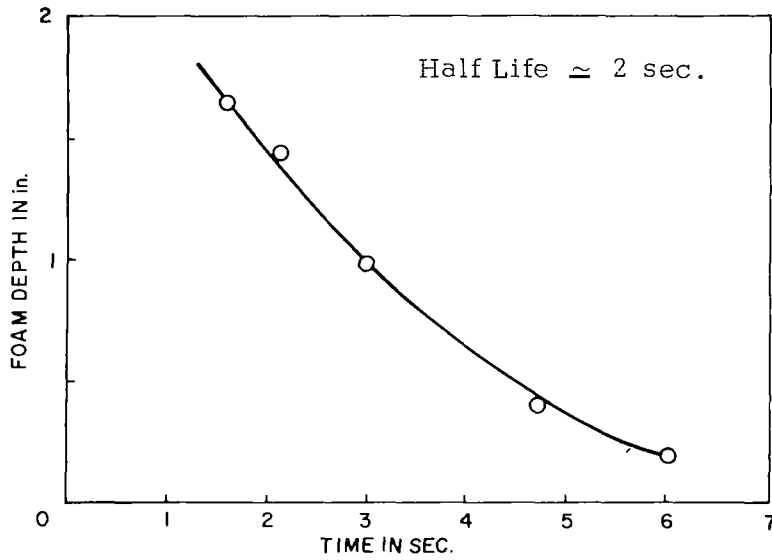
FIGURE 2. Foam Decay Curve for 640 Turbine Fuel.

FIGURE (a) FOAM PRODUCED BY LOW LEVEL MECHANICAL AGITATION
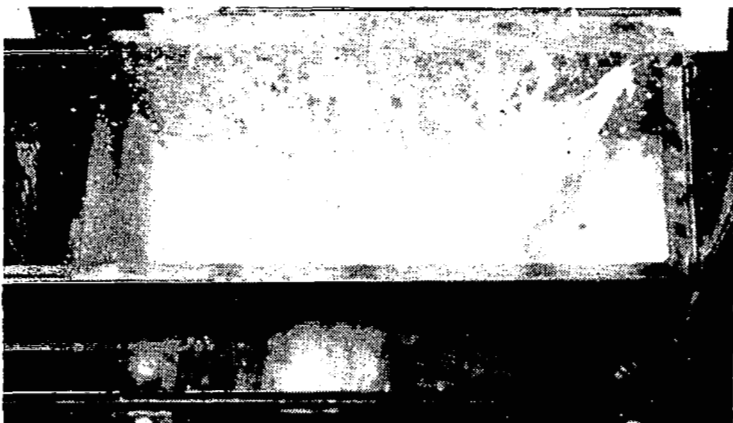
FIGURE (b) FOAM LAYER PRODUCED BY VIGOROUS MECHANICAL AGITATION
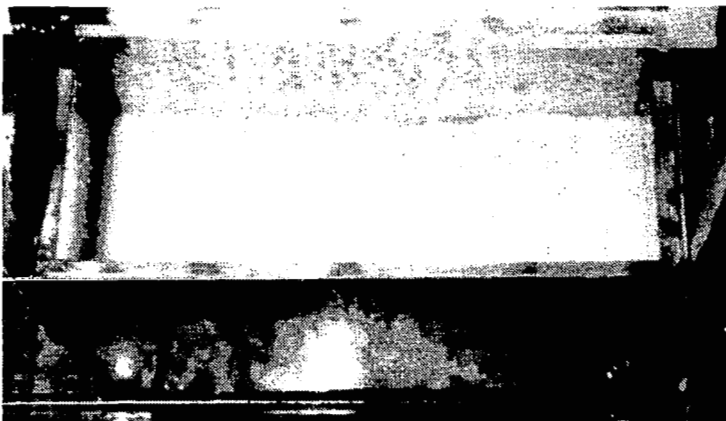
FIGURE (c) SEMI-STABLE FOAM PRODUCED BY VIGOROUS MECHANICAL AGITATION

FIGURE 3. Foam Production in 640 Turbine Fuel

A Paillard Bolex 16 mm camera was employed to monitor flame propagation. Kodak Ektachrome ER449 color film was used in these studies. For some studies, Kodak filters 2A, 16, and 29 were used at times to more clearly define the flame corona boundary. Marks were placed on the wall of the foam tank two inches apart, as a calibration for the dimensions of the flame kernel. The increment between successive frames (1/64 sec.) was used as the time standard.

In addition, a capacitor discharge apparatus was designed and constructed for this program. A number of high voltage capacitors were employed, ranging from 0.0023 to 0.5 μ farads. A charging power supply of 1.2 ma provided voltages from 5 to 11,000 volts.

This generated spark discharges from 1 to 10^5 millijoules. For the propagation studies, the discharge energy was fixed at about 50 millijoules. A standard electrode gap of 1/4" was maintained, using pointed copper electrodes approximately 1/8" in diameter.

Test Results

Flame propagation. - Measurements were conducted on the rate of flame propagation through typical hydrocarbon fuel foam. For this work, 640 turbine fuel and JP-6 were selected as representative of relatively low volatility and high volatility fuels. As an additional interest, 640 turbine fuel with 3% of a foaming agent (surfactant) was tested to determine the effect of bubble or cell size on burning velocity. The foaming agent had the effect of producing smaller bubbles in the foam.

As the foam can be produced in a variety of depths, it was considered important to evaluate the effect of foam depth, on flame propagation. Therefore, the rate of flame propagation for all the fuels was evaluated as a function of foam depth.

Color photography was obtained for all foam flame tests. These films were analyzed to obtain the radius of the flame kernel as a function of time. A group of three photographs of 640 turbine fuel is shown in Figure 4. These photographs show 640 turbine fuel foam at a) electrical ignition, b) burning below the foam surface, and c) flame breaking through the surface and spewing burning droplets of fuel to surrounding foam.

A plot of the experimental data of flame velocity versus burning time is shown in Figure 5 for 640 turbine fuel. These values were obtained from an analysis of the film strips. Similar plots for JP-6 and 640 turbine fuel with foaming agent are shown in Figure 6 and 7.

The flame velocity is presented in these plots as a function of foam depth. It is seen that the foam flame velocity was independent of the foam depth under the conditions studied.

A standard procedure of placing the electrodes at fixed distances under

8
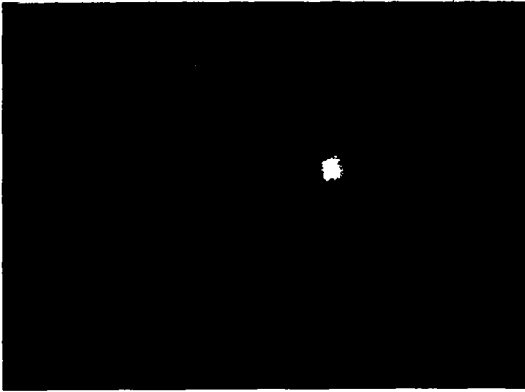
ELECTRICAL SPARK AT IGNITION
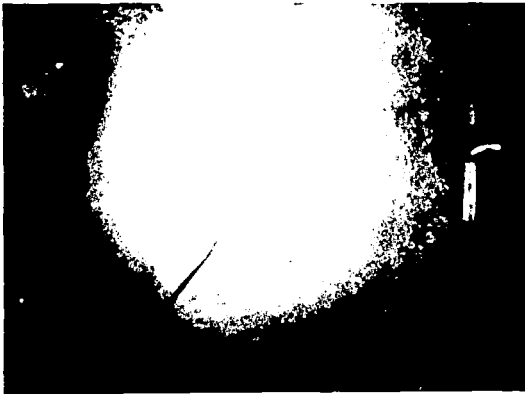
FLAME ZONE 0.015 SECONDS LATER
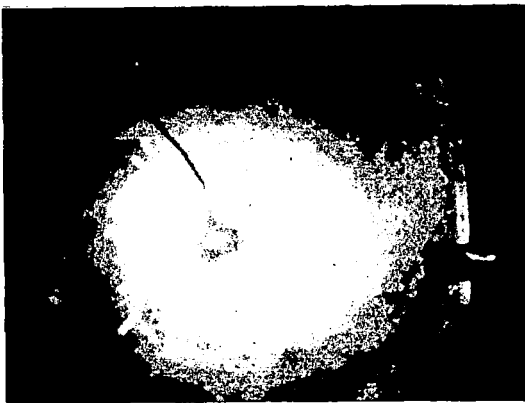
FLAME ZONE 0.063 SECONDS LATER

FIGURE 4. Flame Propagation in Typical Fuel Foam
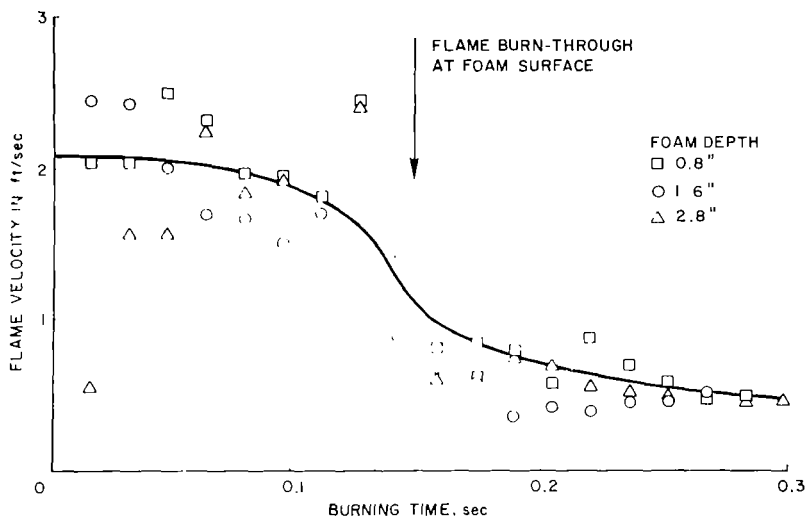
FIGURE 5. Flame Velocity Vs. Burning Time for 640 Turbine Fuel.
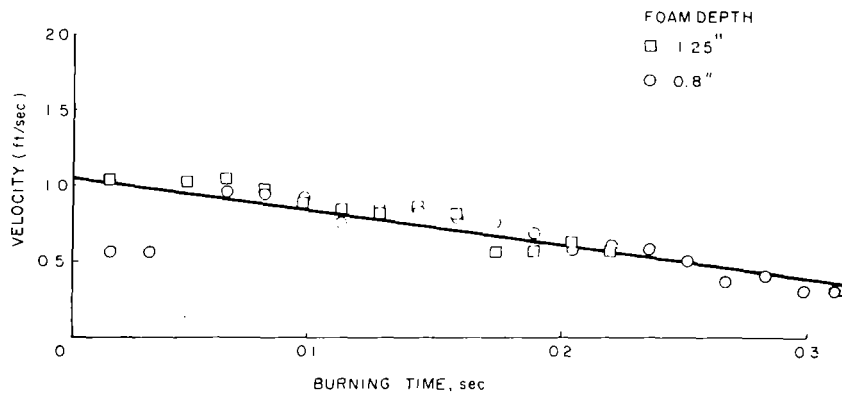
FIGURE 6. Flame Velocity Vs. Burning Time for JP-6.

10
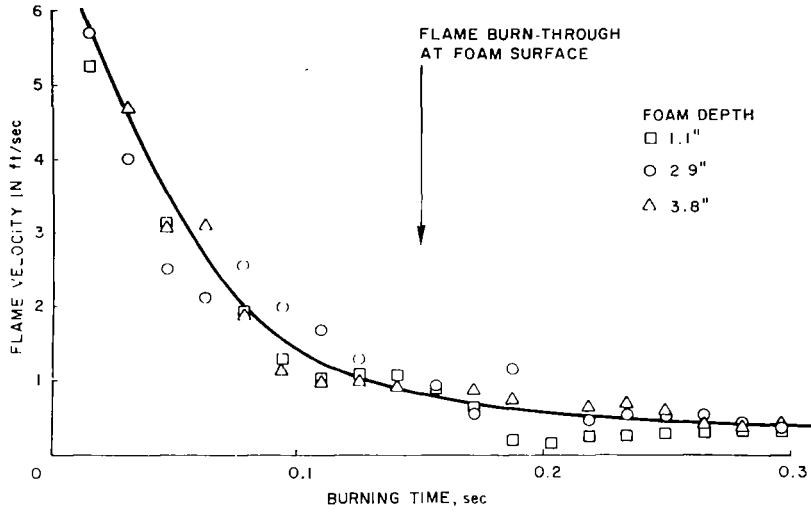
FIGURE 7. Flame Velocity Vs. Burning Time for 640 Turbine Fuel with 3% Foaming Agent.
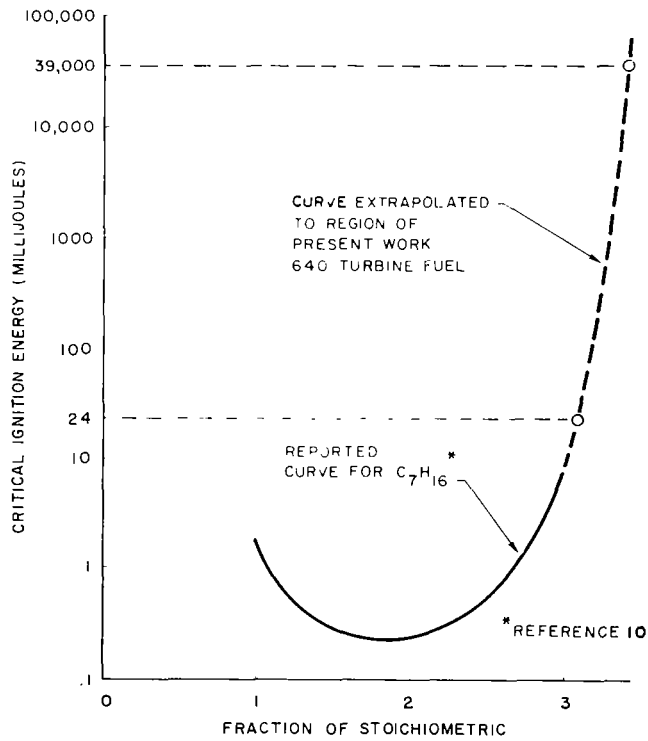
FIGURE 8. Critical Ignition Energy.

11

the foam was employed. This resulted in ignition always occurring at the same distance beneath the foam surface. Once ignited, the flame would burn through the surface of the foam in about 0.15 sec., in all cases. This characteristic time is indicated on Figures 5 and 7.

The burning flame beneath the foam generates hot, expanding gases. These expanding gases tend to push the flame front ahead, and in this burning stage the apparent velocities can be many times the normal burning velocity. After the flame has burned through the surface the hot gases are relieved upward away from the foam. After this point the burning rate slows.

This type of burning phenomenon is indicated in Figures 5 and 7. For 640 turbine fuel with foaming agent, a large initial burning rate of about 5 feet/sec. is observed. The burning rate then drops rapidly to a constant rate of about 0.5 feet/sec. after the burnthrough time of 0.15 sec.

The pure 640 turbine fuel (Figure 5) displays more of a step change from a propagation velocity of about 2 feet/sec. in the initial stage to a lower velocity of about 0.5 feet/sec. Again the transition is observed at 0.15 seconds burning time. Apparently, the larger burning rate observed with the fuel with foaming agent present is due to the smaller cell size of the foam.

The JP-6 did not foam as readily as the 640 turbine fuel. This lack of foam stability may be due to the additional refining operations necessary to produce JP-6 fuel. Also, the bubble size was larger with JP-6. A plot of burning rate vs. time for JP-6 is shown in Figure 6. This fuel did not demonstrate a large initial velocity as the others did. The final velocity was, again, approximately 0.5 feet/sec.

In summary, the initial high velocities observed may be due to the burning gas expanding against the flame front. However, this effect was much more pronounced with foams of smaller cell size.

Ignition.- A series of tests were conducted to determine the critical ignition energy for 640 turbine fuel. Ignition energy was measured at various locations in the foam. Emphasis was placed on determining where in the foam-air fuel system a spark could most readily be discharged. The result of this portion of the investigation is shown in Table 1.

A foam depth of three inches was employed with an electrode gap of 1/4". The breakdown potential was found to be 5,500 volts at the foam/air surface, 5,800 volts in the bulk foam, and 11,000 volts at the foam/liquid interface. It was not possible to discharge a 11,000 volt spark in the bulk liquid. Measurements greater than 11,000 volts could not be made with the present apparatus. The discharge potential in air was not measured but was obtained from Chemical Engineers' Handbook, 1959.

The critical ignition energy for 640 turbine fuel was found to be 24 millijoules at the foam/air surface and 39 joules in the bulk foam. Ignition did not occur when a spark was triggered at the foam/liquid interface, even at the highest energy of our equipment which was approximately 50-60 joules.

TABLE I

SPARKING AND IGNITION LEVELS OF 640 TURBINE FUEL/AIR FOAMS

	Location	Spark Breakdown Conditions		Critical Ignition Conditions	
		Potential Volts	Energy Joules	Potential Volts	Energy Joules
A)	Air	300*	---	---	---
B)	Foam/Air Surface	5,500	0.006	11,000	0.024
C)	Bulk Foam	5,800	.008	11,000	39
D)	Foam/Liquid Interface	11,000	39	**	---
E)	Bulk Liquid	**	---	**	---

*   Reference 11.

**   Greater than 11,000 Volts required to spark or ignite.

It is noted that the energy necessary to ignite the foam was greater at the bottom of the foam than it was at the surface. It is possible to interpret this fact in terms of a fuel/air ratio--critical ignition energy diagram. It is well known that the energy required for ignition is a function of fuel-air ratio. The results of the ignition of the 640 turbine fuel foam at the foam-air surface and in the bulk foam have been displayed on a fuel/air diagram in Figure 8. Here the experimental points are plotted on an extension of a fuel-air ratio-critical ignition diagram for C_7H_{16} from Reference 10. It is felt that the curve for C_7H_{16} should be similar to the 640 turbine fuel at the lower energy region. From the extrapolation of the curve, the critical ignition energy, 24 millijoules, indicates a fuel/air ratio slightly greater than 3 times stoichiometric at the foam/air surface. The value of 39 joules indicates a fuel/air ratio of about 3.5 times stoichiometric deep in the bulk foam.

In these studies, the fuel/air ratio was not monitored. However, the indirect evidence indicates foam does become fuel rich with increased foam depth.

REFERENCES

1. Liebman, Irael; Spolan, Irving; Kuchta, J. M., and Zabetakis, M. G., "Ignition of Tank Atmospheres During Fuel Loading," Paper for Presentation at a Session on Safe Product Handling and Static Electricity During the 30th Midyear Meeting of the American Petroleum Institute's Division of Refining, in the Queen Elizabeth Hotel, Montreal, Que., Canada, May 11, 1965.

2. Davis, "Interfacial Phenomena," Academic Press, 1961.

3. Bartkowiak, A., Lambiris, S., and Zabetakis, M. G., "Flame Propagation Through Kerosene Foams," Combust. Flame 3(3), 347, Sept. 1959.

4. Thomas, A., "Flame Propagation Through Air-Fuel Foams," Presented at 6th Symposium (International) on Combustion. Butterworths Scientific Publication (London) 1959, p. 126.

5. Gates, Albert M., Senior Engineer, Research Div.; Blose, John B., Engineer, Electrical Engineering Div., Philadelphia Electric Co., "Research Reveals Oil-Handling Hazards," Electric Light and Power Journal, January 1963.

6. Rogers, D. T., McDermott, J. P., and Munday, J. C., "Theoretical and Experimental Observations on Static Electricity in Petroleum Products," The Oil and Gas Journal, p. 160, 1965.

7. Tottori, K., Engineering Faculty, Toyama University, "Static Electricity in Oil Tanks," Symposium on Static Electrification, (London), Brit. J. Appl. Phys. Suppl. No. 2, March 1953.

8. Klinkenberg, A., "Production of Static Electricity by Movement of Fluids Within Electrically Grounded Equipment," Proc. Fourth World Petroleum Congress, Section VII-C, paper No. 5, 253-64, Carlo Colombo, Rome, 1955.

9. Nitka, H., "Electrostatic Charging of Liquids, Its Formation, Prevention and Risk," Report No. 16, German Chemical Industry (I. G. Farbenindusrrie A. G.), translated by Norbert Platzer, U. S. Bureau of Mines, 1949.

10. Gerstein, Melvin and Allen, Robert D., "Fire Protection Research Program for Supersonic Transport," T.D.R. No. APL TDR-64-105, October 1964.

11. Perry, John H., Chemical Engineers Handbook, Third Edition, McGraw-Hill, 1950.

FLAME PROPAGATION IN FUEL VENT DUCTS

In transport aircraft, the fuel tanks are vented to the atmosphere to prevent excessive pressure differentials between the internal and external surfaces of the tank. As the aircraft changes altitude there is a flow of gas either into or out of the fuel tank, depending on whether the aircraft is climbing or descending; more exactly on whether the internal tank pressure is higher or lower than the pressure at the vent outlet. As a result of this "breathing" process, flammable fuel-air mixtures often exist within the vent line and the tank itself. It has been recognized for a number of years that these vapors, once ignited, can propagate through the vent lines and into the tanks, causing destructive fires and explosions.

In evaluating this type of hazard, the industry has always considered the ascent as the most hazardous portion of the flight. With a reduction in external pressure, fuel vapors from the tank flow outward toward the vent exit forming a flammable path from the vent exit to the tank. As a result, most research work has been directed toward the characterization of this hazard.

The descent of an aircraft has always been considered a relatively safe flight profile from the standpoint of flame propagation because with an increasing ambient pressure, only fresh air is flowing into the vent system. One factor often overlooked, however, is the fact that when an aircraft encounters turbulence or drops one wing, fuel from the tanks can run into the vent lines. The fuel ultimately flows back into the tanks leaving the walls of the vent wet with fuel. Thus, even during descent and level flight one often finds both fuel and air present in the vent lines.

The objective of our test program was to evaluate the propagation characteristics of flame in a system consisting of fresh air flowing along a fuel-wetted vent line. Tests were run with both low and high volatility pure hydrocarbons in the presence of air velocities ranging from 0 to 10 ft. per second.

Experimental Apparatus

For this series of tests, a simulated vent duct was constructed consisting of a 4" diameter aluminum tube, 10' long, fitted with an air blower, ionization probes, a fuel cup and a liquid nitrogen trap to cool the temperature of the air stream. Figure 1 shows a diagram of the apparatus employed. A Hasting Model G-10 air meter was employed to measure the air stream velocity. The temperatures of the air stream and tube were held between 15 and 18°C for these tests. Pure n-heptane, n-octane, n-nonane and n-decane were selected to represent typical liquid hydrocarbon fuels. The n-heptane employed was AMSCO (American Mineral Spirits) brand technical grade and other hydrocarbons were Phillips 66 brand technical grade. Chromatographic
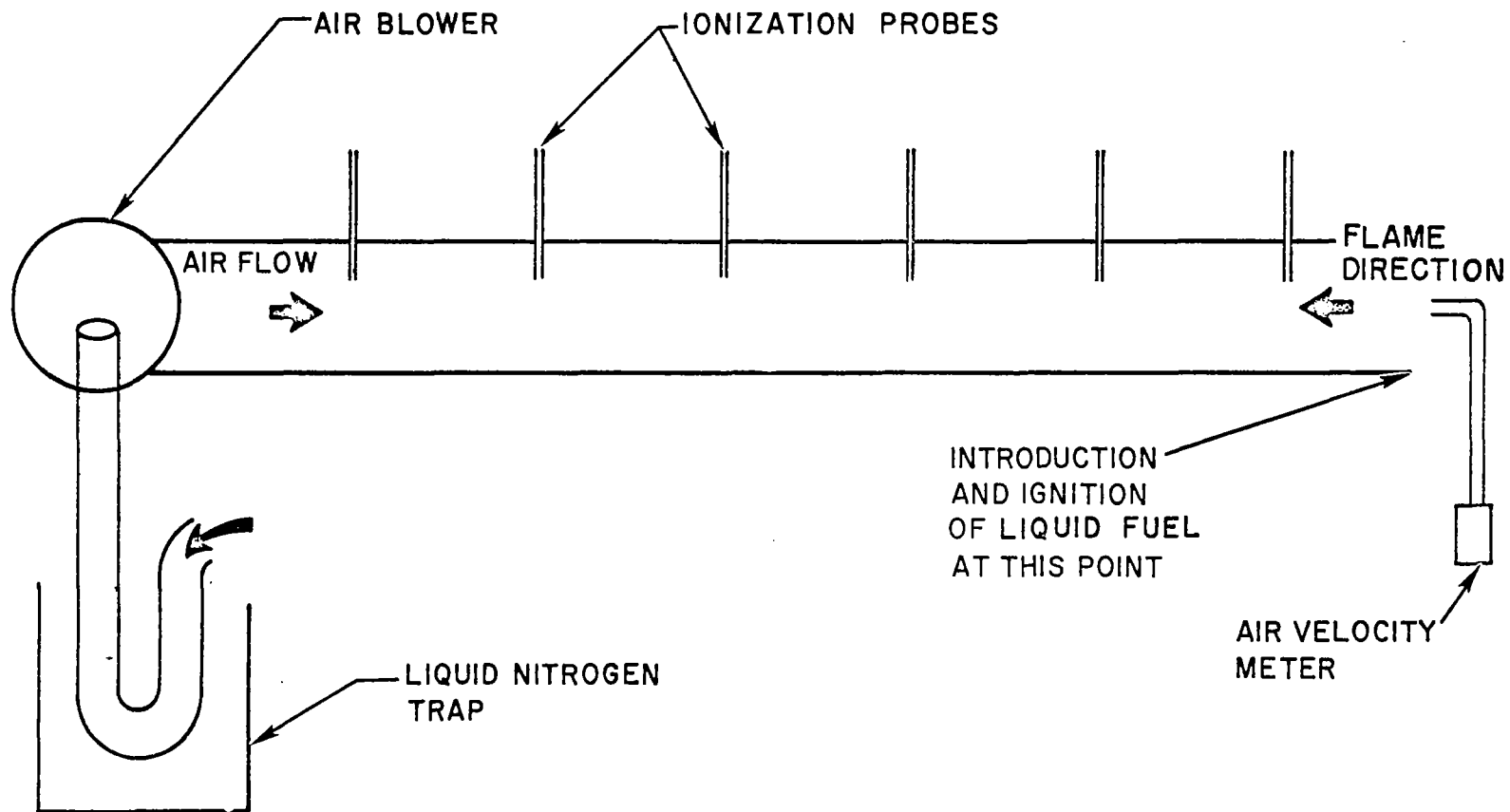
FIGURE 1. Flame Propagation Apparatus, Simulating an Aircraft Fuel Vent Duct.

analysis of the n-heptane indicated less than 1% n-octane as an impurity. The other hydrocarbons displayed no detectable impurity peaks on the chromatograph.

Before each experiment, air, cooled from the liquid nitrogen trap, was passed through the tube. When the tube temperature reached $15^{\circ}C$, 20 ml of the liquid fuel were quickly placed into the apparatus in a manner to wet the entire length of tubing. Next the airstream flow was adjusted to the desired velocity in the tube, and the fuel was ignited at the downstream end with a wick. The rate of flame propagation against the airstream was measured at three different locations in the tube.

Some of the propagation rates were low enough that these measurements could be made visually. However, in the faster runs ionization probes were employed. A 3" diameter glass apparatus was used to obtain photographic evidence of the propagating flame. A series of three photographs showing typical flame propagation of n-heptane against an airstream velocity of 2 feet/sec. is shown in Figure 2.

Test Results

The flame propagation tests were run at temperatures of $15^{\circ}C$ to $18^{\circ}C$. At these temperatures three of the hydrocarbon fuels, n-octane, n-nonane and n-decane, were below their lean flammability limits. Only n-heptane, the highest volatility fuel, was within the flammability range, see Table I. A short wick was used at the end of the tube to ignite the fuel. Without air flowing in the duct, the fuels which were below their lean limit would not propagate in the tube, even in the presence of the heat from the burning wick. N-heptane, on the other hand, supported flame propagation along the length of the tube following ignition without air flowing in the duct.

TABLE I

LOWER TEMPERATURE LIMITS OF FLAMMABILITY

	$^{\circ}C$
n-heptane	-4
n-octane	18
n-nonane	31
n-decane	46

The experimental results are listed at the end of this section. The measurements of rate of flame propagation in the aluminum duct are listed in Table III. The results obtained from color photography on the rate of flame propation in the glass apparatus are listed in Table IV.
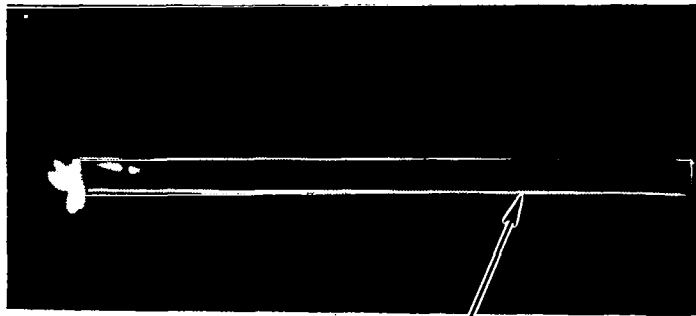
0.06 SECONDS AFTER
START OF BURNING

3 in. DIA. GLASS TUBE

0.6 SECONDS AFTER
START OF BURNING
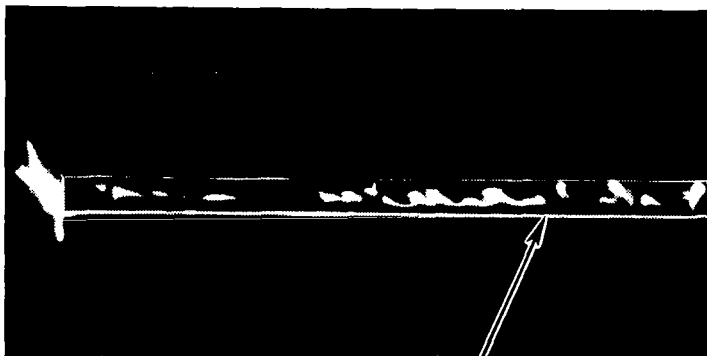
3 in. DIA. GLASS TUBE

I SECOND AFTER START
OF BURNING

3 in. DIA. GLASS TUBE

FIGURE 2. Flame Propagation in Simulated Fuel Vent Duct. Fuel
is n-Heptane.

19

After the initial test series, where propagation was attempted without air flow, a series of tests were run in which a predetermined air velocity was established in the duct prior to ignition. In the presence of flowing air, even at velocities as low as 0.25 feet/ second, flame propagation occurred against the direction of flow for all four fuels. As the air flow in the duct was increased, the rate of flame propagation, against the direction of flow, increased until it reached a maximum as illustrated in Figures 3 and 4. For all fuels tested, the maximum spatial propagation velocity occurred at an air stream velocity of approximately 3 feet/second. As the air stream velocity was increased further, the spatial velocity of the flame began to decrease until it became stationary with respect to the duct at an air stream velocity of approximately 6 feet/second. Due to the difference in volatility, each of the fuels exhibited slightly different propagation characteristics as described below.

N-heptane (Figure 3) demonstrated two types of propagating flames: a blue vapor flash, and a yellow diffusion flame. The spatial velocity of the blue vapor flash decreased linearly with increasing air stream velocity. This is demonstrated on Table IV in that the sum of the air stream velocity and the rate of flame propagation is approximately a constant. At an air stream velocity of 6 feet/second a standing flame (with respect to the tube) is obtained. The spatial flame velocity is the observed linear rate of flame propagation with respect to a fixed point in the tube.

The yellow-diffusion flame, observed for n-heptane, displayed an increasing spatial flame velocity against an increasing air stream velocity up to a maximum flame velocity of 2.5 feet/second. After reaching this maximum spatial velocity at an air stream velocity of about 3 feet/second the spatial velocity decreased to zero at an air stream velocity of 6 feet/second.

The fuels n-octane, n-nonane, and n-decane (Figure 4) all demonstrated the same type of yellow flame and the same type of spatial velocity curve as described for n-heptane. No blue vapor flash was observed for these fuels. The maximum spatial velocities were much lower than observed for n-heptane. These are shown in Table II.

The reason that the yellow diffusion flame increases its velocity with increasing air flow can probably be attributed to an increase in the oxygen supplied to the flame and to better mixing of the burning constituents. Both of these factors tend to increase the size of the flame, which in turn, increases the rate of vaporization of the liquid fuel in the duct. As the flame spreads along the duct, an even greater heat release is obtained and this leads to an increased rate of vaporization and ultimately to an increased rate of flame propagation.

In addition to promoting flame propagation, the increasing velocity of the air stream eventually works to slow flame propagation. Above an air stream velocity of 3 feet/second, the flame begins to be slowed in its spatial velocity until it ultimately is reduced to zero net velocity, which occurs at an air stream velocity of 6 feet/second.
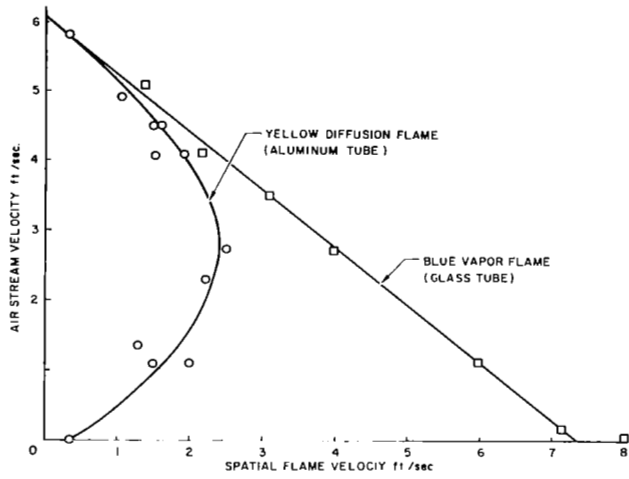
FIGURE 3. Spatial Flame Velocity vs Air Stream Velocity for n-Heptane.
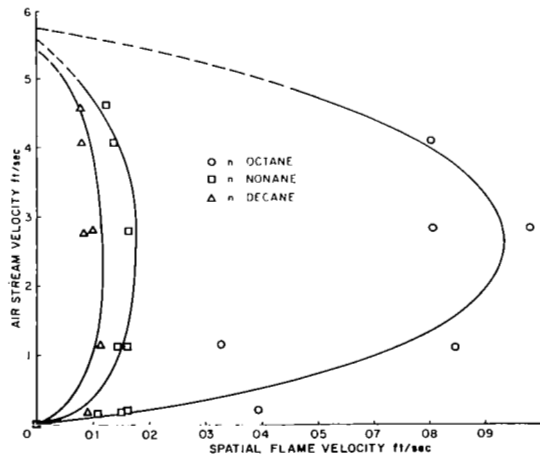
FIGURE 4. Spatial Flame Velocity vs Air Stream Velocity for n-Octane, n-Nonane, and n-Decane.

21

In this 4" duct the transition from laminar flow to turbulent flow occurs at an air stream velocity of about 2 to 3 feet/second, using a Reynolds number of 2300. The term diffusion flame applies directly to flame propagation in the laminar region. Above this air stream velocity a transition to a turbulent or eddy diffusion flow occurs. Although, the type of flame may be somewhat different in the higher velocity region, the term diffusion flame is employed throughout.

The relationship between volatility (or molecular weight) and spatial flame velocity is shown in Figure 5 for the four hydrocarbons studied. It is noted that at high volatility (low molecular weight) the propagation is many times that of the lower volatility (higher molecular) hydrocarbons. A dashed region is indicated between n-heptane and n-octane because of the lack of experimental data between these two points, in the transition region.

TABLE II

MAXIMUM RATE OF FLAME PROPAGATION IN FUEL DUCT

Hydrocarbons	Maximum Flame Velocity* (feet/sec)
n-heptane (vapor flash)	8
n-heptane (diffusion flame)	2.5
n-octane (diffusion flame)	0.09
n-nonane (diffusion flame)	0.02
n-decane (diffusion flame)	0.01

*Initial conditions:

Air temperature: $15-18^{O}C$

Total pressure: 1 atm--sea level
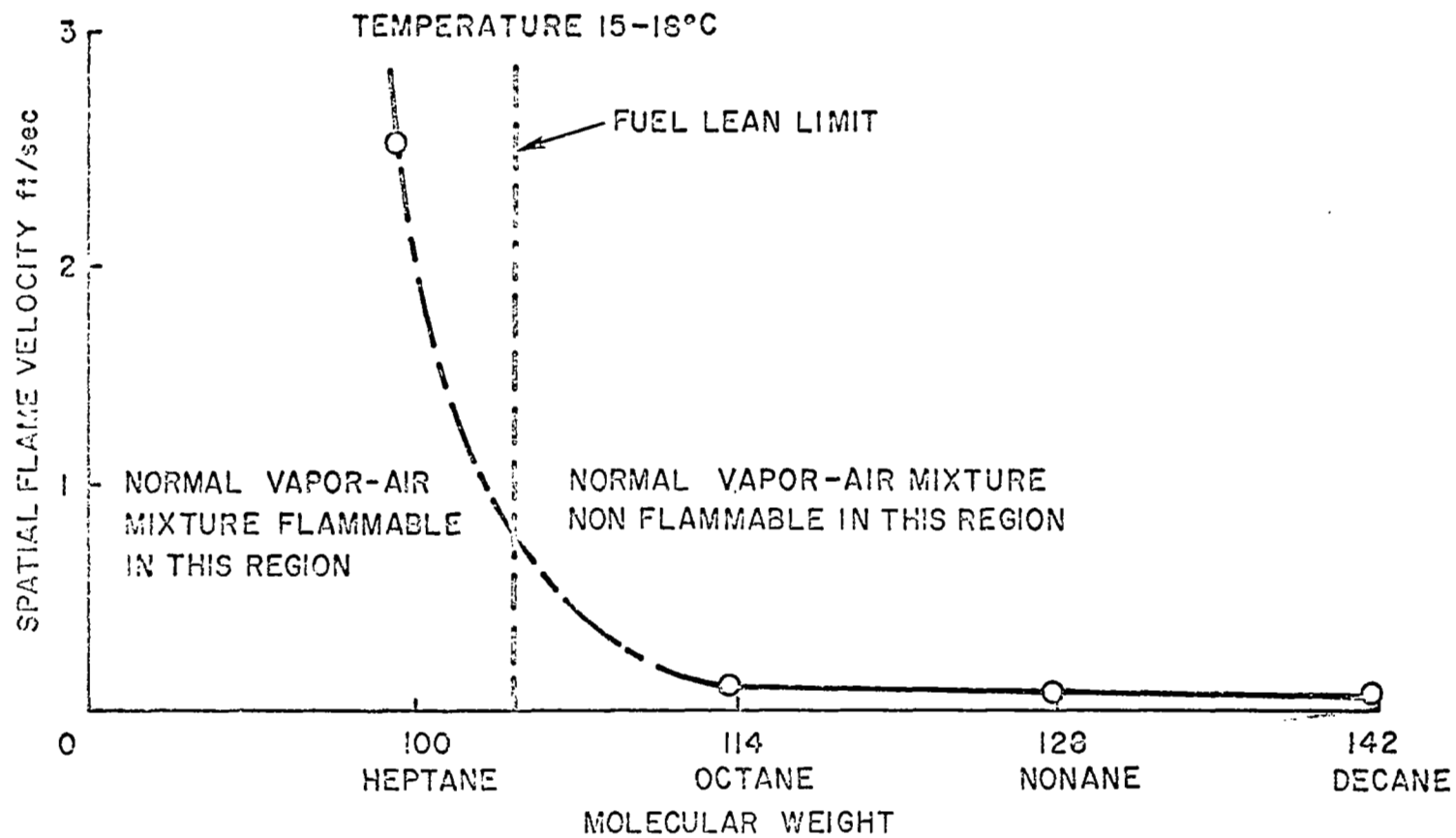
FIGURE 5. Maximum Spatial Flame Velocities vs Molecular Weight of Liquid Hydrocarbon.

TABLE III
FLAME TESTS IN ALUMINUM FUEL DUCT

Rate of Flame Propagation

Run No.	Fuel	Air Stream Velocity		Location (1)		(2)		(3)		Initial Duct Temp. °C	Remarks
		feet/sec.	in/sec.	in/sec.	feet/sec.	in/sec.	feet/sec.	in/sec.	feet/sec.		
1	n-Heptane	4.66	56.0								Control Test
2	"	4.66	56.0					14.4	1.2	23.7	
3	"	4.66	56.0					15.6	1.3	13.4	
4	"	4.60	55.0					11.5	0.96	8.8	
5	"	4.16	50.1					18	1.5	16.2	
6	"	5.33	64.1							15.4	Problem in measuring velocity
7	"	10.05	124.0							14.8	" " " "
8	"	9.80	118.0								" " " "
9	"	9.80	118.0								" " " "
10	"	5.92	71.0					3.71	0.31	15.6	
11	"	4.16	50.0					22.4	1.87	17.3	
12	"	2.73	3.4								Problem in measuring velocity
13	"	1.17	1.4					24.0	2.0	18.0	
14	"	0.167	2.0					3.6	0.3	18.2	
15	"	1.17	14.0					18.0	1.5	18.6	
16	"	1.17	14.0								" " " "
17	"	2.73	34.0					30.0	2.5	16.6	
18	"	1.67	20.0					16.8	1.4	15.2	
19	"	2.5	30.5					27.6	2.30	16.7	
20	"	3.33	41.0					30.0	2.5	16.3	" " " "
21	n-Octane	0.167	2.0							18.6	
22	"	1.17	14.0			0.402				16.6	
24	"	2.73	34.0	0.876	0.073					16.4	
25	"	2.73	34.0					1.09	.091	16.1	
26	"	1.17	14					0.92	.077	16.6	
27	"	4.16	50.1			0.87	.0725			15.5	
28	"	4.66	56.0	.233						16.6	
30	"	.167	2.0	.490	.041					14.3	
33	n-Heptane	0	0.0	10.9	.90					18.2	

TABLE III   (CONTINUED)

FLAME TESTS IN ALUMINUM FUEL DUCT

Rate of Flame Propagation

Run No.	Fuel	Air Stream Velocity		Location (1)		(2)		(3)		Initial Duct Temp. °C	Remarks
		feet/sec.	in/sec.	in/sec.	feet/sec.	in/sec.	feet/sec.	in/sec.	feet/sec.		
35	n-Nonane	0.167	2.0	0.198	0.0165					16.6	
36	"	0.167	2.0					.190		16.5	
37	"	0.167	2.0	1.33	0.0117						
38	"	1.17	14.0	0.160	0.0133	17.2	0.0143	.189	0.0158	14.6	
39	"	1.17	14.0	0.185	0.0154					15.8	
40	"	2.73	34.0	0.185	0.0154	0.209	0.0174	.206	0.0172	16.3	
41	"	4.16	50.1	0.160	0.0133	0.174	0.0144				
42	"	4.66	56.0	0.140	0.0117	0.150	0.0125			11.9	
44	n-Decane	0	0	fire at end of tube						18.7	
45	"	0.167	2.0	0.104	0.00365	0.120	0.010			18.0	
46	"	0.167	2.0	0.102	0.0085	0.114	0.0095			18.6	
47	"	1.17	14.0	0.114	0.0095	0.130	0.0108			18.4	
48	"	2.73	34.0	0.109	0.0091	0.122	0.0101				
49	"	2.73	34.0	0.089	0.0074	0.105	0.0087			11.2	
50	"	4.16	50.1	0.096	0.0030	0.109	0.0091			16.5	
51	"	4.66	56.0			.0.096	0.0080			16.4	

25

TABLE IV

COLOR PHOTOGRAPHY OF n-HEPTANE IN GLASS FUEL DUCTS

Run Number	V_A Air Velocity feet/sec	Blue Vapor Flame V_F Vapor Flame Propagation feet/sec	$V_A + V_F$ Constant
60	1.17	6.0	7.2
60-A	1.17	4.0	5.2
61	0.167	4.0	4.2
61-A	0.167	7.2	7.3
62	0	8.0	8.0
62-A	0	7.2	7.2
64	2.73	4.0	6.7
64-A	2.73	4.0	6.7
65	3.1	3.5	6.5
66	4.16	2.2	6.4
67	5.10	1.4	6.5

MECHANICAL DAMAGE TO AIRCRAFT SKINS FROM LIGHTNING

Introduction

Lightning can produce structural damage to aircraft in three ways: first, mechanically; i.e., from blast effect, burning holes, etc.; secondly, through heating, and last, by pitting or erosion.

In studying fire hazards associated with natural electrical discharges, the program dealt with those portions of the lightning stroke which produced the heat and the holes. In a natural discharge there are often several high amplitude current spikes connected by a low amplitude, long duration current. The heat generated by the long duration current, followed by the blast effect of the high current spike can produce a hole in metal aircraft skin. It has been suggested that the size of the hole formed is proportional to the charge transferred (1) (2), for any given thickness of skin. If this is true, a series of curves correlating hole size to charge transfer would be a useful tool in determining the typical charge transfers encountered by aircraft in flight.

Since a comprehensive series of lightning tests were planned on aircraft skins, sufficient tests were included in the schedule to define the problem of hole burning and its relation to charge transfer for such materials as aluminum, stainless steel, and titanium. A series of tests were also run to determine metallurgical changes in the metal resulting from the intense local heating around the hole or, for that matter, around the strike zone when no hole was produced.

Test Apparatus

The experimental work on metal damage included two test series. The first tests were run at the G.E. High Voltage Laboratory and consisted of lightning strikes to metal samples to develop a correlation between coulomb transfer and hole size. The second test series involved changes in metallurgical properties of metal samples resulting from the intense heat created by the charge transfer. These tests were conducted in the Dynamic Science Laboratories. A description of each test setup follows:

Hole burning tests.- A test chamber was constructed for this test series as shown in Figure 1. It was constructed with one side panel and bottom panel removed, permitting panels of transparent mylar film to be taped in place during the tests. This test chamber served for the hole burning tests and also for the combustible vapor ignition tests which followed. The top of the chamber was fitted with a set of toggle clamps to permit panels of the various test metals to be easily installed and removed. Grounding of the test chamber, to allow return of the lightning discharge currents, was accomplished through a large lug fixed to one side panel. A 1/4" tungsten electrode was
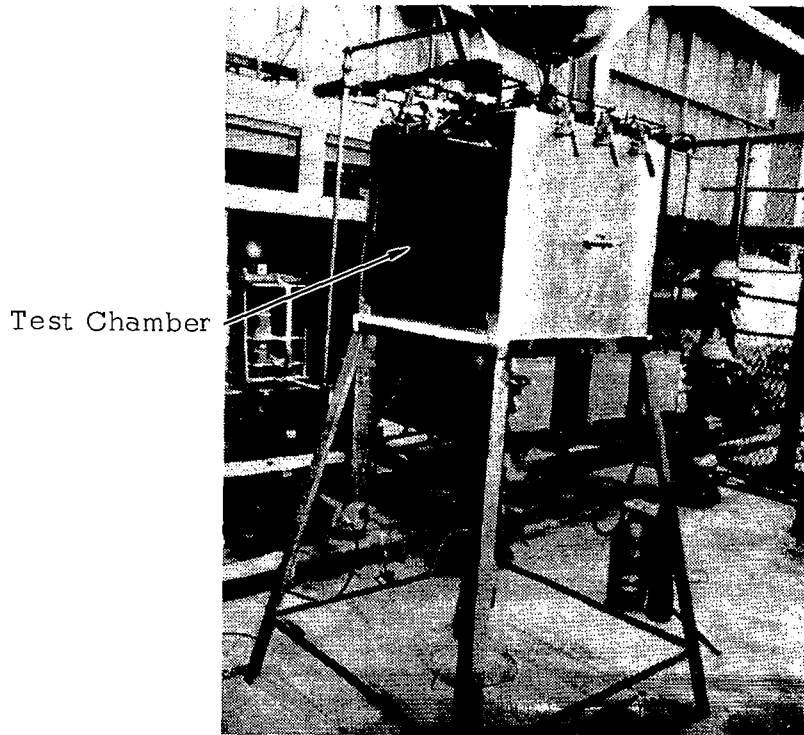
Test Chamber

FIGURE 1. Test Chamber for hole burning tests conducted
at General Electric High Voltage Laboratory
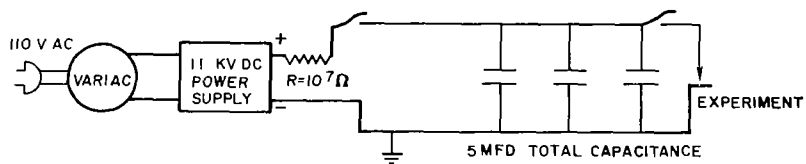
FIGURE 2. Electrical Discharge Circuit for Metallurgical
studies conducted at Dynamic Science

held rigidly positioned above the test panel and served to direct the discharge current to the desired spot on the test panel.

The initial high current spike was supplied from the G.E. high current generator consisting of a 6μfd. capacitor bank charged to a potential of 100,000 volts. The low amplitude continuing current was supplied from their 500 volt, 1000 kva dc rotating generator. Measurements of the current values were made with the use of low resistance karma metal high current shunts placed in the return circuits of both sources. Oscillograms of the current waves were obtained for each discharge, using a GE HC-25 oscilloscope (for the high current spike) and Tektronix 545 and 532 oscilloscopes (for the continuing currents). Electronic timers were used to trigger the high current generator and the continuing current flow in the proper order.

Metallurgical damage.- The electrical test apparatus used in the metallurgical tests is shown in Figure 2. It consists of a 5μ fd capacitor bank charged to a potential of 11,000 volts. When discharged, it delivered 300 joules of electrical energy to the metal sample. A 1/8" tungsten electrode directed the energy to the desired location.

The discharge time for the circuit is approximately 10 microseconds.

Experimental Technique and Test Results

Hole burning.- All tests employed an initial current spike of 38,000 amperes rising to its crest in 7.5μs and decaying to 50% of crest current in 12.5μs, Figure 3. This value was chosen because it is within the range of current which has been measured in actual lightning strokes (1). Continuing currents ranging in magnitude between 40 and 300 amperes and in time duration between 0.25 and 1.60 seconds were applied following the high current discharge, Figure 3a. In most cases, a test sequence would be run with either the current or discharge time held constant and the remaining parameter varied through a range which would provide coulomb transfers similar to those measured in natural discharges.

For the tests made on 20 and 40 mil aluminum, the electrical parameters were set to maintain a constant current of 115 amperes, and discharge times were varied between 0.30 and 1.5 seconds. There was some variation in current during the course of the discharge as a result of changes in the resistance of the arc. These variations rarely caused the current amplitude to fluctuate more than plus or minus 20%.

For the 60 mil aluminum, it was necessary to increase the average current level to 288 amperes in order to obtain charge transfers great enough to burn a hole in this thicker metal within the time periods (from 0.5 to 1.5) sec.) chosen. Tests on 60 mil thicknesses of titanium had the discharge time held constant at 0.5 sec., in order to obtain a hole size comparison with a similar discharge time on 20 mil titanium. Using this time increment (0.5 sec.), tests had to be made at current levels between 288 and 690 amperes in order to
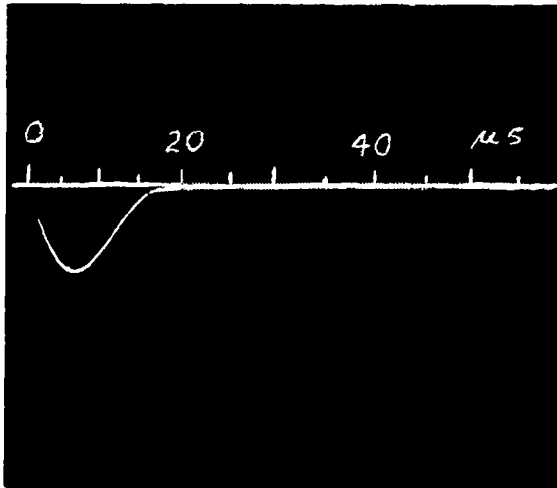
Crest is 38kA at 7.5 μsec.

Tail reaches 50% value at 12.5 μsec.

FIGURE 3. Initial high amplitude, short duration
current wave shape, common to all
simulated lightning current discharges
applied during hole burning tests.

NOTE: Trace has downward deflection due to
placement of current measuring shunt
in ground return circuit.
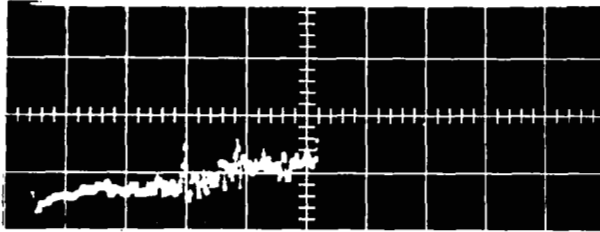
Continuing current.

Average current is 143 amperes for 0.90 sec. resulting in discharge of 128 coulombs.

Major divisions are 46 amperes and 200 msec.
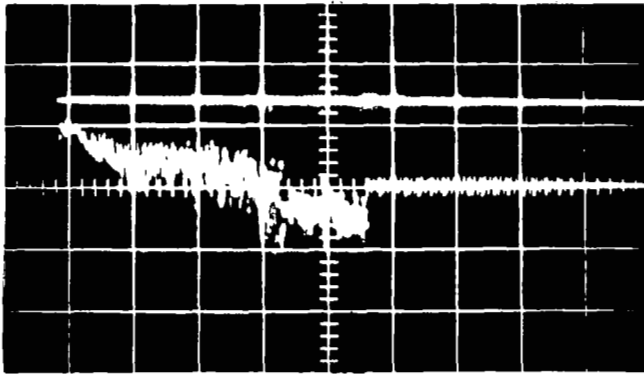
Arc voltage.

Major divisions are 150 volts and 200 msec.

FIGURE 3a   Oscillograms of continuing current and corresponding arc voltage for hole burning test on .040 inch aluminum. Note gradual decrease in current amplitude and increase in arc voltage, indicating draw-out of arc as aluminum was eroded away. (test no. 72)

31

obtain the same range of hole sizes in the 60 mil thickness.

Tests were run on .020", .040", and .060" thicknesses of titanium and aluminum. Tests were also run on .030" stainless steel. Additional tests were planned for stainless steel during the final test series; however, these were temporarily delayed to permit a series of simulated fuel vent system tests as part of a redirection in scope of this contract.

Results

Hole burning.- The results of the hole burning tests for titanium, aluminum and stainless steel are shown graphically at the end of this section. Perhaps the most significant first impression is the wide scatter in the data points which, in essence, say that for any given coulomb transfer a wide range of hole sizes might result. Before beginning an analysis of the data, perhaps a few words are in order concerning possible causes for this wide scatter of data points.

As described previously, the electrode was rigidly positioned about 1/4" above the test sample. This gap was ionized by an initial high current discharge of approximately 38 k amperes. Following this, there was a longer continuing current which flowed from the electrode to the sample, ranging in magnitude between 40 and 300 amperes depending on the charge transfer desired. The metal was damaged by the intense heat created by the long, continuing current discharge. This damage was characterized by molten metal around the discharge zone which generally resulted in the formation of a hole if the charge transfer was of sufficient duration. An examination of the data reveals that the size of the hole often varied considerably for the same charge transfer even when all other factors remained constant. A careful examination of a number of test samples reveals a possible cause. When the current was flowing between the electrode and the test sample it had a tendency to move around on the metal before it finally stabilized and started burning a hole. When the current arc moved over the metal it distributed the associated heating effects over a relatively large area of the metal. Thus a metal sample often exhibited a great deal more damage than could be characterized by the area of the hole.

In retrospect, this mobility of the arc can probably be traced to the choice of cathode and anode. A dc arc, such as that used for the hole burning experiments, is polarized and the anode and cathode processes are distinctly different. For example, the cathode is bombarded by ions from the discharge column, while electrons strike the anode. Potential distribution in the arc is usually such as to produce the highest voltage gradient across the cathode sheath. The cathode spot tends to be highly mobile, whereas the anode spot is almost always stationary, changing only in size and shape as the discharge develops. Current densities are generally higher at the cathode.

The nature of the polarity of lightning strokes to aircraft in flight is not known. If the stroke enters the aircraft at one point and leaves at another,

both polarities will be involved. All the tests made during the hole burning experiments were made with the test sample serving as the cathode and the arc electrode as anode. Since the highest voltage appears across the cathode sheath, it is probable that tests to date represent the more hazardous polarity: on the other hand, the fact that the anode spot is more stationary permits the heat to concentrate at one point and this could result in the earlier formation of holes and ultimately a more uniform distribution of data.

Regardless of the reason, the data obtained to date does show a considerable variation among the hole sizes for a given amount of charge transfer to the test metal.

In fact, the scatter is so great that a line derived by least squares or by other techniques may have little meaning. Nevertheless, there is a distinct trend in the data which indicates that the size of the hole is a function of the charge transferred. The wide scatter in results is partially due to the fact that quantitative evaluation of the damage to the metal was limited to the measurement of the actual size of the hole formed. In a majority of cases, it was apparent from visual observation that additional damage had occurred. The region adjacent to the hole, for example, frequently showed tracking and burning which did not result in burnthrough, but which nevertheless was caused by charge transfers to these regions. Some melting and resolidification of metal along the edge of the holes was also evident. Since there was no quantitative way of determining how much of the charge transfer actually produced the hole, the data was plotted in Figures 4 through 14 as if all of the charge was effective in burning the hole.

With the foregoing in mind, it seems appropriate to assign greater significance to the data on the "upper" side of the region shown on the figures rather than to that appearing on the lower side, since a larger portion of the charge transfer must have been effective in burning the larger hole. The upper points thus more closely represent the areas of holes which can be burned by the corresponding charge transfer. This conclusion is strengthened upon close observation of the damaged metal, where the greatest "side" effects of tracking and burning are frequently associated with the smaller holes burned by a particular charge transfer.

Thus, to obtain a better visual picture of the results and to permit a comparison between one set of data and another, lines have been drawn along the upper side of the data points and along a mean path through the center to form a "zone" of damage related to charge transfer. On this basis comparisons can be made among the results obtained.

Aluminum.- Most of the testing of aluminum was accomplished by use of a constant continuing current amplitude while varying time durations as needed to obtain appropriate variations in charge transfer. Currents of about 115 amperes were used for the tests of the 20 and 40 mil thicknesses, and a current of 288 amperes was used for charge transfer to the 60 mil thickness, since use of the lower current amplitude would require time durations in excess of those found to be characteristic of actual strokes.

The size of the hole burned in aluminum for a constant charge transfer appears to rise almost exponentially as one goes from .060" to .040" to .020" thicknesses. Referring to Figures 4 through 7, a charge transfer of 20 coulombs, the lowest amount applied during these tests, was found to burn a 45 mm^2 hole in the 20 mil thickness, and slightly more than 60 coulombs were required to burn a similar size hole in the 40 mil thickness. No holes of this size were burned in the 60 mil thickness however until over 200 coulombs had passed through the metal. A comparison of results obtained from tests on the three thicknesses of aluminum shows that an increase in metal thickness results in a reduction in the area of hole burned, for identical stroke discharges. A 100 coulomb discharge, for example, burned holes of between 300 and 700 mm^2 in 20 mil aluminum, and holes of between 0 and 140 mm^2 in a 40 mil thickness. The same discharge burned only a pin hole, or no hole at all, in a sheet 60 mil thick. For all thicknesses, increasing amounts of charge resulted in increases in the hole sizes, but existing data is insufficient to establish an exact relationship.

Titanium.- Most of the titanium tests were run by establishing a constant time duration of the discharge and varying the current as needed to obtain the desired variations in charge transfer. In titanium as in aluminum, the size of hole burned for a given charge transfer again appears to rise exponentially as one progresses from the thicker material such as .060" to the thinner metal such as .020".

A 100 coulomb discharge to a 20 mil sample burned holes of between 50 and 200 mm^2 (as compared with 300 and 700 mm^2 for aluminum), and 0 and 20 mm^2 in a 40 mil sample (as compared with 0 and 140 mm^2 for aluminum). The same discharge was insufficient to burn all the way through a 60 mil thickness of titanium (as compared with a pin hole in aluminum). As before, increasing amounts of discharge produce increases in corresponding hole sizes, but the linearity of the relationship is not clearly defined. In one instance, the existing data shows that a twofold increase in the amount of charge transferred to 40 mil titanium resulted in a hole size approximately 4.5 times greater. This relationship can be approximated, of course, only within the 100 through 300 coulomb charge transfer range which was run.

During these tests a charge transfer of 60 coulombs was found to burn holes of between 0 and 65 mm^2 in the 20 mil thickness. A discharge of 100 coulombs or more burned holes of between 0 and 30 mm^2 in the 40 mil thickness, and the smallest hole formed during the tests on 60 mil thicknesses of aluminum occured after 180 coulombs had been discharged. These holes ranged between 20 and 60 mm^2.

Stainless steel.- Tests were made on 30 mil thicknesses only. Holes were burned in this metal at charge transfers above 60 coulombs, see Figures 12 and 13. The shortened test program failed to permit sufficient tests to establish the relationship between charge transfer and hole size above this level.

Conclusions.- The results obtained from this phase of testing provide only a vague relationship between hole size and charge transfer. Where the results are less scattered a linear relationship between hole size and charge

transfer is apparent; however, in no case can a single line be drawn to define the relationship; rather a "region" or "zone" is more appropriate. Undoubtedly, the lack of a more comprehensive method of evaluating damage to the metals was responsible for at least some of the scatter obtained. Also, more uniform results might be obtained by reversing the polarity of the discharge and taking advantage of the stable anode spot.

Tests showed that both titanium and stainless steel are more resistant to hole burning than aluminum. This might be expected since the melting point of aluminum (1200°F) is less than either titanium (3000°F) or stainless steel (2550°F). The few tests run on stainless steel show that it has about the same resistance to hole burning as titanium. Here again this is not unreasonable since their melting points are very close.

The following table shows comparisons of results obtained for an identical stroke carrying 100 coulombs of charge applied to the various metals and thicknesses tested.

100 Coulomb Discharge

		Type of Metal	
	Aluminum	Titanium	Stainless Steel
Thickness		Hole Sizes (mm^2)	
20 mil	300-700	50-200	----
30 mil	----	----	40-80
40 mil	0-140	0-20	----
60 mil	Pin Hole	No Hole	----

Initially, it would appear that titanium is much less susceptible to a lightning stroke than is aluminum, since considerably less titanium metal is eroded away by a given charge transfer than aluminum. This conclusion cannot be extended to the evaluation of hazard when these metals are utilized in fuel-tank walls, since ignition tests on titanium have proved that ignition will occur from discharges much lower in magnitude than those required to produce a hole.

In the hole burning tests two techniques were used to vary the coulomb content of the discharge. The first technique was to fix the duration of the discharge and vary the current amplitude. The second technique was to fix the current amplitude and vary the discharge time. When both techniques were tried on one metal sample and the total charge transfer held constant, larger holes were burned on the test which had the highest current amplitude. Since the energy associated with the discharge is directly proportional to

the time duration and proportional to the square of the current amplitude, it is clear that greater energy release must be associated with higher current discharges, even though the duration is proportionately decreased so that the charge transferred remains the same. This is probably the reason why larger holes were burned during the tests where the current discharge was held constant. Comparisons of tests made under the two conditions for 20 mil thicknesses of titanium, for example, can be seen from observation of the test results as plotted in Figures 8 and 9. These results indicate that the rate of charge transfer to the test metal is significant, as well as the amount of charge transferred.

The hole burning tests have served to provide a rough approximation of a zone of the damage which can be inflicted upon various metals by lightning discharges. These tests have shown that the rate of charge transfer is an important factor in determining the damage that can occur. As a result of these tests it is clear that more consideration must be given to the assessment of damage. Merely measuring the size of the hole is not sufficient. Some consideration must also be given to peripheral damage and evidence of overheating in the vicinity of the strike zone. Additional work should continue into the investigation of the effects of polarity on damage. Future tests run with a less mobile arc and with the time of discharge held constant might provide a better defined set of data points, particularly if the interpretation of damage can be modified to consider the area surrounding the strike zone. In the meantime, some use can be made of the "zones" or range of charge transfers which have been identified with hole sizes in this report.

Results

Metallurgical studies.- In this investigation, the material samples were repeatedly struck with an 11,000 volt discharge such as shown in Figure 2. All discharges were directed at one spot on the material so that we could evaluate the cumulative damage. After each strike, the thickness of the material was measured with a ball head micrometer. The material samples measured 1/2" in width and 2" in length. Tests were run on thin samples of aluminum, titanium, and stainless steel. Sample thickness varied from 0.005 up to 0.016".

Actual test procedures involved a large number of samples of each material and for each thickness. The first sample of each type was struck once, then examined. The second sample of each type was struck twice, then examined. The third sample of each type was struck three times, then examined, etc. Testing was terminated when a hole was produced by these successive strikes. The metal was allowed to cool between each discharge.

In the table below are listed the number of electrical discharges required to produce a hole in these materials:

TABLE I

Total Energy and Number of Electrical Strikes Required to Produce a Hole in Test Materials

Alloy	Thickness Inches	No. of Electrical Strikes to Produce a Hole N	Total Energy 300N Joules
Aluminum	0.012	5	1500
Aluminum	.016	6	1800
Titanium	.005	3	900
Titanium	.016	13	3900
Stainless Steel	.010	24	7200

Microstructure.– Metallographic analyses were conducted on the 0.005" and 0.016" commercially pure titanium metal. The analysis was conducted after a number of electrical discharges had been directed to the same spot on a sheet of material. What is seen in the photomicrographs is an edge-on view of the specimen cut across the center at the point of electrical discharge.

Figures 14 and 15 show the structure near the center of the discharge zone on 0.005" thick commercially pure titanium. Figure 14 shows the effect of one discharge, Figure 15 the effect of two discharges, and Figure 16 the effect of three discharges. The first discharge produced fusion and overheating in the surface zone. Figure 17 shows this overheated structure at higher magnification. The immediate surface layer had been melted. Then under this zone was a layer of material which had not been melted but which had been heated above the beta transus temperature. The second discharge produced substantial melting and thinning of the material. Figure 18 shows a crack in the fusion zone after the second discharge. The third discharge produced a hole in the 0.005" material. Figure 18 shows the structure at the edge of the hole. The white layers represent a severely oxidized zone. The entire thickness beneath this layer had been heated to a temperature above the beta transus. Subsequent rapid cooling produced the acicular alpha structure.

Figures 19, 20 and 21 show the structure of the 0.016" thick 6Al-4V alloy after having been exposed to 1, 5, and 13 discharges, respectively. Again, the fusion and overheated transition zones can be readily seen. Note again, the general thinning resulting from additional discharges. Figures 22 and 23 show the surface effects at 920 and 1200 x magnification.

In summary, these electrical discharges produced a region of high oxidation near the surface. As much as 90% of the material was oxidized in two

discharges of equal magnitude. There was no evidence of carbide or nitride formation from these discharges.

Mechanical properties.- Tensile strength and elongation tests were conducted to provide information on changes occurring in the mechanical properties of these aircraft materials. For these tests samples were selected of 0.015" 6Al-4V titanium alloy which had been subjected to 0, 2, and 10 discharges.

These specimens were 1/2" wide and 2" long. A standard apparatus, was employed for these tests. Figure 24 shows two of these specimens after testing.

The results are shown in the following table for 6Al-4V titanium alloy.

No. of Electrical Discharges	Tensile Strength P.S.I.	Elongation %
0	155,000	12
2	148,000	6
10	96,000	2

The minimum governmental accepted strength for this alloy is 150,000 psi. It can be seen in our tests, two discharges reduced the tensile strength below the acceptable limits.

For ductility the minimum accepted standard is 10%. Here it is found two discharges produced an elongation of 6%, almost one-half the accepted minimum. This result is particularly significant in that one single lightning strike would certainly reduce the ductility below the accepted minimum.

The overall weakening of the material can be attributed to four factors:

1. Creation of thermal stresses (opposite of annealing) from rapid heating and cooling.

2. Raising temperature of specimen above its beta transus temperature, quenching in brittle high temperature crystal form.

3. The general thinning of the material from each discharge.

4. Mutual heating of a portion of the specimen above its melting point, also producing a condition of very low ductility.
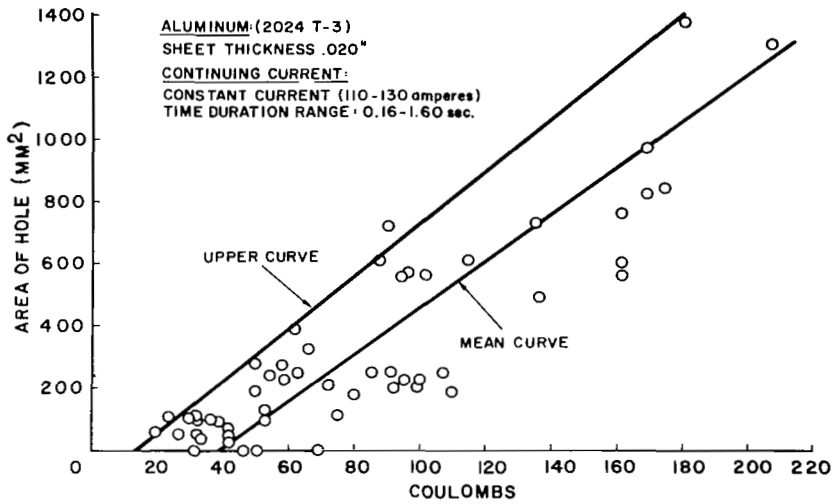
FIGURE 4. Area of Hole Formed Vs. Coulomb Content of Lightning Strike.
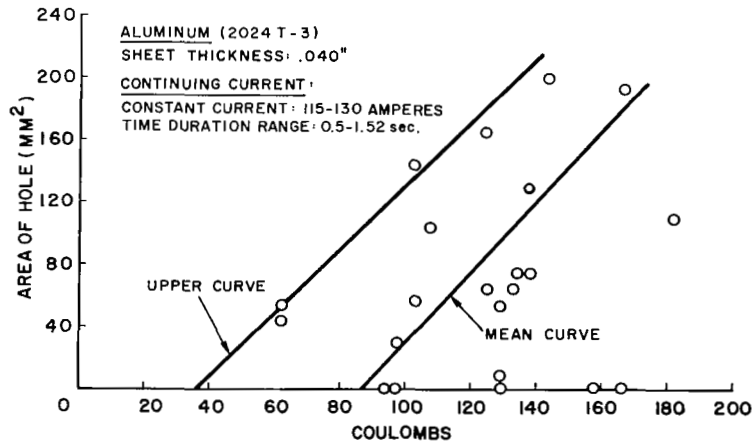
FIGURE 5. Area of Hole Formed Vs. Coulomb Content of Lightning Strike.

39
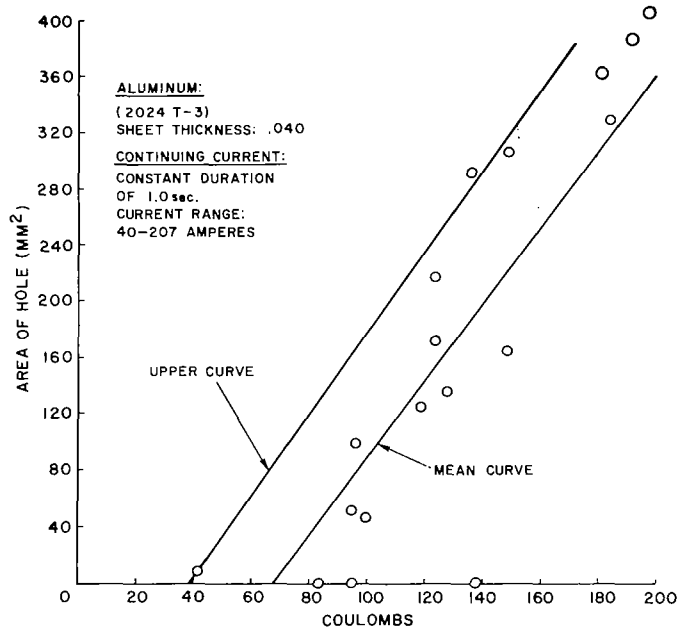
FIGURE 6. Area of Hole Formed Vs. Coulomb Content of Lightning Strike.
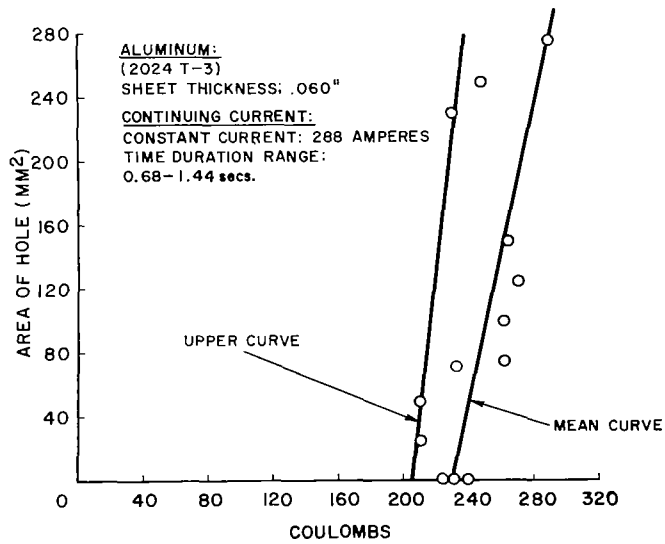
FIGURE 7. Area of Hole Formed Vs. Coulomb Content of Lightning Strike.
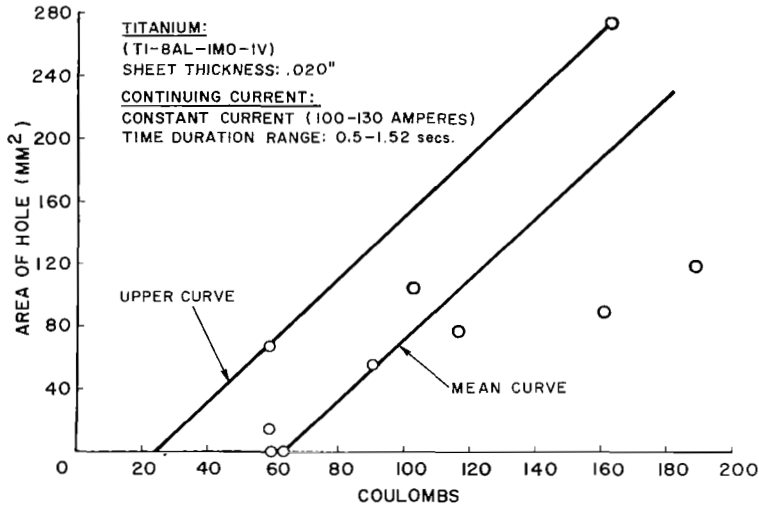
FIGURE 8. Area of Hole Formed Vs. Coulomb Content of Lightning Strike
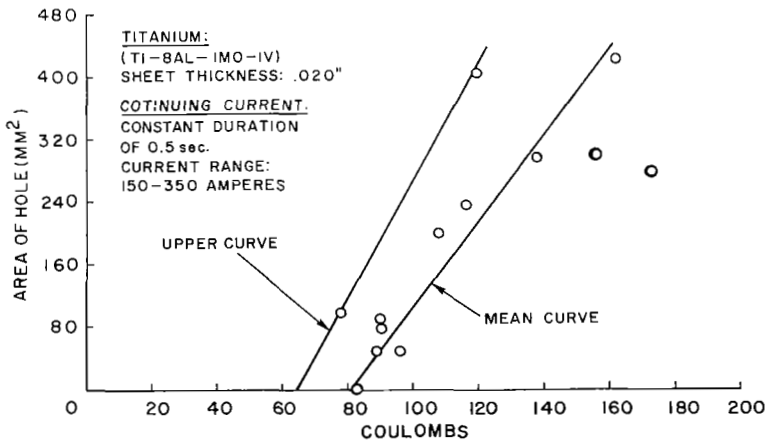
FIGURE 9. Area of Hole Formed Vs. Coulomb Content of Lightning Strike.

41
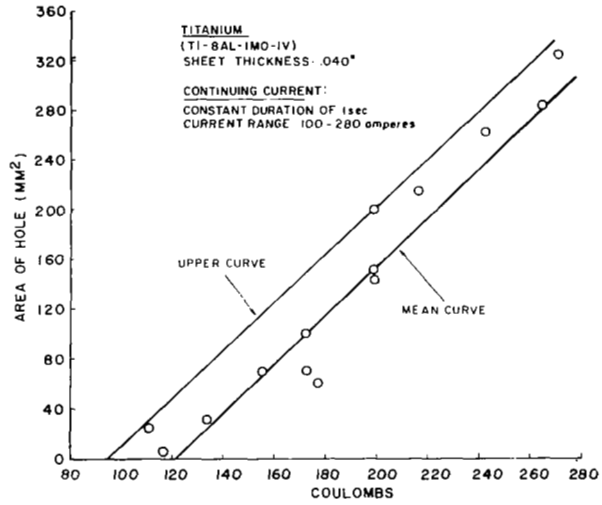
FIGURE 10. Area of Hole Formed Vs. Coulomb Content of Lightning Strike.
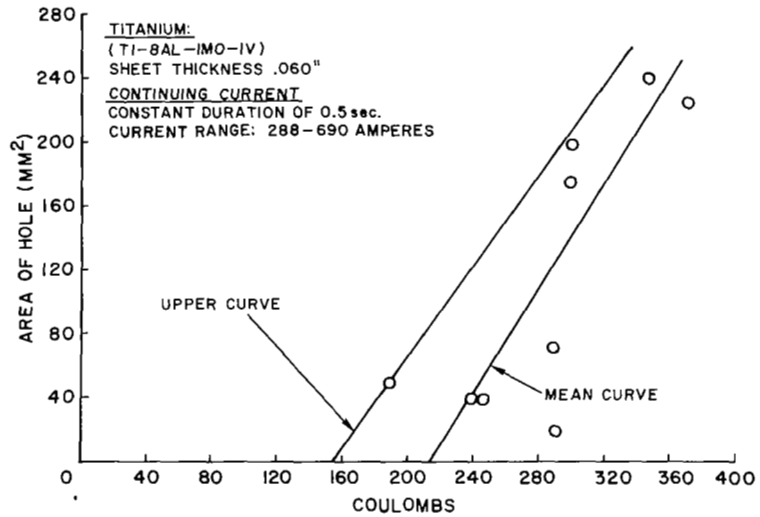
FIGURE 11. Area of Hole Formed Vs. Coulomb Content of Lightning Strike.

42
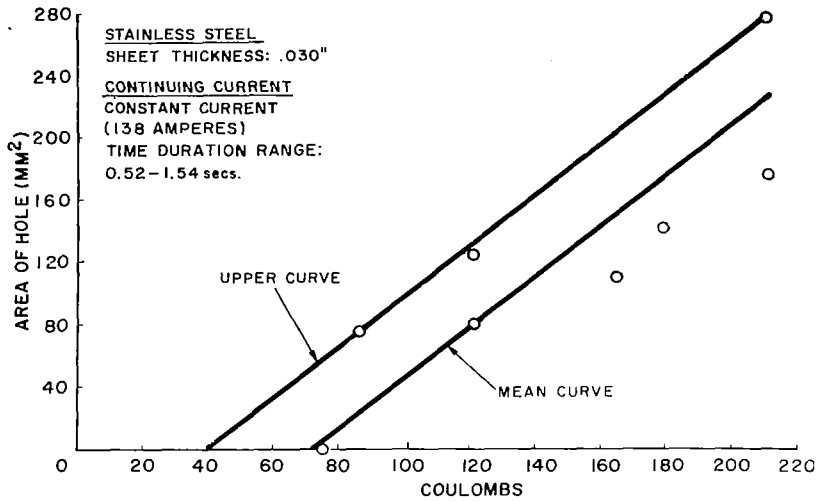
FIGURE 12. Area of Hole Formed Vs. Coulomb Content of Lightning Strike.
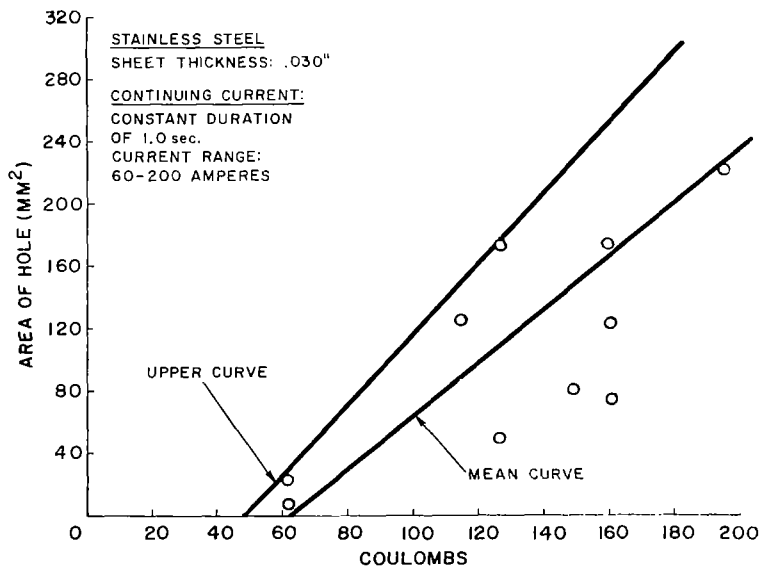
FIGURE 13. Area of Hole Formed Vs. Coulomb Content of Lightning Strike.

43
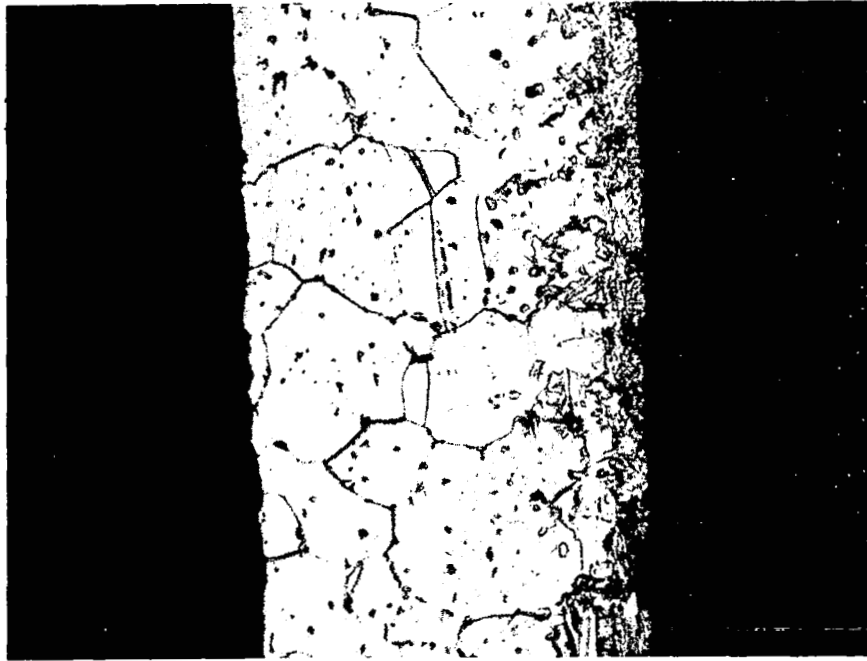
FIGURE 14. Pure Titanium, 0.005" Thick, 500X, One Electrical Discharge.
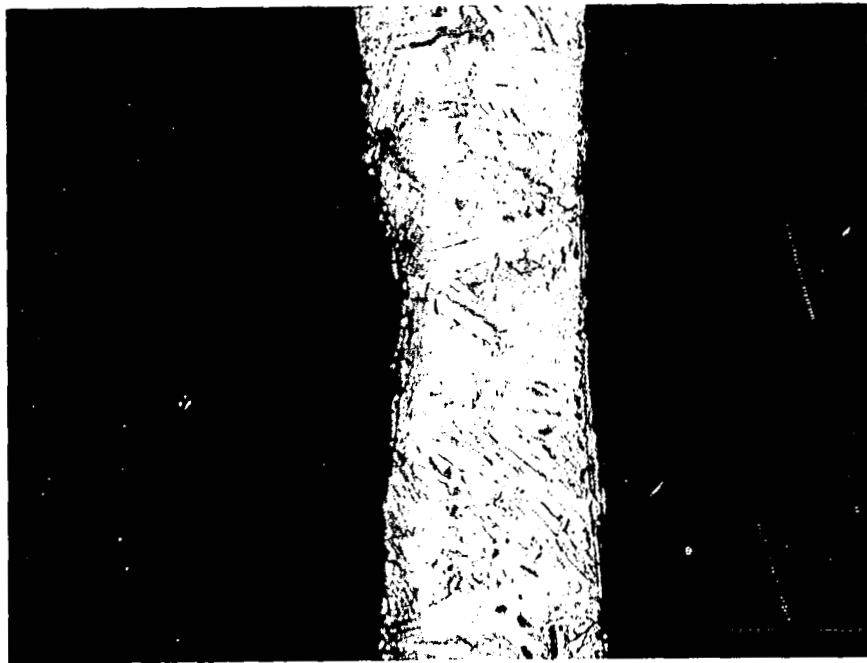
FIGURE 15. Pure Titanium, 0.005" Thick, 500X, Two Electrical Discharges.
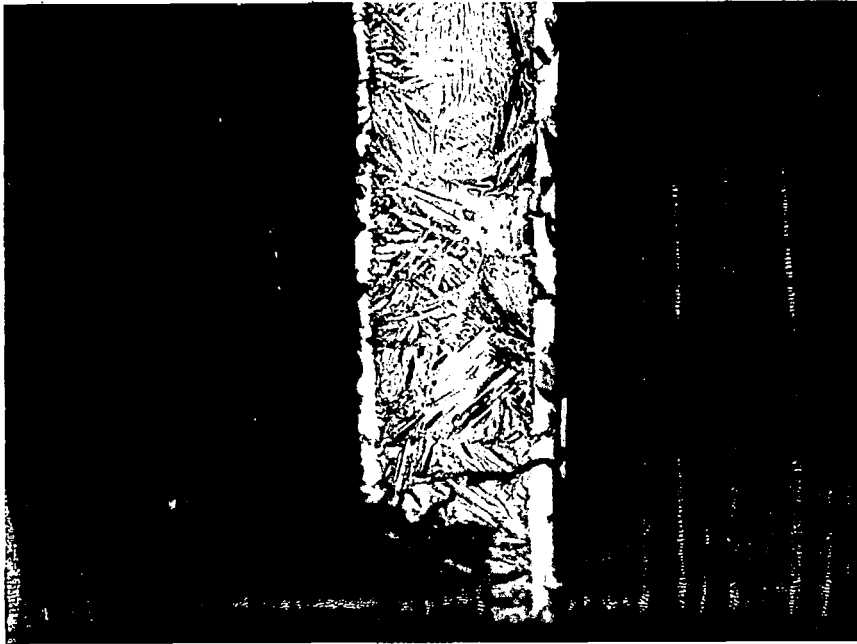
FIGURE 16. Pure Titanium, 0.005" Thick, 500X, Three Electrical Discharges. Note Appearance of Herringbone Structure Characteristic of Brittle High Temperature Beta Form. Also, Note Presence of Highly Oxidized Region at Surfaces.
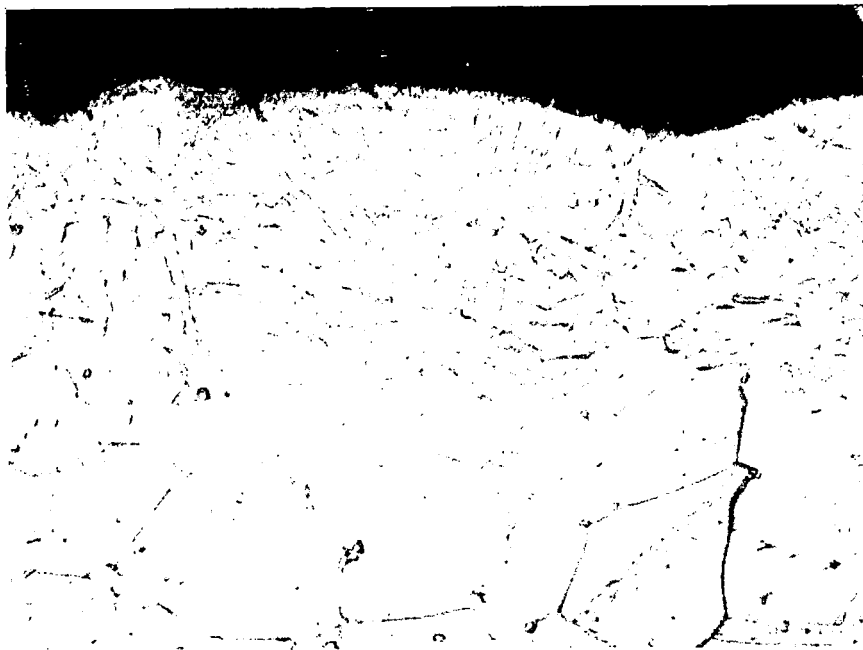
FIGURE 17. Pure Titanium, 0.005" Thick, 900X, One Electrical Discharge. Note Region of Overheating and Fusion Next to Surface. The Immediate Surface Layer had been Melted.
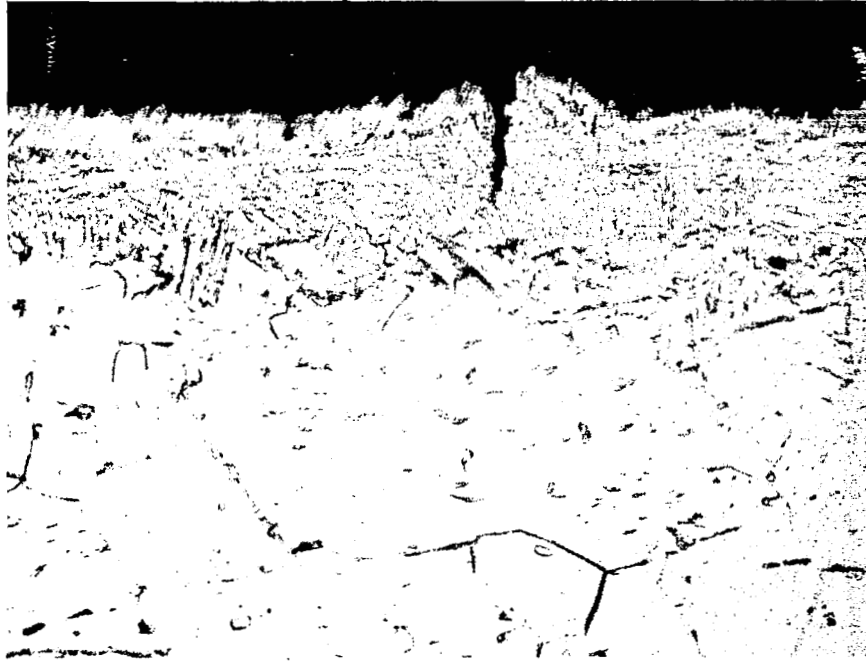
FIGURE 18. Pure Titanium, 0.005" Thick, 920X, Two Electrical Discharges.
Note Crack in Fusion Zone.
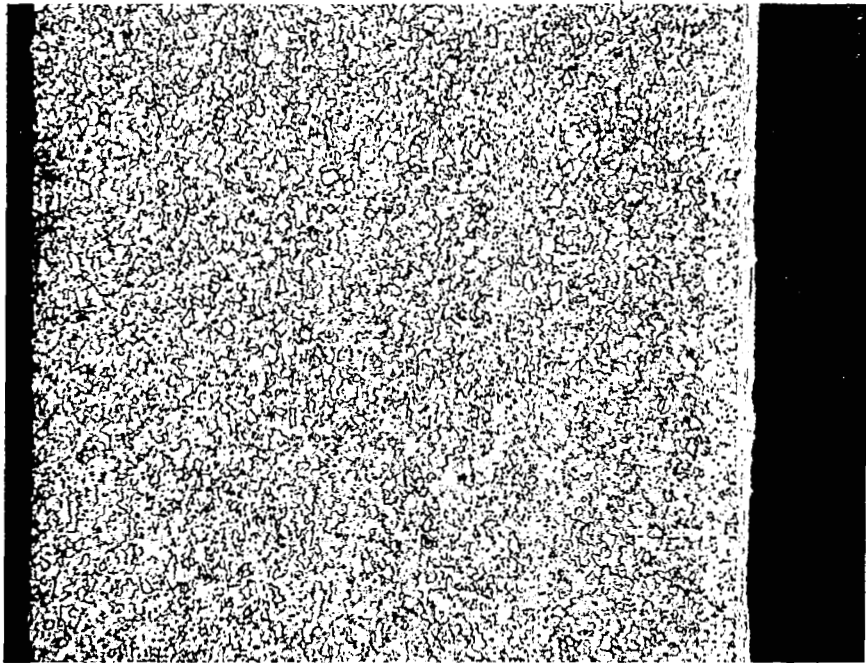
FIGURE 19. 6 Al.-4V Titanium Alloy, 0.016" Thick, 260X, One Electrical
Discharge. Note Oxidized Surface.
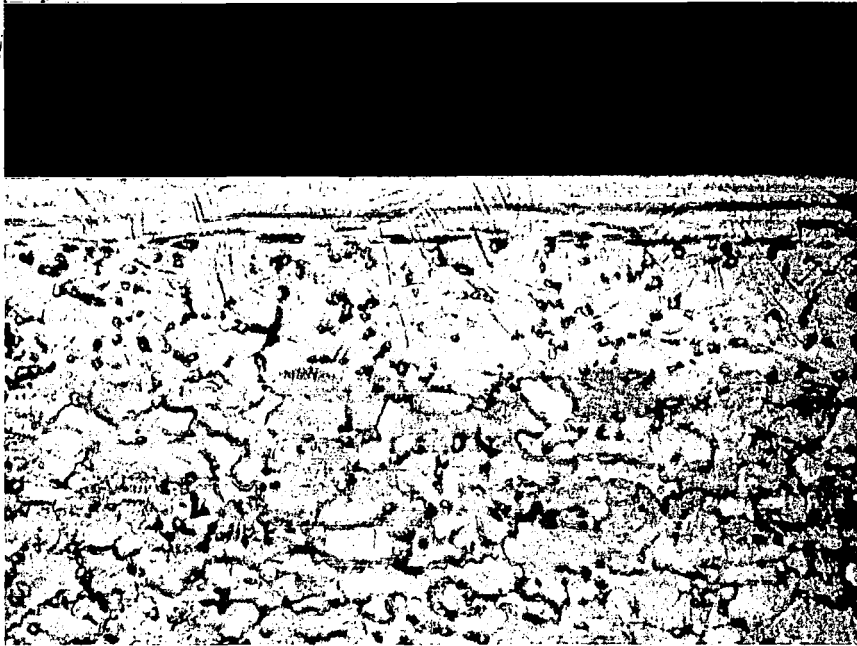
FIGURE 20. 6 Al.-4V Titanium Alloy, 0.016" Thick, 920X, One Electrical
Discharge. Note Herringbone Structure of Oxidated State.
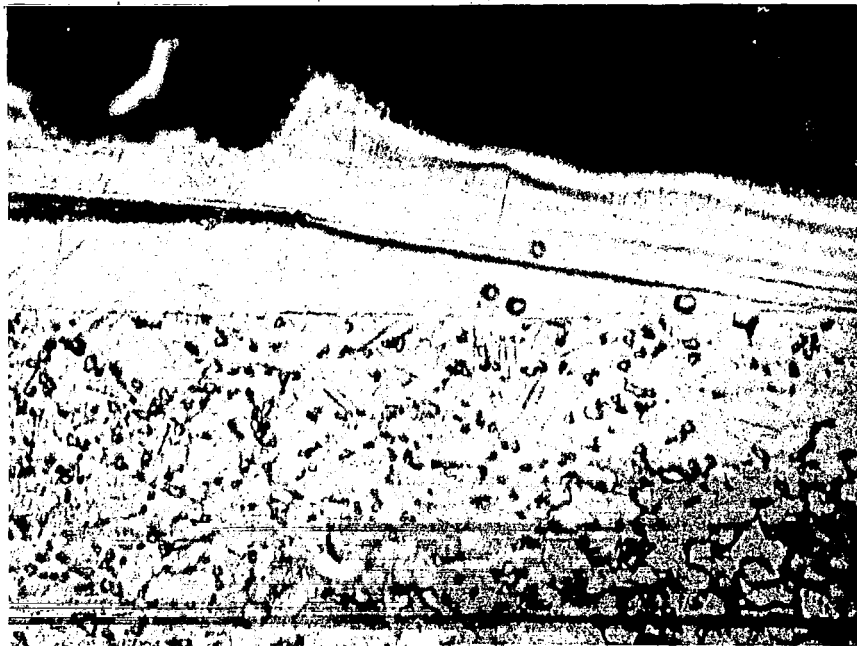
FIGURE 21. 6 Al.-4V Titanium Alloy, 0.016" Thick, 1200X, Five Electrical
Discharges. Note under High Magnification Amorphous Structure
of Oxidized Titanium at Surface, with High Temperature Beta Form
Underneath.

47
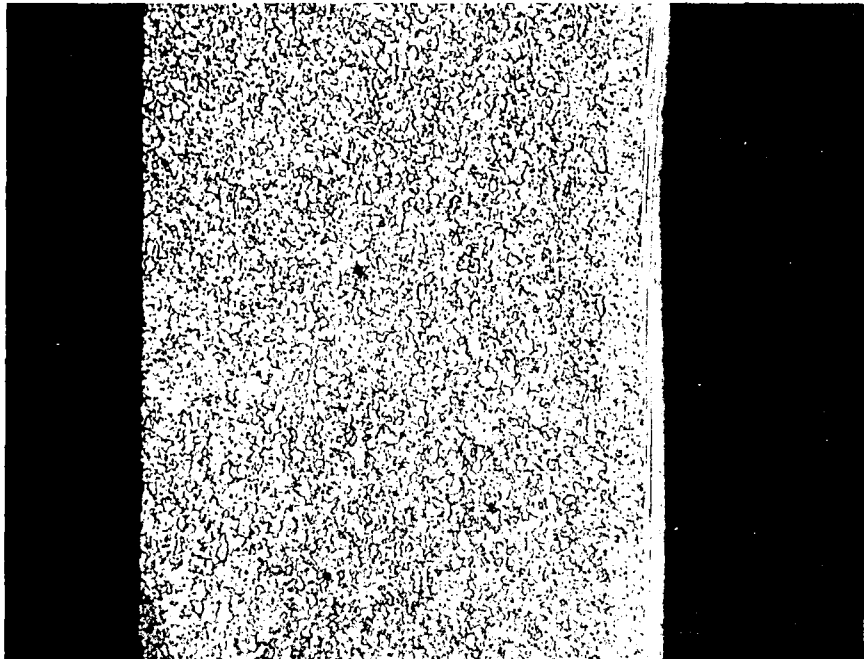
FIGURE 22. 6 Al.-4V Titanium Alloy, 0.016" Thick, 200X. Five Electrical
Discharges. Note Highly Oxidized Surface.
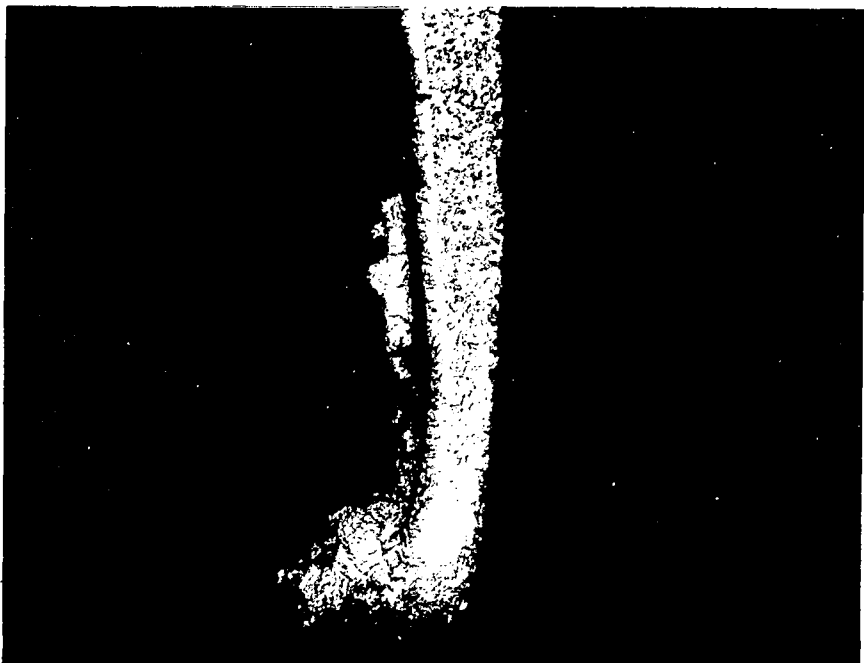
FIGURE 23. 6 Al.-4V Titanium Alloy, 0.016" Thick, 260X, Thirteen Electrical
Discharges. Again Note Oxidation and General Thinning
Resulting from Additional Discharges.
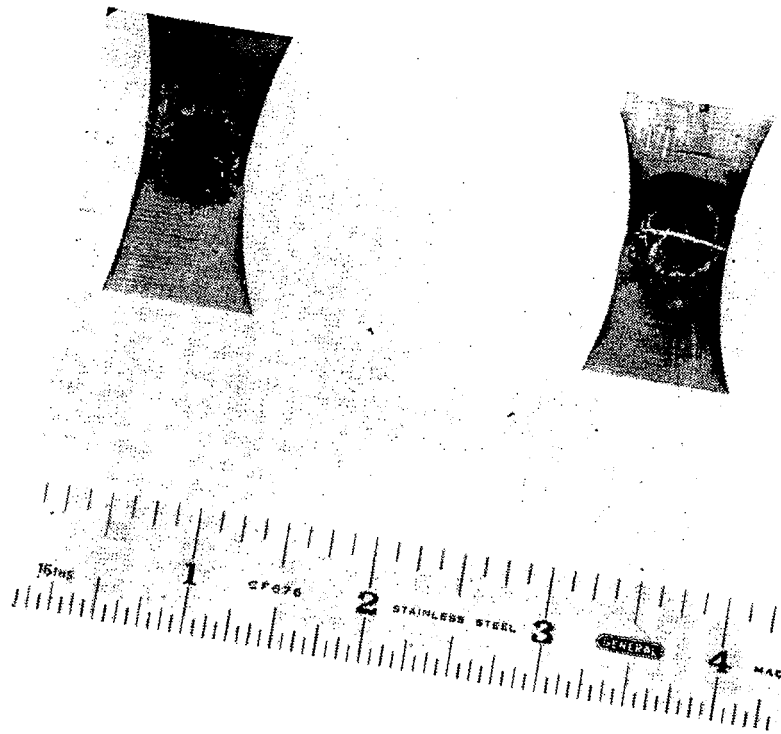
FIGURE 24. Photograph of 0.016" titanium specimen subjected to tensile strength and ductility tests after being struck by electrical discharges. The specimen on the left is the result of two electrical discharges, where the specimen on the right is the result of ten discharges.

REFERENCES

1. Schmidt, H. A., N. S. Kovar, D. E. Stogryn, M. Gerstein, "The Study of a Facility to Investigate the Effect of Natural Electrical Phenomena on Aircraft and Spacecraft," Prepared under NASA Contract No. NASW-853 (1964).

2. Newman, M. M. and J. D. Robb, "Lightning and Transients Research Institute Report 395, Comparative Lightning Damage to Aluminum and Stainless Steel-1.

FUEL IGNITION THROUGH AIRCRAFT SKINS

Introduction

The work on lightning strikes to aircraft skin was primarily concerned with defining ignition mechanisms of fuel in contact with the underside of the skin. The investigation was not limited to ignition produced by burning a hole through the skin but was equally concerned with the possibility of lightning producing a localized temperature "hot spot" on the undersurface of the skin which would remain at an ignition temperature for a sufficient period of time to ignite a combustible mixture. The relationship between ignition delay and ignition temperature for a typical hydrocarbon is shown below.
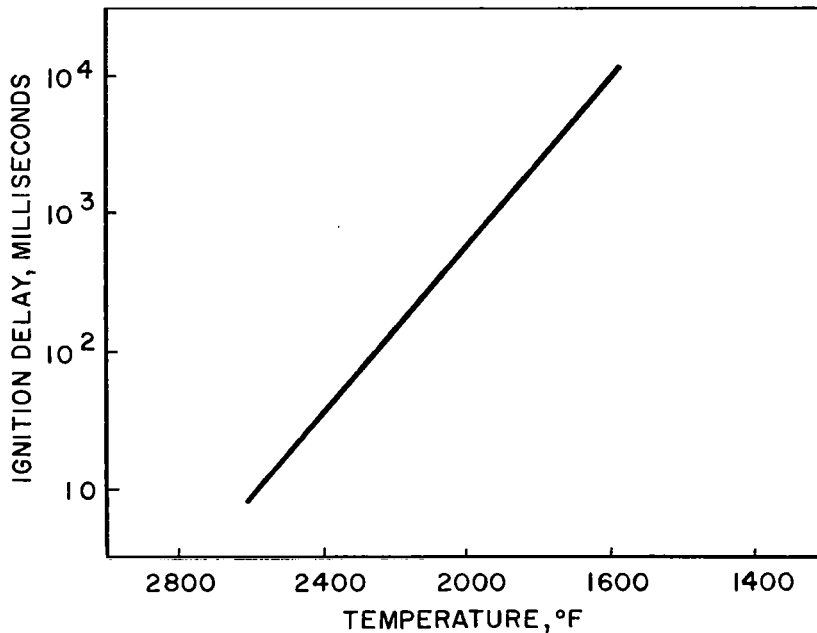
At $1200^\circ F$, the melting point of aluminum, the ignition delay is approximately 30 seconds. It would be impossible for a hot spot to maintain that temperature for such a period of time considering the excellent thermal conductivity of aluminum. Therefore, hot spot ignition has not been a problem with aluminum skin.

Titanium and stainless steel on the other hand, have relatively low thermal conductivities and high melting points ($3000^\circ F$ and $2500^\circ F$ respectively). Lightning striking these materials could produce temperatures in the strike zone up to their melting points without producing a hole. Referring again to the above curve, the ignition delay at these temperatures is in the

millisecond range. Considering the lower thermal conductivity of these materials, there was good reason to believe that an electrical discharge could create a "hot spot" which would produce ignition.

Thus our program, which was largely experimental, was designed to characterize the temperature gradients created by electrical discharges, varying in their coulomb content, and to relate these to their ignition capability in terms of ignition delay time and the fuel-air ratio of the combustible mixture. Tests were run on copper, aluminum, stainless steel and titanium in thicknesses ranging from .020 to .060 inches.

Towards the end of the program a mathematical model was developed to correlate the experimental data and to facilitate parametric studies of ignition hazard in terms of the physical properties of the material, the fuel-air ratio and the energy transferred by the electrical discharge.

In summary the program objectives were: 1) to obtain the coulomb levels of lightning discharges necessary to ignite a typical fuel-air mixture through metal surfaces of aluminum, titanium, and stainless steel, 2) to measure the time of fuel ignition after initiation of the lightning strike for the above materials, and 3) to determine the mechanism by which fuel ignition occurs in these cases.

Test Apparatus and Techniques

The same test chamber which was used for the hole burning experiments and which is described in the previous section was employed for these tests. Two high speed cameras were positioned to record the ignition and the temperature distribution on the undersurface of the metal sample. Through the mylar walls of the chamber a Hi-Cam camera in front of the test chamber was loaded with high speed Kodak Ektachrome film and photographed the discharge, burnthrough and vapor ignition. A Fastex high speed camera below the chamber was set up to view the undersurface of metal sample. It was loaded with Kodak infrared film and recorded the temperature distribution around the strike zone and the ignition and propagation of the flame.

Fuel ignition times were established from the analysis of both the color and infrared films. A check on these measurements was obtained through use of a sensitive microphone placed into the test chamber.

A sketch of the electrode configuration and its relation to the metal sample is shown in Figure 1. The electrical discharge consisted of a two-component wave which is characteristic of a natural stroke. It consisted of a 38kA high current spike with a rise time of 7.5 microseconds and a decay time of 12.5 microseconds. This initial spike was followed by a low amplitude current flow of between 90 and 150 amperes lasting for periods up to 1 second, depending on the charge transfer desired (Figure 2a). In addition a few tests were conducted with a three component wave shape such as shown in Figure 2b. In addition to the 38kA initial peak and the low amplitude continuing current, a middle component of about 1400 amps lasting for 80 milliseconds was employed. This was the same test arrangement employed in the hole burning experiments, all discharges were of positive polarity with the test metal as cathode.

52
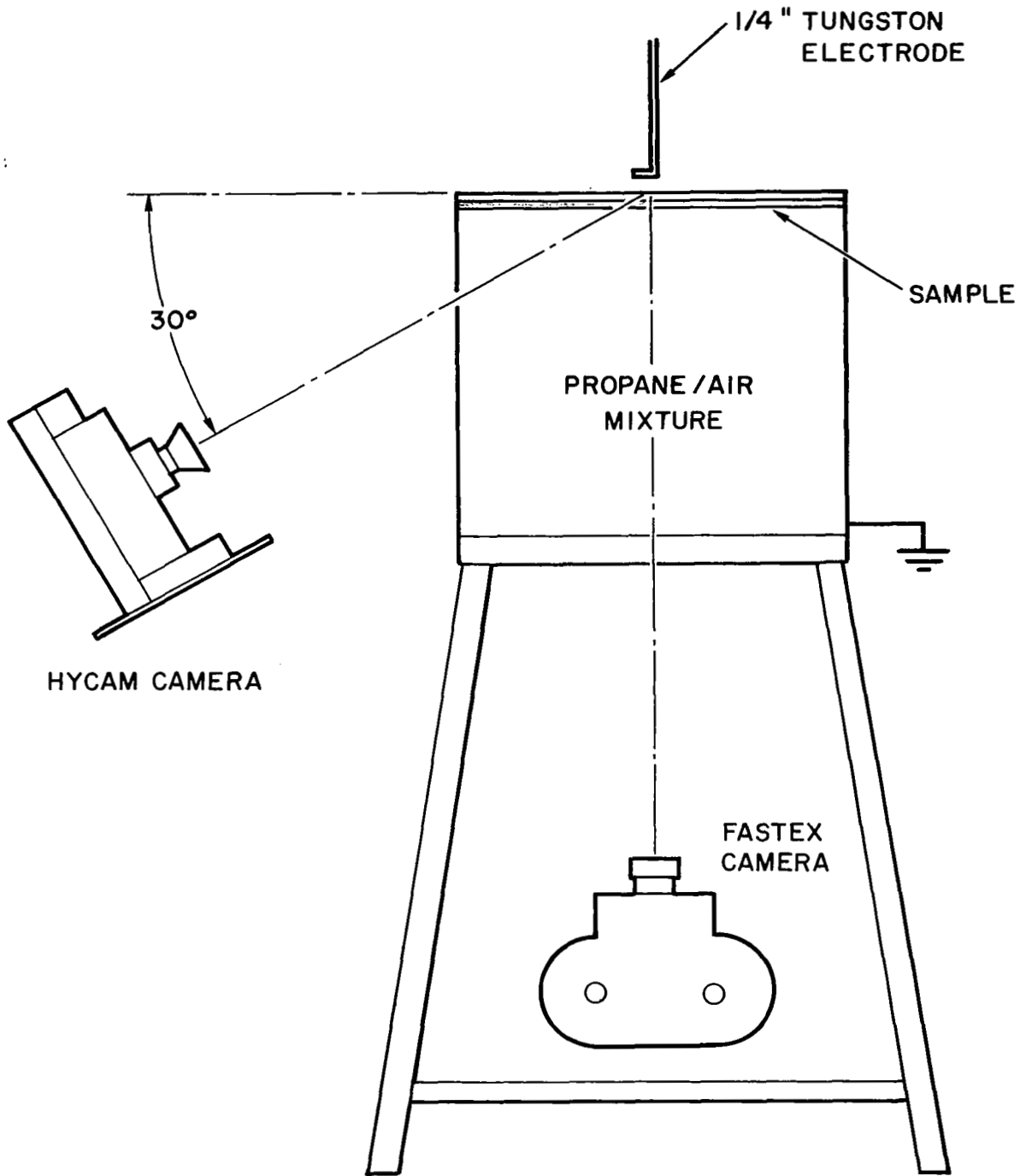
FIGURE 1.   Test Apparatus for lightning fuel ignition studies.
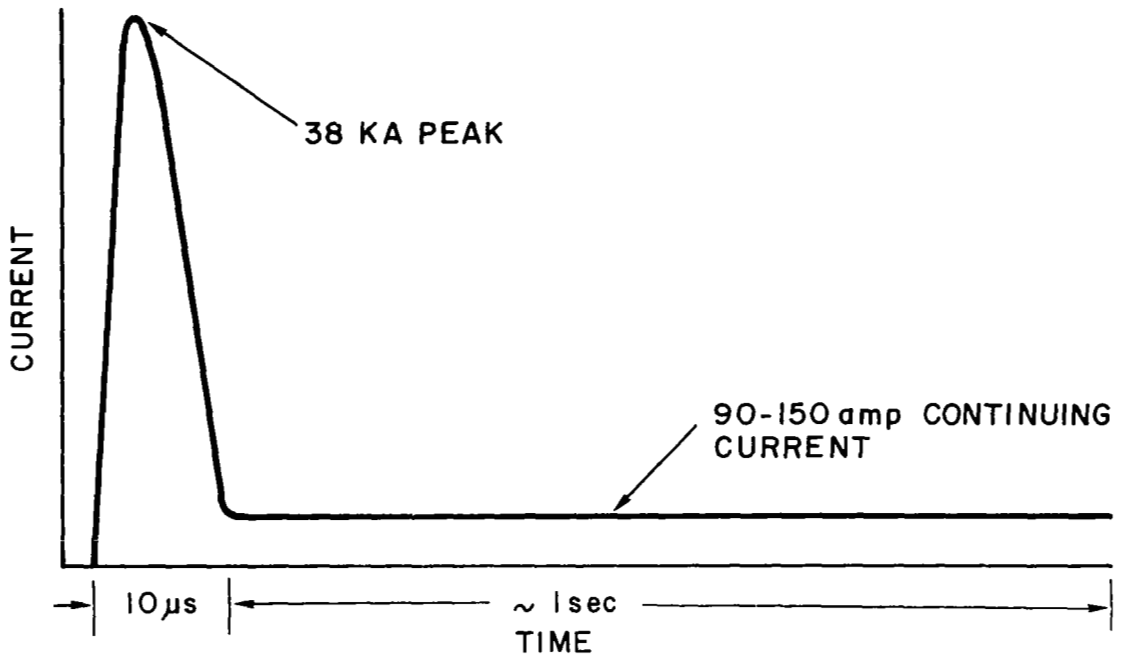
FIGURE 2a. Two Component Wave Shape
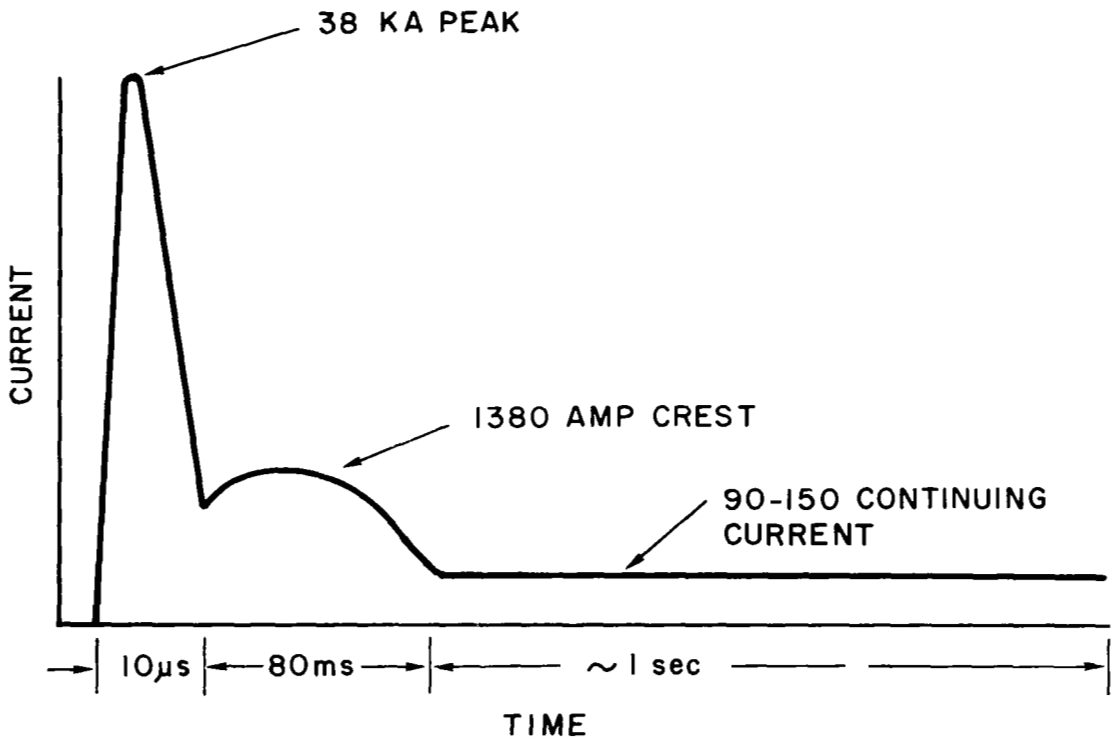
FIGURE 2b.   Three Component Wave Shape

FIGURE 2.   Typical Current-Time Relationship of Simulated Lightning
Discharges Employed.

The tests were conducted by selecting an amperage discharge level for the continuing current portion of the strike and then varying the coulomb content of the stroke by changing the time duration of the current flow. To relate charge transfer to ignition, each time the metal skin was struck the time duration of the current flow was increased until ignition occurred. On aluminum and copper a hole was required before ignition was achieved. On titanium and stainless steel, it was possible to ignite the mixture without burning a hole. In the case of these metals, the duration of current flow was increased until a hole was burned in the metal sample. The ignition times and the ignition mechanisms were compared under these circumstances i.e., by hole burning, with the mechanisms and delay in the presence of a hot spot only.

For aluminum a current level of approximately 90 amperes was employed. For titanium and stainless steel, a current of 130 to 140 amperes was used. For a combustible mixture propane and air in a ratio that was 1.5 times stoichiometric was employed. This ratio is generally considered to have the lowest ignition temperature. To test this, a few tests were also run at 0.75 and 2.25 stoichiometric.

In addition to the photographic coverage, instrumentation consisted of a temperature sensitive paint applied to the undersurface of the skin. By this means it was possible to record peak temperatures for radial distances away from the strike zone.

Test Results

Titanium.- The results of the tests on 20 mil titanium showed that a two-component discharge such as shown in Figure 2a with a charge content of 5.5 coulombs transferred by an average current of 90 amperes for a period of 61 milliseconds is sufficient to cause ignition of the fuel-air mixture 1.5 times stoichiometric. At this level no hole is produced; the ignition resulted from a hot spot only. The hot spot formed is very small and appears as only a discolored circular area about 1 to 2 mm in diameter on the underside of the strike zone. The results of all tests are listed in Table IV (Appendix). In addition, Figure 3 shows a series of three photographs of a 100 coulomb lightning strike to 20 mil titanium.

Tests performed in the same manner upon 40 mil thicknesses of titanium also resulted in ignition occurring at charge transfers as low as 5.75 coulombs. The waveform of such a discharge is shown in Figure 4. This charge was transferred by an average current of 93 amperes for 63 milliseconds. Other tests made at this and greater amounts of charge transfer resulted in ignition. It is very interesting to note that 20 and 40 mil thicknesses of titanium both require the same amount of charge transfer to cause ignition.

The results of the tests on 60 mil thicknesses of titanium did not follow the same pattern of low coulomb ignition threshold levels associated with the 20 and 40 mil thicknesses. These tests showed that for charges transferred at a rate of about 115 amperes for a period of .95 seconds a total
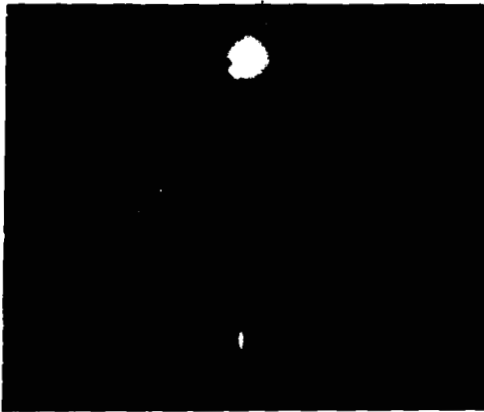
FILM AT BURN THROUGH−40 MILLI−SECONDS AFTER START OF DISCHARGE

FILM 43 MILLISECONDS AFTER START OF DISCHARGE
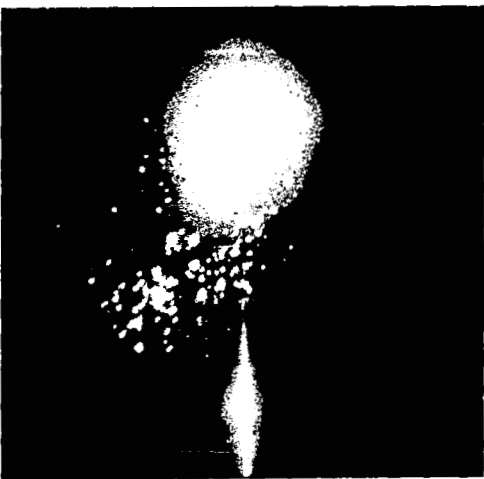
FILM 50 MILLISECONDS AFTER START OF DISCHARGE

FIGURE 3. High Speed Photography (3500 frames/second) of a 100 coulomb lightning discharge to 20 mil titanium sheet. Camera is viewing the underside of sheet at burnthrough. Ignition of fuel vapor present can not be readily seen in these films.

of 107 coulombs of charge was necessary to cause ignition. It is not understood why the 60 mil sample requires a much greater coulomb content for fuel ignition than the 20 and 40 mil samples. It is recommended that a 50 mil sample be tested to help clarify this question.

Figure 5 shows the metal discoloration on the underside of the test metal resulting from the transfer of 125 coulombs for 60 mil titanium. A summary of the coulomb ignition thresholds for a 1.5 stoichiometric propane-air mixture is given in Table I for all materials studied.

TABLE I

COULOMB IGNITION THRESHOLDS FOR 1.5 STOICHIOMETRIC PROPANE-AIR MIXTURE

Material Thickness	Titanium (Ti-8Al-1MO-IV)	Aluminum (2024T-3)	Stainless Steel (Series 304)
	Coulombs	Coulombs	Coulombs
0.020"	5.5	not determined	4.4
0.040"	5.75	20	12
0.060"	100/125	46	41

All thicknesses of titanium sheet tested ignited fuel vapor by a hot spot; a hole was not required. Titanium, with its high electrical resistivity (Table II) generates a larger amount of heat than materials such as aluminum. Also, the heat generated is contained in the strike region for a relatively long time due to its low thermal conductivity. As a result a high temperature region exists in the vicinity of the lightning strike for a much longer period of time than for aluminum.

Knowledge of the time of fuel ignition after the initiation of the lightning stroke (Table III) is important to establish the ingition mechanism. Thicknesses of 20 and 40 mil titanium displayed ignition times of about 44 and 72 milliseconds respectively at electrical discharges of the order of the coulomb ignition threshold. The mechanism of fuel ignition by hot spots is most likely the transfer of heat from the hot undersurface to the gas by conduction. When a sufficient amount of the gas has the required amount of thermal energy, ignition occurs.

Some tests were conducted on 20 mil titanium with a three-component discharge wave at levels much greater than the threshold, as shown in Figure 2b. It was found that ignition occurred in the 2nd component at a current of 1350 amps and a time of 5 milliseconds. At ignition, about 6.5 coulombs had been transferred to the metal which is in agreement with the threshold figure. Ignition occurred before burnthrough about 40 milliseconds later. This demonstrates that even with high current strikes, such as those found in nature, fuel ignition occurs following a fixed coulomb transfer which is very near the threshold region. This demonstrates the hazard that exists from fuel vapor ignition by a surface hot spot.

TABLE II

TABLE OF PHYSICAL PROPERTIES

	Melting Point °F	Thermal Conductivity BTU/ft² Sec °F/in	Resistivity Microhm-cm	Specific Heat BTU/lb/°F	Heat of Fusion BTU/lb	Density lbs/in³
Aluminum - 1100-0	1200	1540	3	0.24	169	0.100
- 2024-T-3	950	840			167	0.098
Stainless Steel						
-304	2550	105	70	0.12	108	0.286
Titanium -100-A	3200	112	60	0.135	137	0.164
- Ti-6Al-4V	3000	52	170	0.13		
- Ti-8Al-1M-1V	3000	50	200	0.13		
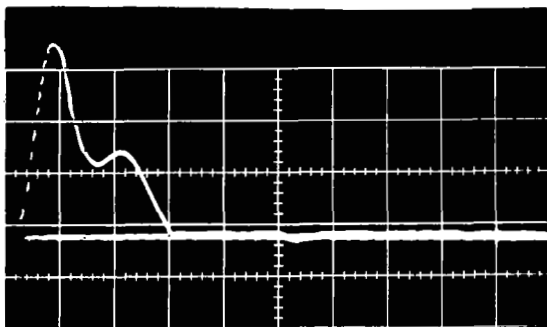
Continuing current
Major divisions are 46 amps and 20 msec.
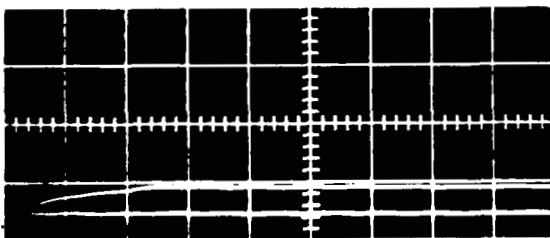
Integral of continuing current
Major divisions are 11.5 coulombs and 20 msec.

FIGURE 4.   Oscillograms of 5.75 coulomb continuing current
             discharge applied to .040 inch titanium (TI-8AL-
             1MO-1V) resulting in formation of a small hot
             spot and ignition of fuel-air mixture.
             (test no. 235)
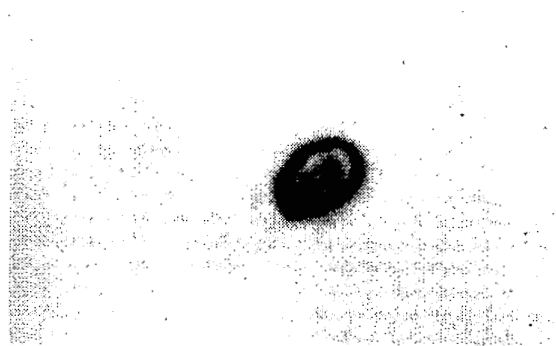
FIGURE 5.   Metal discoloration resulting from hot spot
             formation on under side of 60 mil thickness of
             titanium resulting from a 125 coulomb charge
             transfer to the top side. Hot spot was
             sufficient to cause ignition of fuel vapor.
             Hot spot is shown full scale.

TABLE III

DISCHARGE AND IGNITION TIMES AT COULOMB IGNITION THRESHOLD REGION

Thick-ness	Titanium			Aluminum			Stainless Steel		
	Cou-lomb	Discharge Time (ms)	Ign. Time (ms)	Cou-lomb	Dis. Time (ms)	Ign. Time (ms)	Cou-lomb	Dis. Time (ms)	Ign. Time (ms)
0.020"	6	56	44				4.4	48	125
							*8.0	55	105
0.040"	8	62	72	22	130	130			
				*37	300	100			
0.060"	107	950	900						

* Above threshold level.

Photographic evidence was obtained of the burnthrough for some of these tests conducted at very high coulomb levels. It was found that molten titanium particles from the burnthrough are blown into the tank at high velocities. The high speed photography indicates these particles travel at a speed of about 200 feet/second measured at a distance of one inch below the surface. It was also observed that these particles ignite the fuel vapor as they travel through the container. The particles are travelling much faster than the flame front which is probably burning at about 10 feet/second. In this case the particles act as a match, lighting the gas through which they are passing.

Aluminum.- Tests were made upon 40 and 60 mil aluminum in the same manner as those made upon titanium. The tests upon 40 mil thicknesses of aluminum were all made at identical rates of charge transfer of about 125 amperes. Here, the time duration was gradually increased until ignition occurred. It was found that 20 coulombs were necessary to cause ignition of the fuel-air mixture for the 40 mil sample. For the 60 mil thickness of aluminum, a minimum of 46 coulombs of charge must be transferred to cause ignition. This transfer required current flow for an average of 0.35 seconds. A hole was always formed simultaneously with ignition for the aluminum tests.

One of two mechanisms can cause ignition with hole formation:

1. Molten aluminum metal blown into the interior of the fuel tank is responsible for fuel ignition.

2. The plasma directly is responsible for fuel ignition.

Both of these mechanisms require the occurrence of a hole for ignition Molten aluminum from the hole blown into the combustible mixture would be capable of igniting the propane/air since the spontaneous ignition temperature of propane is 920°F and the temperature of molten aluminum alloy is at least 950°F. Ignition at this temperature however would have a delay time on the order of minutes. As can be seen from Table II, there is essentially no ignition delay (discharge time-ignition time = 0). Therefore the mechanism described in Item 1 above does not seem reasonable.

Ignition by the second mechanism, the plasma directly, has much more merit. It would be expected that this ignition mechanism would have very little or no delay time as in the case observed here.

Stainless steel.- Tests upon 20 mil stainless steel were made at a continuing current of between 80 and 100 amperes at durations of 50 milliseconds. Ignition resulted after 4.4 coulombs of charge had been transferred. No holes were formed at the point of lightning strike and only a small discolored area on the underside of the sheet was observed.

The 40 mil thickness was tested with an average continuing current amplitude of 140 amperes with varying amounts of time duration. Twelve coulombs were sufficient to cause ignition to occur. The 12 coulomb test resulted in no hole being formed, and only a discolored area on the underside was found, similar to the 20 mil tests.

Similar tests on 60 mil thicknesses of stainless steel at the same current amplitudes showed that the ignition threshold is 41 coulombs. For these threshold tests, no holes were found to be present when ignition occurred.

Ignition time measurements were conducted on the 20 mil stainless steel sample only. An ignition time of 125 milliseconds was measured at the coulomb ignition threshold. Since no holes were formed upon fuel ignition it is concluded that the ignition mechanism is the same as for titanium.

Copper.- A few control tests were performed on some 30 mil commercially pure copper sheets. As copper melts at 1900°F, it was of interest to check its ignition mechanism for this type of experiment. It was found that copper always formed a hole prior to fuel ignition. It is concluded that lightning strikes to copper will always burn a hole and ignition occurs by the plasma, as is the case for aluminum. It was found that 60 coulombs were required to burn a hole and ignite the fuel.

Fuel ignition times.- A plot of fuel ignition time vs. the amplitude of the continuing current is shown in Figure 6 for a number of tests. The experimental points are for 20 and 40 mil titanium. As thicknesses of 20 and 40 mil titanium show equivalent coulomb ignition thresholds, they are treated equally in this plot. In all cases the duration of the lightning strike was greater than the ignition delay time, except one test with 40 mil titanium. Therefore, the curve drawn does not include any weight from this point. As can be seen this point is a little above the curve.
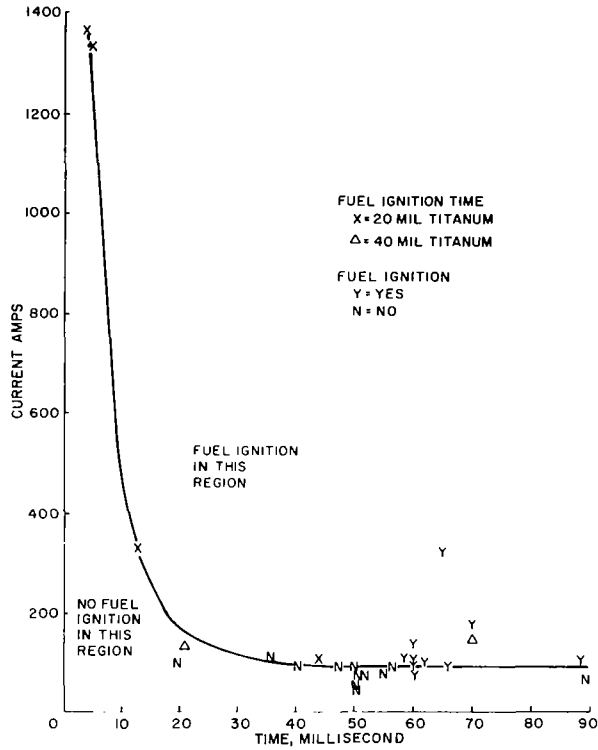
FIGURE 6. Fuel Ignition Time vs Continuing Current
Amplitude for 20 & 40 Mil Titanium. 1.5
Stoichiometric Propane/Air Mixture.
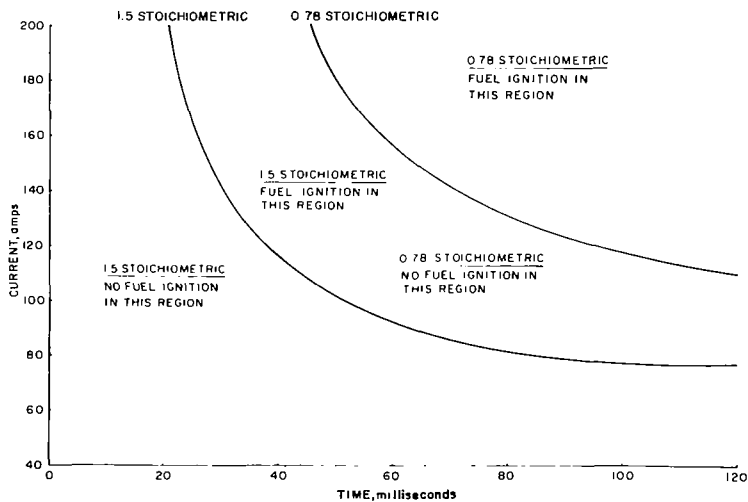
FIGURE 7. Coulomb Ignition Boundaries for Hot Spot
Ignition 20 & 40 Mil Titanium.

63

The plot shows the general trend that would be expected for this situation. At high current levels a short ignition time is noted. At low current levels very long times are indicated. This type of curve is of the form:

$$t(I-i) = c$$

where t = fuel ignition time

I = continuing current

i = a threshold current, below which ignition cannot occur

c = a constant in units of coulombs

The threshold current is the value, below which no ignition would occur no matter how long the current is applied. Stated another way, it is the ignition threshold at an infinitely long time. The constant (c) in the above equation is roughly equal to the coulomb ignition threshold for 20 and 40 mil titanium.

For tests made at the coulomb ignition threshold, the ignition times were similar to the arc duration time. Therefore, the region above the curve in Figure 6 represents conditions in which fuel vapor can be ignited prior to the end of the discharge. The region below is the safe region, in which no ignition occurs. The curve is the coulomb ignition boundary for 20 and 40 mil titanium. To check this curve with the data collected, all experimental points were plotted on the graph. An N indicates no ignition; a Y indicates ignition.

Figure 7 shows a portion of this smooth curve at 1.5 stoichiometric fuel/air. From the few tests done at 0.78 stoichiometric a second curve is shown above the other curve in this Figure. As can be seen, the coulomb ignition threshold is greater for 0.78 stoichiometric than for 1.5. As pointed out before, a fuel-air ratio of 1.5 stoichiometric is the most easily ignited; any other ratio will require greater energy.

Temperature of metal skin at time of fuel ignition.- As part of this work, a temperature profile was determined for the titanium samples at the time of fuel ignition. To determine the temperature, a test series was conducted in which the temperature of the metal was determined as a function of the radial distance from the center of the strike. To do this, a series of "Temp-i-laq" coatings were applied to the undersurface of the material. These coatings show a characteristic phase or color change at a specified temperature. The temperature radial distribution was determined at the coulomb ignition threshold for 20 mil and 40 mil titanium. This was, in both cases, 5-6 coulombs. Figure 8 shows this experimental relationship. In addition, a minimum ignition temperature for ignition by a hot spot was established by this technique. For these tests, copper sheets were also tested. These tests employed propane/air at 1.5 times stoichiometric.

64
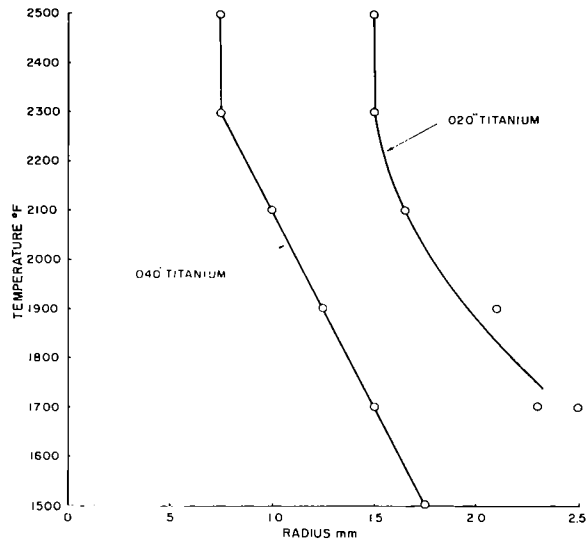
FIGURE 8. Radial Variation of Skin Temperature
About Point of Lightning Strike.

As it was found that aluminum (M.P. 1200°F) and copper (M.P. 1900°F) both require a hole for ignition, the minimum ignition temperature by a hot spot must be above 1900°F. It was found that stainless steel, which melts at 2500°F, ignites fuel by a hot spot. Therefore, this is the upper temperature boundary. From the "Temp-i-laq" measurements, it is observed that the temperature of the underside of the material is between 2300°F and 2500°F. Therefore, the hot spot ignition temperature for a propane/air mixture when struck by a lightning discharge is

$$2400°F \pm 100°F.$$

It is also noted that this ignition temperature is probably dependent upon the size of the hot zone exposed to the gas.

Mechanism of Energy Transfer Through the Metal Skin

The knowledge of how energy (heat) is transferred through the metal skin is important to the proper selection of ways to reduce and eliminate hot spot fuel ignition. To clarify this question, a mathematical analysis was conducted on this problem. The objective was to predict the maximum temperature reached by the skin during a typical, but well-defined lightning strike, and secondly, predict the temperature distribution radially in the skin.

Problem.- Temperature distribution for an infinitely large plane metal sheet during a typical lightning strike was investigated. It was assumed that the ratio $k/\rho c_p$ and $\overline{R}$ are constants where k, c_p, o, and $\overline{R}$ are respectively the thermal conductivity, specific heat, density, and resistivity of the metal. A bolt radius $\overline{r}$ is introduced in order to remove the mathematical singularity at the point where lightning strikes the metal sheet. The governing equation for the temperature distribution reads as follows:

$$\rho c_p \frac{dT}{dt} - k \nabla^2 T = Q(x, y, t) \tag{1}$$

where $Q(x, y, t)$ is the power generated by electrical resistance. Here x and y are the cartesian coordinates in the plane of specimen, and t is time. Using Ohms Law, the power generated can be written as

$$Q(x, y, t) = I^2(x, y, t)\overline{R}. \tag{2}$$

Denoting $I_0(t)$ as the current intensity generated by the lightning strike,

$$I(x, y, t) = I(r, t) = I_0(t) \qquad \text{for } r < \overline{r}$$

$$= \frac{\overline{r}}{r} I_0(t) \qquad \text{for } r > \overline{r}$$

where $\qquad r = (x^2 + y^2) \qquad$ and $\tag{3}$

$$\nabla^2 = \frac{\partial^2}{\partial x^2} + \frac{\partial^2}{\partial y^2}$$

To evaluate the maximum temperature reached, equations (1) and (2) are rearranged and evaluated in a Greens function. The Greens function, expressing temperature in terms of a triple integral, is then integrated over time, radial distance and a geometry factor. The details of the integration over time, radial distance and a geometry factor are not included here, as they are quite lengthy, but a final solution for the special case r = 0 is shown below.

Maximum temperature of metal skin at r = 0.- The Greens function can now be evaluated for r = 0, the maximum temperature at the center of the lightning strike, for a thin titanium metal skin. For this particular case, the equation becomes much more simple and many terms in the integrated expansion are found to be very small or zero. Thus,

$$T(r = 0, t = \overline{t}) = T_O + \frac{R I^2 \overline{t}}{\pi^2 \overline{r} \rho c_p}$$

is the equation to be evaluated, where

$\overline{R}$	=	resistivity of metal	=	3.20×10^{-4} Ω- m
I	=	current through arc	=	90 amps
$\overline{t}$	=	duration of lightning strike	=	0.061 sec
$\overline{r}$	=	bolt radius	=	1.1×10^{-3} m
c_p	=	heat capacity of metal	=	6.63×10^2 Joules/K_g - ^{O}C
ρ	=	density of metal	=	$4.50 \times 10^3 K_g/m^3$
T_O	=	metal temperature before strike	=	25^OC

These are the experimental conditions for an ignition threshold lightning strike in 20 mil titanium. When evaluated for these conditions a maximum temperature reached during the lightning strike is obtained.

$$T_{max} = 1700^O C$$

$$or = 3100^O F$$

From Table II, it can be seen that fuel ignition for 20 mil titanium occurred at 44 milliseconds with a strike duration of 56 milliseconds. The ignition temperature can be computed as follows:

$$T_{ignition} = 3100(\frac{44}{56})$$

$$= 2450^O F.$$

This result is in line with our experimental value of $2400 \pm 100^O F$.

It is important to state that $\bar{r}$, the bolt radius, was the measured value on a number of materials. What was measured was the radius of a region showing strong color change and material deformity. Whether or not this is the best value to use for the bolt radius is subject to question. This point is raised because the bolt radius comes in as $\bar{r}^4$, so any uncertainty in $\bar{r}$ will be much more uncertain as $\bar{r}^4$. Therefore, the result should be expressed as

$$T_{max} = 2450 \pm 300^{\circ}F$$

due to the uncertainty in $\bar{r}$.

Temperature distribution in skin.- It was desired to calculate the temperature distribution radially from the point of strike as an additional means of suggesting ways of reducing the hazard of hot spot fuel ignition. Ideally, this would correlate closely with the experimentally determined curve for 20 and 40 mil titanium (Figure 8). This solution would require integration of the Green's function over the appropriate variables. The most straight-forward way to do this is by computer. Unfortunately, this was not done in this contract. A correlation of this type would lend much more confidence to this model and its ability to predict other temperatures, such as that obtained with a composite or a material with an ablative on it. Use of this type of model to predict the ignition hazard can greatly reduce the number of lightning experiments required to establish the temperature distribution. The computer problem was not completed due to a contractual redirection in the technical scope of the program.

Conclusions

In summary, the following conclusions are drawn:

1) Fuel ignition by "hot spots" from lightning strike is possible with all titanium and stainless steel alloys studied.

2) Aluminum always burned a hole in conjunction with fuel ignition.

3) Very low charge transfers (5-6 coulombs) can ignite fuel vapor through 20 and 40 mil titanium; the 60 mil sample was twenty times more resistant (100 coulombs).

4) The ignition times were on the order of a few milliseconds for a a typical lightning discharge to 20 and 40 mil titanium.

The reasons for the apparent inconsistency in the results from the test upon 20, 40, and 60 mil thicknesses of titanium are not clear. Additional testing upon 50 mil titanium in conjunction with additional work on the mathematical model should help in answering this question.

Complete results of all ignition tests are presented in Table IV in the Appendix.

References

1. Robb, J. D., E. L. Hill, M. M. Newman, and J. R. Stahmann, "Lightning Hazards to Aircraft Fuel Tanks," NACA TN 4326 (1958).

2. Schmidt, H. A., N. S. Kovar, D. E. Stogryn, M. Gerstein, "The Study of a Facility to Investigate the Effect of Natural Electrical Phenomena on Aircraft and Spacecraft," Prepared under Contract No. NASW-853, (1964).

IGNITION AND FLAME PROPAGATION IN AIRCRAFT FUEL VENT SYSTEMS

Introduction

Approximately three months before the end of the contract work, Dynamic Science and General Electric were requested, by the aircraft industry, to conduct a series of tests on a simulated S-tube and surge tank assembly similar to that found on the 707 jet transport.

It has been recognized for a number of years that lightning can ignite fuel vapors at the vent exit and that the flame can then propagate through the vent lines to the tanks, causing destructive fires and explosions (1). There has been continuing work on this problem to develop protective techniques that will prevent a flame from reaching the fuel tanks. This has involved inerting systems, techniques for flame suppression, and the use of flame arrestors. The success of these systems depends, to a large extent, on the characteristics of the flame and the environment in the vent system at the time ignition occurs. The experimental investigation was designed to determine maximum flame speeds that might be encountered following a lightning-induced ignition and to test the effectiveness of a prototype flame arrestor developed by NASA engineers at the Lewis Research Laboratories.

Lightning strikes are characterized by one or more high amplitude, short duration spikes, separated by periods of long duration, low amplitude continuing current flow. The initial high current discharges, often as high as 50 kA or 100 kA, produce an intense blast pressure which tends to accelerate the rate of flame propagation following ignition. Some experimenters have reported flame speeds approaching 1000 feet per second following lightning-induced ignition (2). Obviously, flame speeds of this magnitude would require different means of control than would the relatively slow laminar or turbulent flames which normally propagate at speeds of 10 to 20 feet per second.

The purpose of these tests was to determine whether flame speeds approaching shock wave velocities occurred in the vent system following lightning ignition and, if so, could their passage be stopped or materially slowed by the presence of a flame arrestor. In the pursuit of these objectives, the following investigations were conducted:

1. Determine the effect of simulated lightning wave shapes, current amplitudes, and location of discharge on the propagation velocity in the vent system.

2. Determine the feasibility of employing a flame arrestor or flame retarder in the vent system as a means of slowing the passage of the flame.

3. Determine modifications to the vent outlet and S-tube geometry that would reduce flame propagation velocity.

Test Equipment

The simulated fuel vent system used in this program is shown in a photograph in Figure 1. It consisted of a simulated vent outlet and short section of 5.5" diameter S-tube leading to a surge tank.

The vent outlet was rectangular in shape, measuring 2" x 8" and was connected to a 5.5" diameter S-tube at a right angle. The S-tube was 42" in length as measured along the center line. It was bent 45°, 24" from the vent end and then 90° as it came out of the surge tank. The surge tank, cylindrical in shape, had an inside diameter of 15-1/2" and an inside depth of 8-5/8". The top of the surge tank was bolted to the chamber and sealed with a neoprene gasket.

A 2" diameter tube was welded on the periphery of the tank wall near the bottom of the tank to serve as a mixing chamber for the introduction of combustible mixtures of propane and air.

A propane-air supply system was attached to this mixing chamber. Control of the fuel-air ratio and the flow of the combustible mixture through the system was accomplished by means of pressure regulation, flow meters and solenoid valves. Commercial grade propane (93.49% propane, 0.212% methane, 4.00% ethane, 1.90% isobutane, and 0.26% n-butane) and dry air were employed in these tests. The fuel-air ratio was fixed at 1.1 stoichiometric (4.2% by volume) for most of the tests. The flow rate of the combustible mixture was maintained at approximately 4.0 cubic feet/minute, which produced a laminar flow in the S-tube at a Reynolds number of about 1200.

The flame arrestor, when employed, was mounted in the surge tank. The arrestor diameter was the same as the inside of the surge tank and it was 2" thick. When installed, its upper surface was approximately 1" below the top of the surge tank. Over the center of the flame arrestor, beneath the opening where the S-tube entered the surge tank, a 12" diameter plate shielded the arrestor from the direct impingement of a fast-moving flame. The plate served to deflect the flame radially outward toward the periphery of the surge tank. A photograph of the arrestor, with the plate removed, is shown in Figure 2.

The arrestor itself was constructed from corrugated stainless steel pressed against a flat backing plate and wrapped in a tight coil around a framework resembling a reel for a movie film. The corrugation approximated a sine wave and, when placed against a flat plate, created openings with a diameter of .050". A detail of this is shown in Figure 3.

For later tests, an area of 17.7 sq. inches was cut away from the lower wall of the surge tank, below the arrestor tank, to provide venting in front of the flame. This blow-out area, present for configurations D and E, was covered with saran wrap prior to each test.
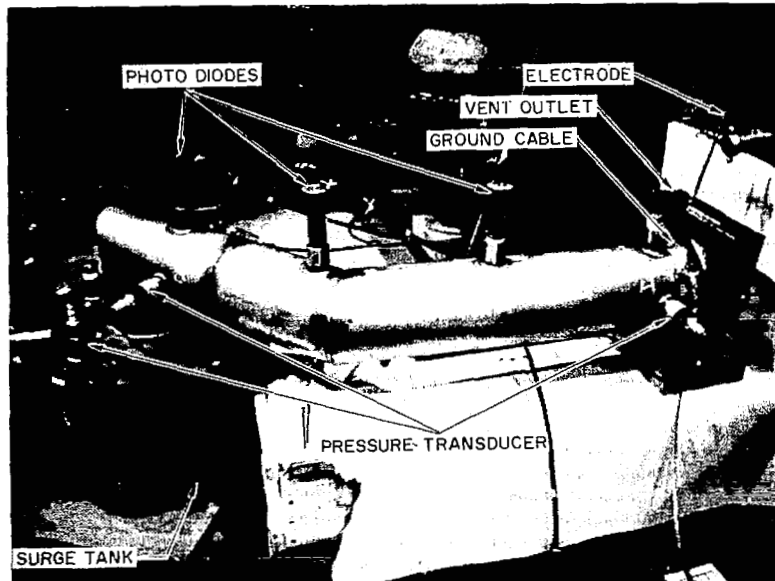
FIGURE 1. Photograph of Vent Test System.

FIGURE 2. Arrestor in Surge Tank.

Material:- Stainless Steel
Corrugation Shape:- Approx. Sine Wave
Depth of Arrestor:- 2 Inches
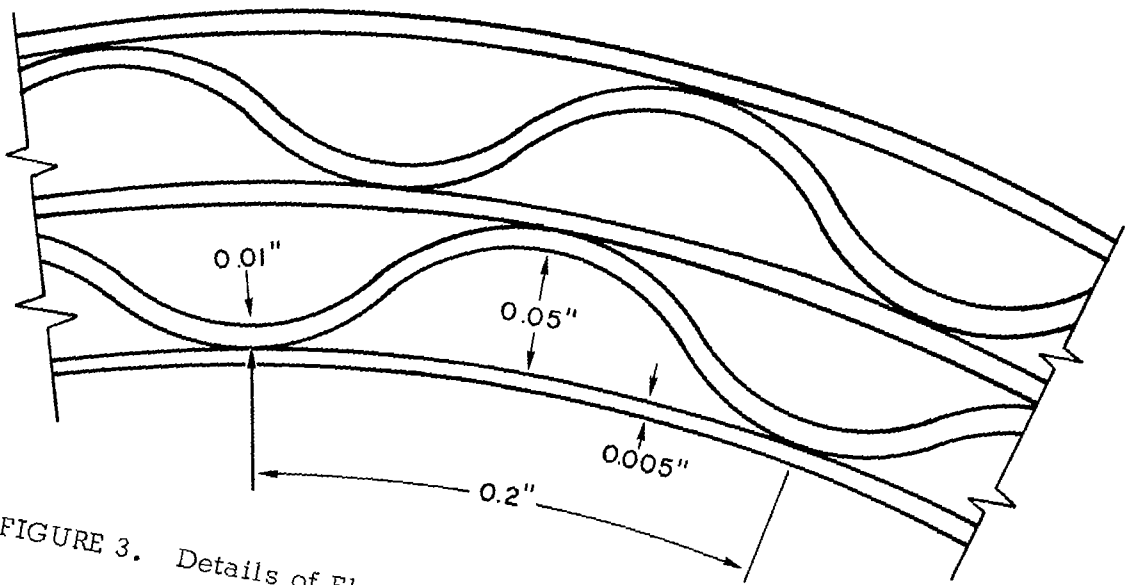
FIGURE 3. Details of Flame Arrestor for Simulated 707 Aircraft Surge Tank.

Instrumentation was required to measure the velocity of the flame as it travelled down the S-tube into the surge tank. It was also important to know if the arrestor stopped the flame or if the flame penetrated the arrestor and entered the surge tank below. Additional data of interest was the pressure pulse transmitted by the lightning blast to the surge tank and the existence of a shock wave in the S-tube following the discharge.

Interest in the shock wave stemmed from previous reports of flame speeds approaching the speed of sound. If such a speed were measured, it would be interesting to relate this to a shock wave, if one were present.

The General Electric High Voltage Laboratory was responsible for the selection and calibration of this instrumentation. Photodiodes were chosen over ionization probes because of their low-impedance, fast response and adequate sensitivity. The diodes were mounted in an insulating material which isolated them from the surrounding metal. The diodes were connected to oscilloscopes and a multi-channel recorder (Honeywell Visicorder) by individual shielded cables which were passed through a shielded conduit. Both cable shields and conduit were grounded outside the test area at the recording equipment. No grounds were made at the transducer end to prevent induced voltages from occurring in the instrumentation circuits as a result of transient ground currents arising from the simulated lightning discharges. The use of a multi-channel recorder permitted all traces to be monitored on one piece of paper. A sample of data is shown in Figure 9.

In addition to the photodiodes, the pressure was monitored at four points in the system as shown in Figure 4. These were the vent exit (A), in the S-tube just outside the surge tank (B), in the surge tank above the arrestor (C), and in the surge tank below the arrestor (D). Pressure sensitive piezo-electric transducers were assembled from lead titanate-lead zirconate ceramic crystals and mounted in insulated housings. The output from these pressure transducers was also placed on the multi-channel recorder.

The location of the instrumentation is shown in Figure 4. For flame speed measurements, six photodiodes were employed, mounted in pipe fittings along the S-tube and above and below the flame arrestor.

Table I below lists the instrument stations referred to in Figure 4, giving the distances between them and the vent outlet.

TABLE I

Segment	Station Distances in Feet	
	Increment	Total
0 – 1,A	0.333	0.333
1 – 2	0.907	1.240
2 – 3	0.886	2.126
3 – 4,B	0.917	3.043
4,B-5,C	1.188	4.231
5,C-6,D	0.375	4.606

Photo Diode Stations

Vent Outlet

Vent

1

2

A

90° Bend

4

3

S-Tube

Gasket

5

B

C

45° Bend

Pressure Transducer Stations

Flame Arrester (When Installed)

Surge Tank

12" Dia. Metal Plate
Installed With Arrester Only

6, D – Photodiode and Pressure Transducer Station
(Below Arrester Location)

Blowout Area
(Configurations D and E Only)

Fuel & Air Entrance
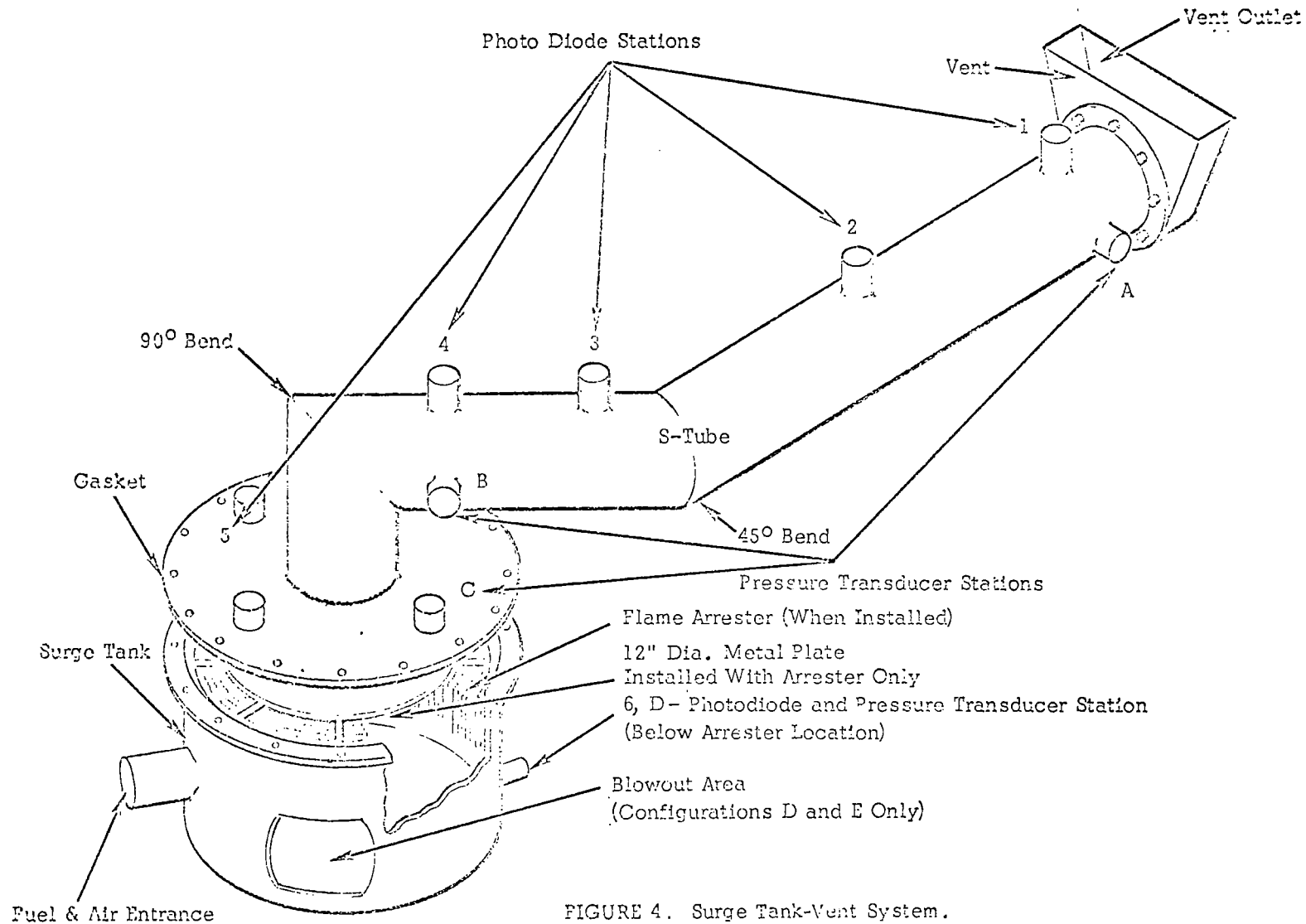
FIGURE 4. Surge Tank-Vent System.

Section 0 was at the center of the vent exit opposite the end of the S-tube. All segments except segment 4,B-5,C were straight line distances measured from center line to center line of the appropriate photodiodes. The length of segment 4-5 was determined by pulling a string tight between the station 4 and 5 pipe fittings and measuring the length thereof.

Test Configurations

A total of five distinct vent system configurations were tested. In tabulating the results of this test program, reference is made to the vent configuration. To permit a proper evaluation of these results, the different configurations are described below:

Configuration A - Flame arrestor installed; no blowout hole cut in surge tank.

Configuration B - Flame arrestor removed; no blowout hole cut in surge tank.

Configuration C - Flame arrestor installed; top of surge tank elevated 1.5" and sealed to surge tank with masking tape.

Configuration D - Flame arrestor installed, 17.7 sq. inch blowout hole cut in surge tank below arrestor and covered with saran wrap prior to each test.

Configuration E - Flame arrestor removed; 17.7 sq. inch blowout hole cut in surge tank below arrestor and covered with saran wrap prior to each test.

Lightning Simulation

The simulated lightning discharges were limited to the high amplitude short-duration current spikes which are characteristic of lightning strokes and which have been found to create the blast pressures believed to produce the high flame speeds in the vent line. No low-amplitude continuing currents were applied for this series of tests.

The General Electric high current generator was used for these tests. Both damped and oscillatory wave shapes were employed with amplitudes ranging from 38 to 195 kA (3). The rate of current rise ($di/_{dt}$) was varied between 8 and 25 kA/microsecond, depending on the wave shape employed. The high current generator was charged to a voltage ranging between 80 kV and 100 kV. Wave shapes typical of those employed in these tests are shown in Figures 5 and 6. Additional waveshape variations are shown in the Appendix, Figures 1, 2, and 3. All discharges were of positive polarity, with the vent system as cathode.

A photograph of the test apparatus in place at the General Electric High Voltage Laboratory with a tungston electrode positioned near the lip of the vent outlet is shown in Figure 7. The output of the high current generator was discharged through this electrode to the vent system.

76
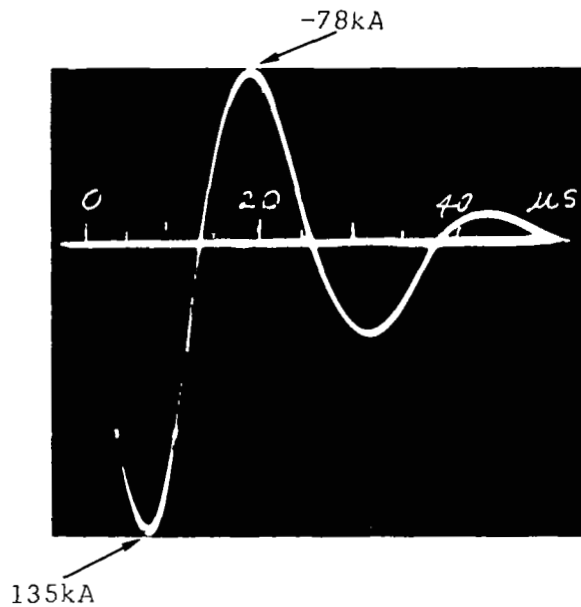
−78kA

135kA

Underdamped oscillatory wave. Crest
is 135kA in 8 μsec. Undershoot is
−78kA. Initial di/dt = 16.9kA/μsec.
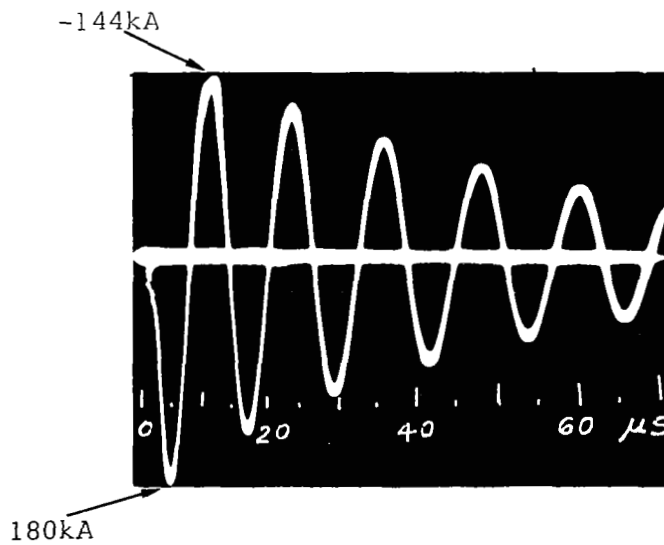
−144kA

180kA

Underdamped, highly oscillatory wave.
Crest is 180kA in 8 μsec. First undershoot
is −144kA. Initial di/dt = 22.5kA/μsec.

FIGURE 5. Typical Wave Shapes Employed
for Lightning-Flame Velocity Tests.
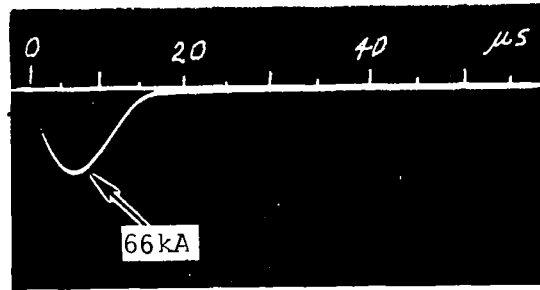
Overdamped (unidirectional) wave.
Crest is 66kA in 7.5 μ sec. Initial
$di/dt = 8.8$kA/μ sec.
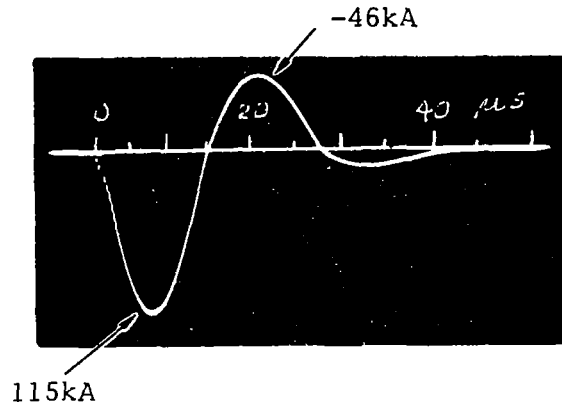
Underdamped, slightly oscillatory wave.
Crest is 115kA in 7 μsec. Undershoot is
-46kA. Initial $di/dt = 16.4$kA/μsec.

FIGURE 6. Typical Wave Shapes Employed for Lightning-Flame
Velocity Tests.

Electrode   Vent Outlet
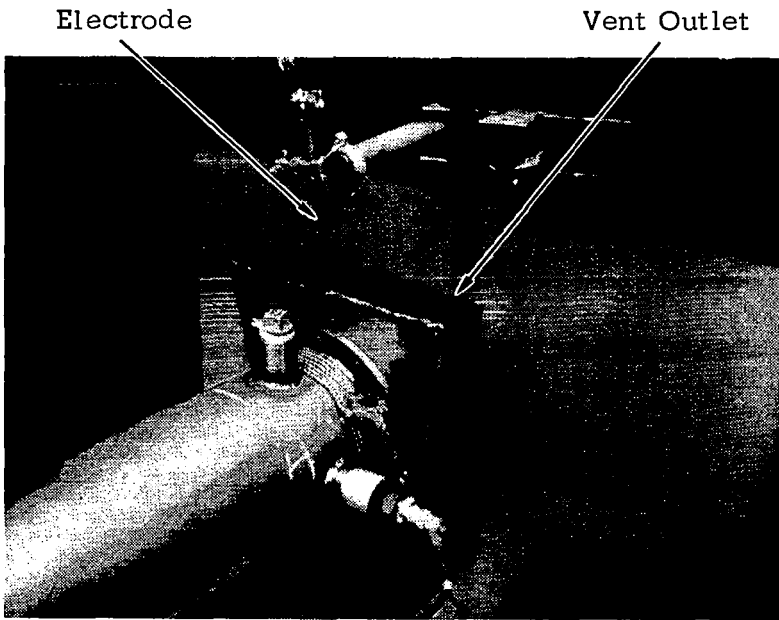
FIGURE 7. Electrode Positioned at Vent Outlet.

For some of the tests, the electrode was positioned at the vent outlet, Figure 8a. It was felt that this most-nearly approximated actual operating conditions. However, a large number of other tests were made with the tip of the electrode positioned well within the vent so that the arc occurred directly across the end of the S-tube, Figure 8b. The object in changing these electrode positions was an attempt to achieve a maximum flame velocity. The discharge current flowing from the electrode to the vent system was conducted away from the vent line through a copper braid wrapped around the neck of the vent line. This prevented current flow through the vent system which might interfere with the instrumentation.

Flame Velocity Calculations

The average velocity of the flame between diode stations was calculated by dividing the time it took for the flame to travel from one station to the other by the known distance between stations. Each photodiode had a restricted angle of view since it was mounted a considerable distance up a supporting tube, away from the center of the S-tube.

Figure 9 illustrates a typical recorder trace and the various photodiode outputs are shown. These have been marked to show the technique used for measuring the time lag between stations. In this case, it took 22 milliseconds for the flame to travel from station 1 to 6, a distance of 4.60'. From this data, an average flame velocity of 210 ft. per second can be calculated.

Test Results

The test objectives were twofold; first, to determine the maximum flame velocity that could be induced in the vent system by simulated lightning ignition. Once established, the second objective was to determine the ability of an arrestor to stop or retard this flame. The vent system as initially tested (Configuration A) had no hole cut in the surge tank. The search for a condition which would allow high flame speeds, along with the realization that an actual surge tank has some effective venting area, led to the testing of the additional system configurations. The configurations were tested in the order listed, beginning with Configuration A.

Configuration A.- The flame arrestor was installed for Configuration A. It was found that damped or underdamped, slightly oscillatory current discharges of 125 kA or more (Figure 6) caused flames to travel down the tube and penetrate the arrestor; while discharges of less than 125 kA amplitude caused flames which were stopped by the arrestor. For each case the maximum overall average velocity was 12 ft. per second. On tests run with this configuration, numbers 523 through 557, a maximum velocity of approximately 20 ft. per second was achieved in the S-tube. Observation of the flame profiles of some of these tests shows the presence of a secondary flame appearing, apparently after the original flame has completely died out, at stations 1 through 5 and possibly at 6. Further analysis indicates that these are actually two separate flames, travelling simultaneously away from a common point of origin near station 4. The speeds of these

Vent

S-Tube

A. Electrode Positioned
at Vent Outlet.

Electrode

Vent

S-Tube

B. Electrode Positioned
0.5" or 0.75" Above
Lower Lip of S-Tube,
Inside of Vent.
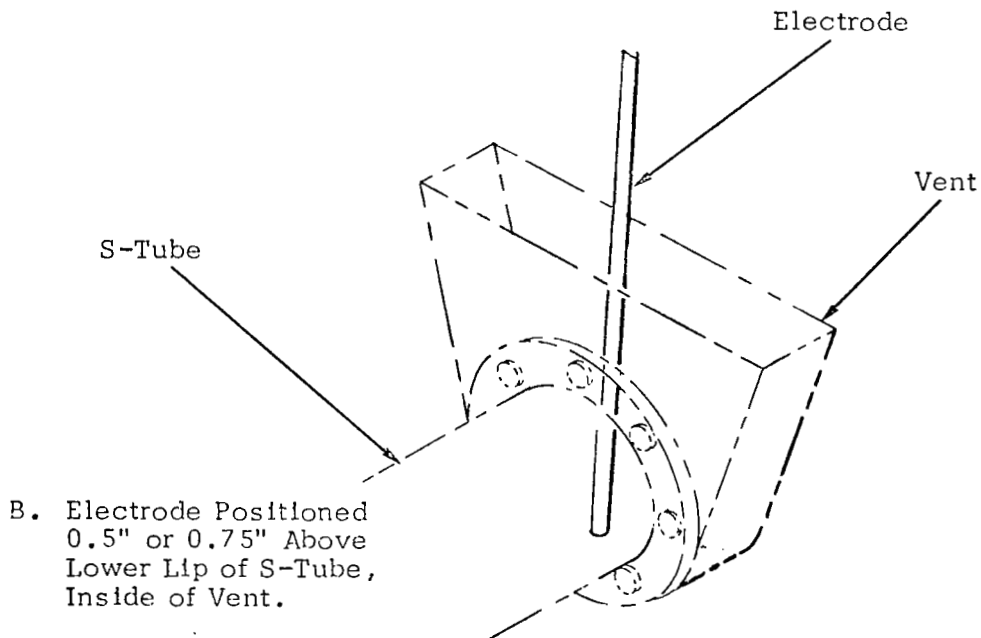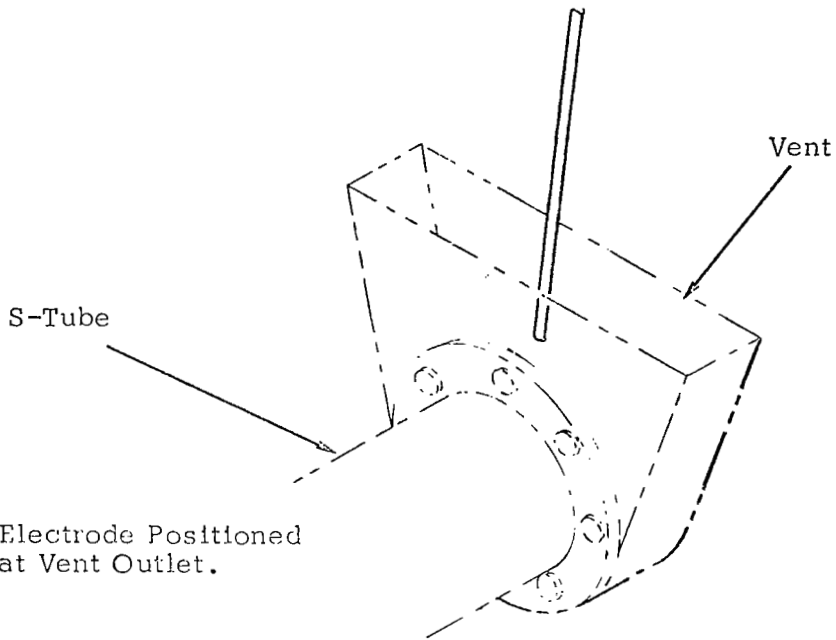
FIGURE 8. Electrode Arrangement at Vent Outlet.

81
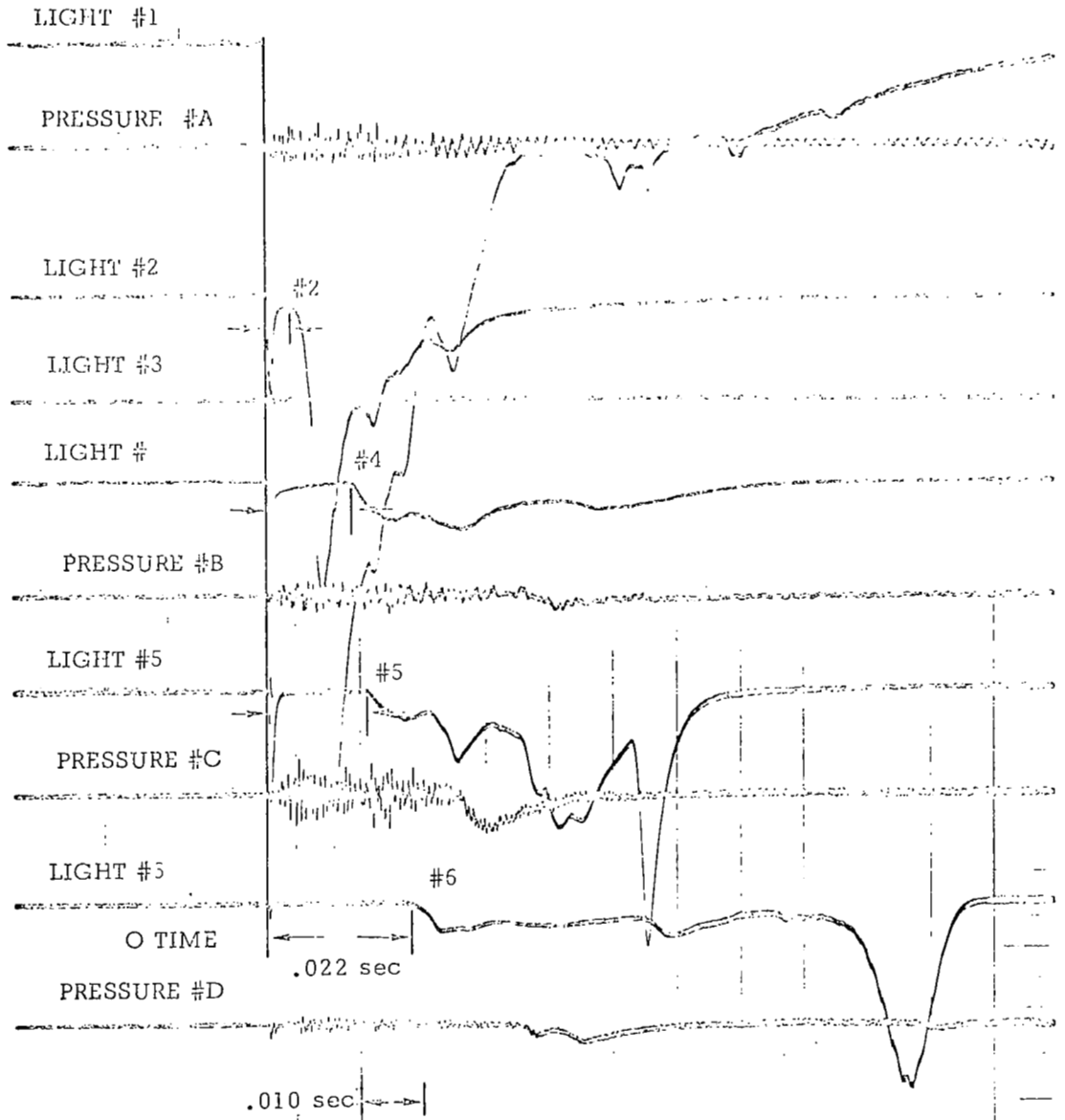
FIGURE 9 –   Visicorder traces showing output voltages of photodiodes and pressure transducers at stations 1 through 6. Configuration D, vent outlet 90% cloth taped. 100 kA, slightly oscillatory discharge from electrode positioned 0.75 in. above lower lip of S-tube, inside of vent. Overall average flame velocity 210 ft. per second (Test #590). Timing lines are at 10 msec. intervals.

flames were mostly between 100 and 400 ft. per second. During these tests, a second flame was observed "popping out" of the vent outlet a split second after the initiation of the first. An example of such a flame is shown in Figure 10. There were indications that a pressure buildup occurred in the surge tank which drove residual flames back up the vent line.

For the tests of this configuration, the best electrode position was a deep penetration of the vent outlet with the electrode directly in front of the 5-1/2" S-tube. This would be expected because by discharging the current in a more-or-less enclosed space, a higher pressure rise was obtained which tended to accelerate the flame.

Configuration B.- This configuration was achieved when the flame arrestor was removed from Configuration A. The results were identical with those tests using Configuration A in which the flames penetrated the arrestor.

Configuration C.- In an effort to determine conditions which would result in increased flame speeds, it was decided to elevate the top of the surge tank 1.5" above the tank, in order to provide a blowout area which would relieve pressure build-up in front of the flames. This blowout area was covered with masking tape prior to each test to prevent the fuel mixture being fed through the surge tank from escaping. The flame arrestor was installed. Using discharges similar to those employed in Configurations A and B, no changes were observed in average velocities (around 11 ft./sec.). The flames not only penetrated the arrestor, but blew the masking tape off. Similar tests were made with the vent outlet partially sealed with cloth tape shielding the discharge below the tape. These tests resulted in overall average velocities as high as 140 ft. per second. In this configuration, the ignition of the gas at the partially closed vent exit permitted the products of combustion to build up behind the advancing flame front producing a much higher propagation rate.

Configuration D.- This series of tests were run with a 17.7 sq. in. hole cut in the surge tank below the flame arrestor in order to simulate the openings provided by the secondary vent lines in an actual system. The electrode position was maintained inside the vent exit for most of these tests, (Figure 8b). Since previous studies of flame propagation have shown that the velocity of flame propagation in a duct is highly dependent on the magnitude of pressure buildup behind it which results from expanding combustion gases, a series of tests were run with 90% of the vent outlet taped shut. Velocities of up to 790 ft. per second were achieved between stations 4 and 5 using a slightly oscillatory wave with a peak current amplitude of 150 kA (tests 589-599). Average overall flame velocities (between stations 1 and 6) of up to 307 ft. per second, were obtained and the flames penetrated the arrestor. It was realized that sealing the vent outlet could not be considered a valid simulation of actual operating conditions and these tests were considered to be of academic interest only.

A more realistic simulation was obtained when the vent outlet was uncovered and the electrode tip was positioned at the center of the vent
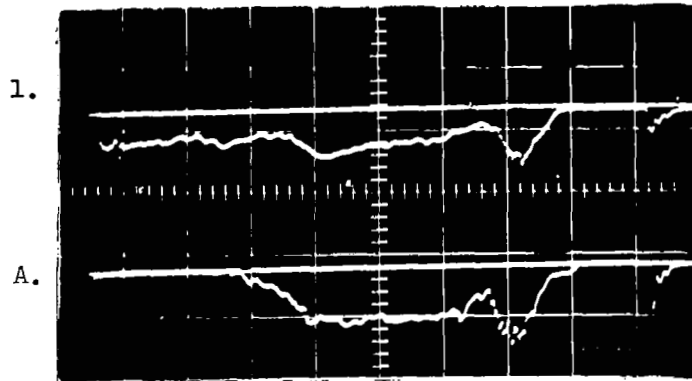
1. Photo-diode output at station 1 (vent end of "S"-tube)
A. Piezoelectric transducer output at station A (same as 1)
   Major divisions are 100 msec and 0.2 volt
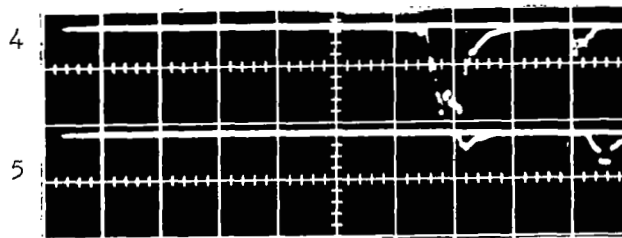
4. Photo-diode output at station 4 (before 90° bend)
5. Photo-diode output at station 5 (above flame arrester)
   Major divisions are 100 msec and 0.2 volt
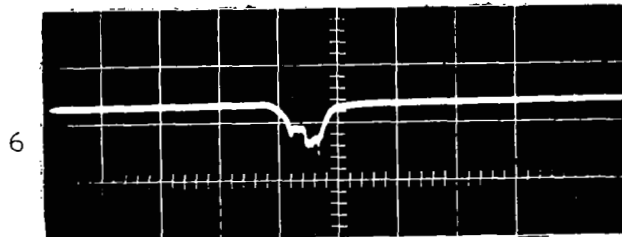
6. Photo-diode output at station 6 (below flame arrester)
   Major divisions are 200 msec and 0.2 volt

FIGURE 10.   Oscillograms showing flame intensity versus time at stations
             1 through 6 in simulated vent system. 125 kA underdamped,
             slightly oscillatory discharge from electrode positioned 0.5
             inch above bottom lip of "S"-tube inside of vent caused igni-
             tion of 4.4% (volume) propane-air mixture. Note secondary
             flame pulses, apparently originating between stations 4 and 5
             and proceeding simultaneously in both directions from point
             of origin at about 150 ft./sec. (test no. 535)

outlet, as in Figure 8a. A maximum flame speed of 60 ft. per second was achieved between stations 4 and 5 when the discharge employed a slightly oscillatory wave having a peak current amplitude of 150 kA. The overall average flame speed for this test was 24 ft. per second between stations 0 and 6.

Some additional tests were run under the above conditions but with the flame arrestor wetted with kerosene prior to the tests. In certain tests where the flame velocity was relatively low (less than 15 ft./sec.) the wetted arrestor was effective in stopping the flame.

In summary, with the vent outlet unsealed and the arrestor in position, a maximum flame speed of 60 ft. per second was recorded in one section of the vent line when the high current discharge (150 kA amplitude) struck the edge of the vent outlet. With the arc discharging across the end of the S-tube beneath the covered vent outlet, flame speeds over 12 times as great were obtained. The presence of a blowout hole below the flame arrestor permitted generally faster flame speeds than was the case without it. Whereas the flame arrestor had stopped flames initiated by discharge currents of less than 125 kA in Configuration A, flames initiated by currents of equal or less ar plitude penetrated the arrestor when the blowout hole was present.

Configuration E.- In this series of tests, the flame arrestor was removed to see what maximum flame speeds might be possible in its absence. As with the other configurations, the wave shape and amplitude and the electrode position were varied to achieve a maximum flame velocity.

For the most realistic case, with the outlet open and the electrode tip at the outlet, maximum flame velocities of up to 156 ft. per second were achieved between stations 5 and 6, using a highly oscillatory wave (Figure 7) with a peak current amplitude of 195 kA. The average velocities between stations 1 and 6 for these tests were up to 66 ft. per second.

A test (No. 646) was made with the vent outlet covered with cloth tape and all other conditions remaining the same. In this case, an average velocity of 121 ft. per second was obtained. The initial rate of propagation, between stations 0 and 2, was 413 ft. per second, illustrating the effect of ignition within a closed vent.

General remarks on flame speed tests.-- Several general remarks should be made about the change in flame velocity as it travelled down the vent tube toward the surge tank in this and the preceeding configurations. Following an initially high speed in the first part of the S-tube (stations 0-2), the flames would decelerate as they passed toward the 45° bend (stations 2-3). Relatively little change was recorded as they passed around the bend (stations 3-4). However, as the flames passed around the 90° bend, a marked increase in velocity was nearly always noted, and, in almost every test the flame recorded a maximum velocity between stations 4 and 5. This appeared unusual because there was no evidence of a progressive increase in velocity as the flame propagated down the S-tube. Since the distance used in calculating this velocity was measured as the shortest distance

between stations 4 and 5, the velocity calculated should have been the minimum actual flame velocity, since the flames could have taken a longer route.

One of these tests performed with Configuration E (No. 649) using a highly oscillatory current discharge of 190 kA amplitude, resulted in evidence of flames moving at well above 1000 ft. per second within the system. In addition, this ignition resulted in a 0.5 inch outward deformation of the outer side of the vent outlet and blowout of a segment of the gasket underneath the top of the surge tank. These effects indicated a much greater than usual pressure build-up within the system. A thorough check was made of the system following this unusual result, which resulted in strong evidence that the high current discharge had caused simultaneous sparking and ignition at several points along the vent system. The explanation is that the vent system was momentarily lifted above ground by an amount equal to an inductive voltage rise in the high current ground circuit. This voltage rise, proportional to the discharge current amplitude, was enough in this case to cause sparkover from the surrounding metal to the piezoelectric transducer ground wires. This sparking was evidenced by discoloration of the PVC surface between the element and the edge of the pipe plug in which it was mounted. This evidence appeared at stations A, B, and C, but not at D, which also had pressure transducer installed. Transducers were frequently inspected and this was the only discharge to occur in this manner during the test series. If a lesson could be learned from this experience, it would be that extreme precautions must be taken in vent design to insure that induced or other voltages, arising in the vent system components themselves or in structures or circuits in any way connected to the vent system, must be prevented from causing such sparking in actual operation. The magnitude of the voltage which caused the sparking in the present case was estimated to be 11 kV. Such voltages are not uncommon in circuits or structures through which lightning currents may pass.

A brief summary of test results is presented in Table II on the following page. Detailed test results are presented in the Appendix.

Flame Arrestor

The performance of the flame arrestor was erratic; however, some general trends were noted that encouraged us in the belief that an effective flame arrestor can be developed for this type application.

The arrestor was partially effective at velocities below 15 ft. per second, i.e., in those tests where it did prevent a flame from reaching the surge tank, the flame speeds were in the range of 5 to 15 ft. per second. A number of tests were run, however, where the arrestor failed to stop a flame travelling at these slower speeds. For the tests run in which the arrestor did not stop the flames, as in Configuration D, the effect of the arrestor was to slow the flames passing through it. Some success with the arrestor occurred when it was wetted with kerosene prior to ignition. In Configuration D the arrestor, when wetted, successfully stopped the flame in four successive tests. The maximum flame velocity, however, did not exceed 16 ft. per second in any of these tests. In other tests where

TABLE II

FLAME VELOCITY TESTS

Brief Summary of Results

TEST CONFIGURATION	TEST VARIATIONS			
	Arc Inside Vent. Outlet open.	Arc Inside Vent. Outlet partially covered with cloth tape.	Arc at Vent Outlet, Outlet open.	Arc at Vent Outlet. Outlet partially covered with cloth tape.
	ft/sec	ft/sec	ft/sec	ft/sec
A. No additional venting. Flame arrestor installed	4.4 – 12.1			
B. No additional venting. Arrestor removed.	8.5			
C. Top of surge tank elevated 1.5". Arrestor installed.	11 – 12.8	13.4 – 140		
D. Hole cut in surge tank. Arrestor installed.	13.2 – 26	4.3 – 307	24	9.8
E. Hole cut in surge tank. Arrestor removed.	5.4 – 74	92	4.2 – 64	121

Note: The numbers listed above are average velocities, calculated by dividing the length of time it took the flames to travel from the electrode (vent) to the bottom of the surge tank, by the total length of the system (4.606 feet). Where a range is shown, a number of tests were made and the numbers given are the minimum and maximum average velocities.

the flames approached the arrestor at greater speeds, the flames succeeded in penetrating the arrestor even though it was wetted with kerosene.

Perhaps the most significant general trend noted was the ability of the arrestor to reduce the velocity of the flame as it passed from station 5 to station 6. There is some indication that the amount of retardation or reduction in velocity is a function of the flame velocity approaching the arrestor, i.e., the higher the flame velocity, the greater the percent of reduction of flame speed. To illustrate this, a plot of the ability of the arrestor to slow the approaching flame is shown in Figure 11. There is a wide scatter in the data, but a trend is evident that the velocity reduction is greater as the approaching flame speed (V_{4-5}) is increased.

The reason for the erratic behavior of the arrestor is not known. Additional work must be undertaken to understand the problem before reliable flame arrestors can be designed.

Other Results

In addition to the principal objectives, considerable information was developed pertaining to the electrical characteristic of the lightning discharge and its affect on flame speed and pressure in the vent system which will be of interest in future testing of this type. These are discussed as follows:

Pressure.- As discussed in the Experimental Results, pressure measurements were not made as frequently or at as many locations during these tests as were light measurements. Limitations of time, for this phase of the test program, precluded the possibility of making complete light and pressure profile measurements, and light measurements were chosen as the most accurate means of measuring flame speeds. Pressure measurements were, however, made occasionally to ascertain the order-of-magnitude of pressure buildup within the system. No pressures greater than 0.5 psi were measured and pressure rises, in most cases, were coincident with rises in light intensity at the same locations. The pressure pulse in the surge tank, below the arrestor, was approximately the same whether or not the flame passed through the arrestor.

No pressure measurements were possible during the test which resulted in a detonation since damaging sparkovers occurred on all three pressure transducers. Nevertheless, ample evidence was present of a much higher than normal pressure buildup, since the gasket blew out and the 1/8" stainless steel vent wall was deformed. Such forces would be very damaging to an actual aircraft system, constructed of lighter materials.

Simulated lightning current amplitude and waveshape.- The amplitude and the wave shape of the current discharge were significant factors in determining the velocity of flame propagation. In general, the higher amplitude currents produced higher velocities; however, the effect of wave shape was more significant than amplitude. A highly oscillatory discharge consisting of a number of repeated cycles of current flow, as shown in Figure 5, was capable of producing flame velocities an order-of-magnitude greater
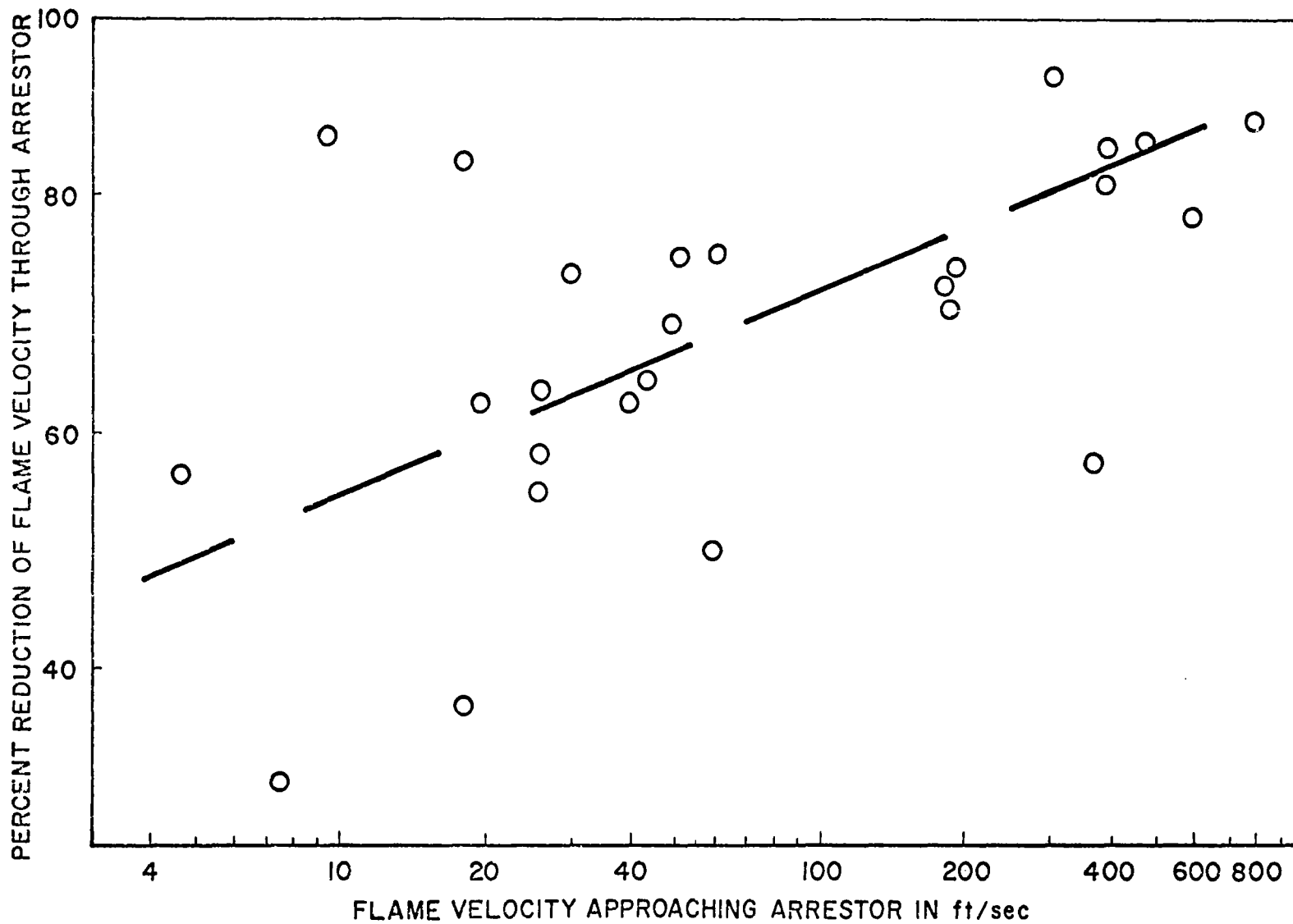
FIGURE 11. Effectiveness of Arrestor in Slowing Approaching Flame.

than an overdamped discharge having the same initial peak current amplitude but consisting of only one unidirectional surge. An examination of a highly oscillatory wave shape shows that over twelve separate pulses occur less than 7 microseconds apart (.007 millisecond). If the initial rate of flame propagation were 1000 ft. per second, for example, after ignition by the first pulse, the flame front would have moved only 0.084" down the tube before being hit by the next pulse. These repeated pressure pulses probably account for the higher flame speeds.

The question arises as to whether or not such an oscillatory current discharge can exist in nature, particularly in the aircraft environment. Measurements of the characteristics of strokes to grounded objects generally exhibit unidirectional characteristics, similar to the overdamped wave shown in Figure 6. Very little is known regarding the characteristics of strokes from cloud to cloud which may intercept an aircraft; however, it is known that strokes to grounded objects often occur more than once in rapid succession, separated by very short periods of time. In such cases the entire succession is usually considered as making up the stroke and reference is made to this as a multi-spike stroke. The effect of the oscillatory wave could be similar in effect to a multi-spike stroke. Thus, there is reason to believe that the use of an oscillatory wave is not entirely unrealistic for these tests.

Electrode gap and position.- Both electrode position and arc length affected the flame speed. During the tests, the current spike was discharged across a gap of 0.5" and 0.75". In every case the smaller gap resulted in slower flame velocities. No velocities above 30 ft. per second were obtained with the 0.5" gap. All the higher flame speeds occurred with the 0.75" gap.

Electrode position was also important to the flame speed. When the electrode was positioned well inside the vent outlet, in fact directly in front of the 5.5" S-tube, much higher flame velocities were achieved than when the electrode was in the center of the vent outlet, discharging to the lip. It is our opinion that this effect merely reflected the increased pressure buildup that could occur when the blast from the discharge was semi-enclosed. Even greater velocities could be achieved by placing tape over a large portion of the vent outlet and placing the electrode inside.

REFERENCES

1. "Investigations of Mechanisms of Potential Aircraft Fuel Tank Vent Fires and Explosions Caused by Atmospheric Electricity," Lockheed California Company, Prepared under NASA Contract NASW-59, May 1963.

2. Horeff, T. G., "Airflow Velocity Effects on Lightning Ignition of Fuel Vent Efflux," Presented at Inter-Agency Coordination Meeting on Aircraft Fire Safety, Wright-Patterson Air Force Base, April 18, 1967.

3. Bremer, E. and Jouid, M., McGraw-Hill, 1959, "Analysis of Electric Circuits," Ch. IX, 135, The Source Free R-L-C Circuit.

91

APPENDIX

INTRODUCTION TO TABLE I - FLAME SPEED TEST RESULTS

The following table lists the results of all of the tests run at the General Electric High Voltage Laboratory with the exception of those in which ignition did not occur. The tests are listed in the order performed. In reading the table, the following notes are helpful:

1. Both the amplitude and waveshape of the discharge current were varied. The table makes reference to the appropriate wave-shape figures shown in Figures 1., 2., and 3. following this introduction.

2. With few exceptions, all elapsed times and velocities are listed as positive numbers, indicating that the direction of travel was from station 0 to station 6, from the left to the right side of the page. In a few cases, however, during the tests on Configuration A, negative numbers appear, indicating a return flame traveling in the opposite direction.

3. When no numbers are listed for a particular segment of the system, no measurements were made at the downstream station of that segment. In these cases, the elapsed time and velocity shown for the next segment downstream (to the right on the table) refer to the elapsed time and velocity across both segments. In the case of Segment 5, C-6, D the lack of data indicates that the flame did not penetrate the arrestor when the words "no indication" are used.

4. Numerous variations were made in the test procedure, such as variation in electrode position or covering of vent outlet, etc. These changes are listed in sentence form and appear between tests, as they were made. Each such sentence remains in effect until that condition is changed by a later sentence concerning the same item. In the case of coverings over the vent outlet, the absence of any sentence to the contrary indicates that no covering was present over the vent outlet.

5. During testing of Configuration C and E where blowout areas were provided, these areas were always sealed with a fragile covering prior to each test, so that the fuel-air mixture would not escape or be contaminated by air prior to the test. For Configuration C, the blowout area below the elevated tank top was covered with masking

tape, 50% of which normally blew off during each test. The blowout hole in the side of the surge tank in Configuration E was covered prior to each test with saran wrap, the extremities of which were taped lightly in place with masking tape. The saran wrap burned or blew away during each test, in which ignition of the fuel-air mixture occurred.
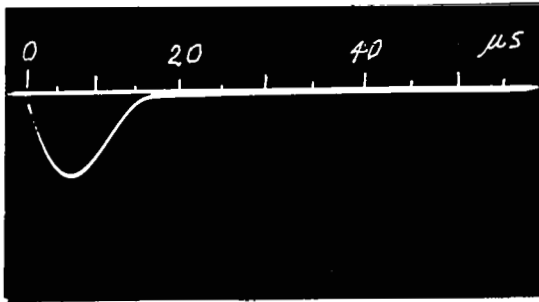
FIGURE 1 (a).

Overdamped (unidirectional) wave
(test no. 527). Crest is 66 kA in
7.5 μsec. Initial di/dt = 8.8 kA/μs
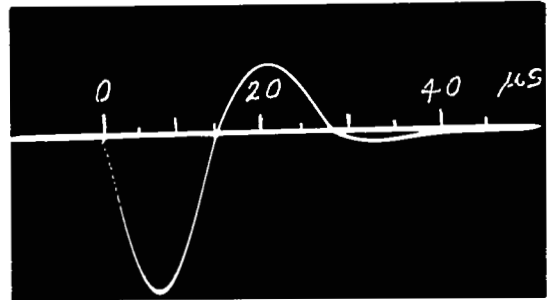
FIGURE 1 (b)

Underdamped, slightly oscillatory wave
(test no. 528). Crest is 83 kA in 8
μsec. Undershoot is -34 kA. Initial
di/dt = 10.3 kA/μsec.
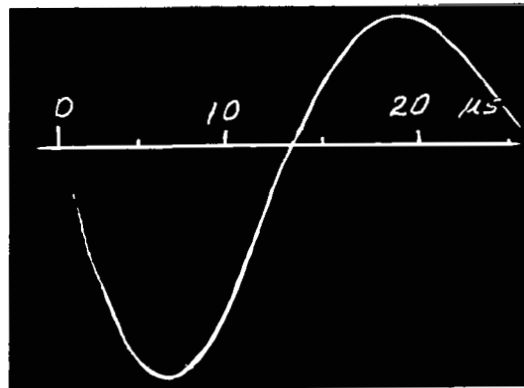
FIGURE 1 (c).   Underdamped, slightly oscillatory wave
(test no. 532). Crest is 126 kA in
7.5 μsec. Undershoot is -68 kA.
Initial di/dt = 16.8 kA/μsec.

FIGURE 1   Examples of oscillograms of different current
wave shapes applied during flame velocity tests.

   Note: All discharges were of positive polarity. Oscillograms
          are shown with downward deflections due to placement of
          current measuring shunt in ground return circuit.
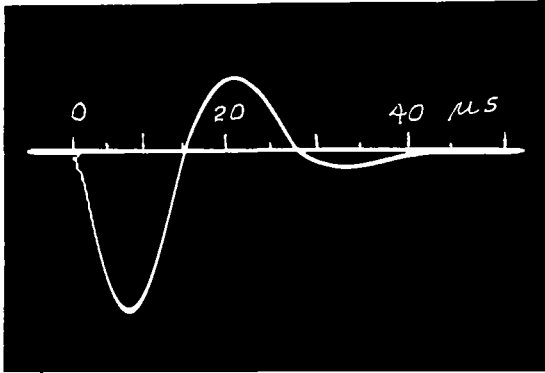
FIGURE 2 (a).

Underdamped, slightly oscillatory wave
(test no. 540). Crest is 115 kA in 7
μsec. Undershoot is -60 kA. Initial
di/dt = 16.4 kA/μsec.
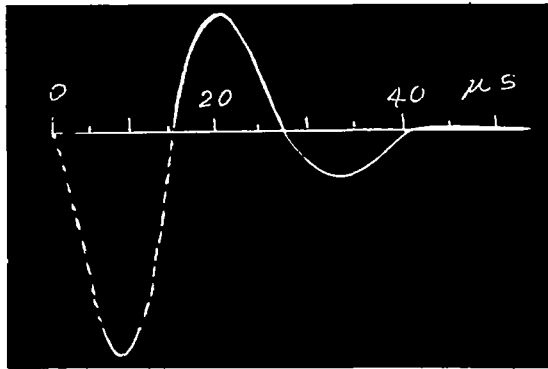
FIGURE 2 (b).

Underdamped, slightly oscillatory wave
(test no. 576). Crest is 85 kA in 7
μsec. Undershoot is -38 kA. Initial
di/dt = 12.1 kA/μsec.
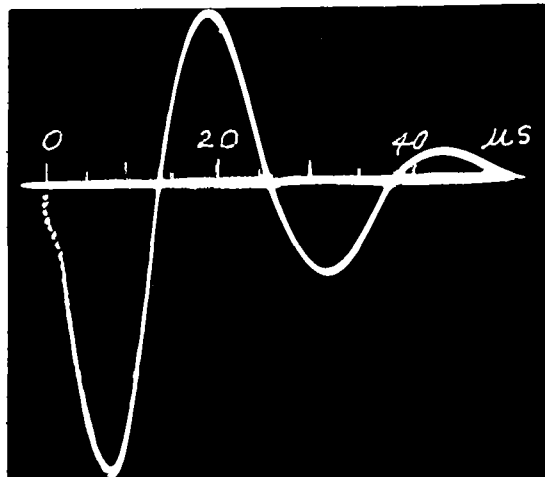
FIGURE 2 (c).   Underdamped oscillatory wave (test no.
612). Crest is 150 kA in 7.5 μsec.
Undershoot is 87.5 kA. Initial di/dt =
20 kA/μsec.

FIGURE 2   Examples of oscillograms of different current
wave shapes applied during flame velocity tests.

Note: All discharges were of positive polarity. Oscillograms
are shown with downward deflections due to placement of
current measuring shunt in ground return circuit.
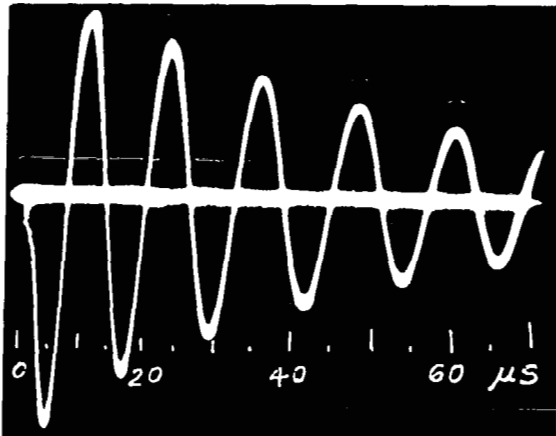
FIGURE 3 (a).

Underdamped, highly oscillatory wave
(test no. 653). Crest is 180 kA in 8
μsec. First undershoot is -144 kA.
Initial di/dt = 22.5 kA/μsec.
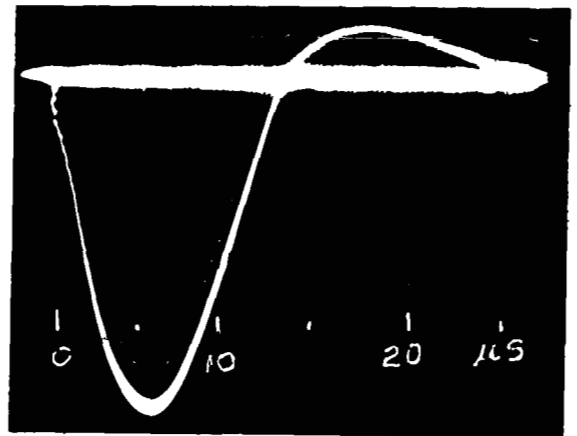
FIGURE 3 (b)

Underdamped, slightly oscillatory wave
(test no. 674). Crest is 130 kA in 7
μsec. Undershoot is -17 kA. Initial
di/dt = 18.5 kA/μsec.
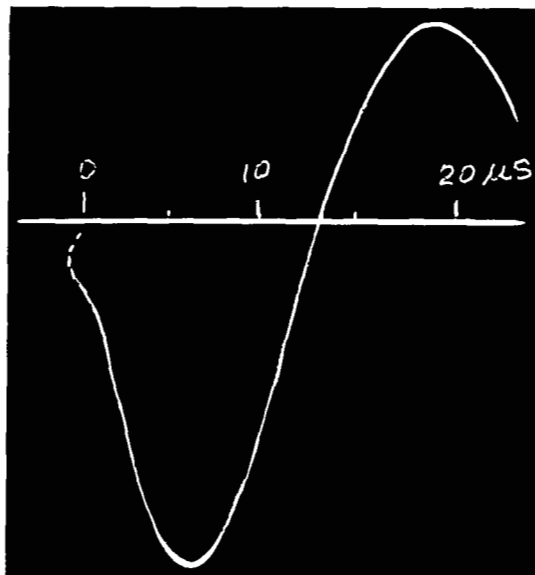
FIGURE 3 (c).   Underdamped oscillatory wave (test no.
682). Crest is 135 kA in 8 μsec.
Undershoot is -78 kA. Initial di/dt =
16.9 kA/μsec.

FIGURE 3   Examples of oscillograms of different current
wave shapes applied during flame velocity tests.

    Note: All discharges were of positive polarity. Oscillograms
           are shown with downward deflections due to placement of
           current measuring shunt in ground return circuit.

TABLE I

Flame Velocity Test Results

Configuration A: No Blowout Area. Arrestor Installed

Test No.	Current kA	Wave (Fig)	Flame Arrestor	1 – 2 t msec	1 – 2 v '/sec	2 – 3 t msec	2 – 3 v '/sec	3 – 4 t msec	3 – 4 v '/sec	4 – 5 t msec	4 – 5 v '/sec	5 – 6 t msec	5 – 6 v '/sec	Avg.Velocity t msec	Avg.Velocity v '/sec	Remarks
523	66	1a	dry	100	12.4			320	5.6	110	10.8			530	8.0	
524	57	1a	dry					630	4.8	180	6.6			810	5.4	
525	57	1a	dry	130	7.0			530	3.4	270	4.4			960	4.4	
526	43	1b	dry	75	16.6			295	6.1	90	13.2			460	9.2	
527	43	1b	dry					340	8.9	85	14.0			425	10.0	
528	82	1b	dry	70	17.7			170	10.6	100	11.9			340	12.5	
530	120	1c	dry	60	20.7			165	10.9	125	9.5			350	12.1	
531	125	1c	dry	105	11.8			225	8.0	85	14.0	85	4.4	500	9.2	
				-3	-302			-8	-226	7	170					Secondary flame
535	125	1c	dry	245	5.1			375	4.8	60	19.8	70	5.4	750	6.2	
								-12	-150	30	395	30	52			Secondary flame
537	125	1c	dry					515	5.9	175	6.8	50	7.5	740	6.2	
								-10	-271	40	30					Secondary flame
538	125	1c	dry					430	7.1	75	15.9	55	6.8	560	8.2	
								-10	-271	10	118					Secondary flame
539	125	1c	dry					835	3.7	95	12.5			930	4.6	
540	125	2a	dry					770	4.0	70	17.0			840	5.0	

Configuration A.

Test No.	Current kA	Flame Wave Arrestor (Fig)	1 - 2		2 - 3		3 - 4		4 - 5		5 - 6		Avg. Velocity		Remarks
			t msec	v '/sec	t msec	v '/sec	t msec	v '/sec	t msec	v '/sec	t msec	v '/sec	t msec	v '/sec	
541	125	2a dry					480	6.3	98	12.1	62	6.1	640	7.2	
									-10	-119					Secondary flame
543	125	2a dry					515	5.9	65	19.8	60	6.2	640	7.2	
									-10	-119					Secondary flame

Flame arrestor wetted with kerosene.

Test No.	Current kA	Flame Wave Arrestor (Fig)	1 - 2		2 - 3		3 - 4		4 - 5		5 - 6		Avg. Velocity		Remarks
544	112	2a wet					465	6.6	165	7.2			630	6.7	
546	112	2a wet					355	8.6	135	8.8			490	8.6	
551	112	2a wet					415	7.4	120	9.9			535	7.9	

Flame arrestor dried off.

Test No.	Current kA	Flame Wave Arrestor (Fig)	1 - 2		2 - 3		3 - 4		4 - 5		5 - 6		Avg. Velocity		Remarks
556	108	2a dry					330	9.2	100	11.9			430	9.9	Arrestor possibly still damp
557	108	2a dry					590	5.2	150	7.9			740	5.7	"

- -

Configuration B: No Blowout Area. Arrestor Removed.

Electrode positioned 0.5" above bottom lip of S-tube, inside of vent.

Test No.	Current kA	Flame Wave Arrestor (Fig)	1 - 2		2 - 3		3 - 4		4 - 5		5 - 6		Avg. Velocity		Remarks
552	108	2a out					415	7.3	85	14.0			500	8.5	

- -

TABLE I

Flame Velocity Test Results

Configuration C: Top of Surge Tank Elevated 1.5" to Provide Blowout Area Above Flame Arrestor. This area was covered with masking tape prior to each test. Flame arrestor installed.

| | | | Locations | | | | | | | | | | Avg. Velocity | | |
| Test No. | Current kA | Flame Arrestor (Fig) | 1 - 2 | | 2 - 3 | | 3 - 4 | | 4 - 5 | | 5 - 6 | | | | Remarks |
			t msec	v '/sec	t msec	v '/sec	t msec	v '/sec	t msec	v '/sec	t msec	v '/sec	t msec	v '/sec	
Electrode positioned 0.5" above bottom lip of S–tube, inside of vent.															
559	104	2a dry					290	10.5	110	10.8	20	18.8	420	11	
Vent outlet 90% sealed with masking tape. Electrode positioned as above.															
560	104	2a dry					215	14.2	45	26	20	18.8	280	16.5	
Electrode positioned 2.0" above bottom lip of S–tube, inside of vent.															
570	95	2b dry	50	25			155	11.7	100	11.9	55	6.8	360	12.8	
Vent outlet 90% sealed with cloth tape. Electrode positioned as above.															
571	95	2b dry	50	25			160	11.3	105	11.3			315	13.4	
Electrode positioned 0.5" above lower lip of S–tube, inside of vent.															
575	95	2b dry					12	254	2	593	19	19.8	33	140	
576	95	2b dry	1	1240			6	300	3	395	25	15.0	35	132	
Fuel–air mixture fed into system at location A.															
562	110	2a dry	7	177	4	221	2	258					13	234	

TABLE I

Flame Velocity Test Results

Configuration D: <u>17.7 sq. inch Blowout Area Cut in Surge Tank. This Hole Was Covered with Saran Wrap Prior to Each Test. Flame Arrestor Installed.</u>

Test No.	Current kA	Flame Wave Arrestor (Fig)	1 - 2 t msec	1 - 2 v '/sec	2 - 3 t msec	2 - 3 v '/sec	3 - 4 t msec	3 - 4 v '/sec	4 - 5 t msec	4 - 5 v '/sec	5 - 6 t msec	5 - 6 v '/sec	Avg. Velocity t msec	Avg. Velocity v '/sec	Remarks
													Locations	**Avg. Velocity**	

Electrode positioned 0.5" above bottom lip of S-tube, inside of vent. Vent outlet 90% sealed with cloth tape.

Test No.	Current kA	Arrestor	1-2 t	1-2 v	2-3 t	2-3 v	3-4 t	3-4 v	4-5 t	4-5 v	5-6 t	5-6 v	Avg t	Avg v
577	85	2b dry							10	423	48	7.8	58	80
578	102	2b dry	50	24.8			180	10.0	140	8.5			370	11.4
579	118	2b dry	5	248			35	52	30	40			70	61
580	118	2b dry	5	248			25	72	40	30			70	61
581	118	2b dry	285	3.2			310	5.8	130	9.1	300	1.3	1070	4.3
582	118	2b dry	80	15.5			120	15.0	45	26	35	10.7	280	16.5
583	118	2b dry	80	15.5			110	16.4	50	24	30	12.5	270	17.1
584	100	2b dry	220	5.7			190	9.5	65	18.3	35	10.7	510	9.1
585	97	2b dry	100	12.4			130	13.9	45	26	45	8.3	320	14.4
586	97	2b dry	90	13.8			130	13.9	45	26	30	12.5	305	15.1

Electrode gap increased to 0.75".

Test No.	Current kA	Arrestor	1-2 t	1-2 v	2-3 t	2-3 v	3-4 t	3-4 v	4-5 t	4-5 v	5-6 t	5-6 v	Avg t	Avg v
587	97	2b dry	80	15.5			110	16.4	40	30	40	9.4	270	17.1

Configuration D.

Test No.	Current kA	Flame Wave Arrestor (Fig)	Locations 1 – 2 t msec	v '/sec	2 – 3 t msec	v '/sec	3 – 4 t msec	v '/sec	4 – 5 t msec	v '/sec	5 – 6 t msec	v '/sec	Avg. Velocity t msec	v '/sec	Remarks
			Vent outlet covered with saran wrap.												
588	97	2b dry	80	15.5			160	11.3	60	19.8	50	7.5	350	13.2	
			Vent outlet 90% cloth taped.												
589	100	2b dry	4	310			7	258	2	594	3	125	16	288	
590	100	2b dry	5	248			8	225	2	594	7	54	22	210	
591	100	2b dry	8	155			15	120	4	297	13	29	40	115	
593	100	2b dry	4	310			6	300	1.5	790	3.5	107	15	307	
595	150	2c dry	2	620			30	60	6.5	183	7.5	50	46	100	Arc occurred from electrode to edge of outlet.
596	150	2c dry	3	413			9.5	190	2.5	475	5	75	20	230	
597	150	2c dry	2	620	3	295	6	153	3	396	6	63	20	231	
598	150	2c dry	8	155	15	59	20	46	10	119	9	42	62	75	
599	150	2c dry	2	620	4	222	6	153	2	594	6	63	20	231	
			Electrode gap decreased to 0.5".												
602	150	2c dry			21	101	15	61	5	237	5	75	46	100	

Configuration D.

Test No.	Current kA	Wave (Fig)	Flame Arrestor	Locations										Avg. Velocity		Remarks
				1 – 2		2 – 3		3 – 4		4 – 5		5 – 6				
				t msec	v '/sec	t msec	v '/sec	t msec	v '/sec	t msec	v '/sec	t msec	v '/sec	t msec	v '/sec	
Electrode gap increased to 0.75".																
604	150	2c	dry	5	248	5	177	6	153	3	396	8	47	27	171	
Vent outlet covered with saran wrap.																
605	132	2c	dry					120	25	25	48	25	15.0	170	27.1	
606	137	2c	dry	160	7.8			360	5.0	260	4.6	190	2.0	970	4.8	
607	137	2c	dry	30	41			90	20	30	40	25	15.0	175	26.3	
Flame arrestor wetted with kerosene.																
609	137	2c	wet	90	12.7			210	8.6	165	7.2	75	5.0	540	8.5	
612	150	2c	wet	30	41	50	17.7	30	31	20	59	13	29	143	32	
Vent outlet uncovered. Electrode positioned in center of vent outlet.																
614	150	2c	wet	58	21	52	17.0	35	26	20	60	25	15.0	190	24	
Vent outlet 90% covered with cloth tape.																
615	150	2c	wet	80	15.5	100	8.9	120	7.6	130	9.1			430	9.8	
Electrode positioned 0.75" above lower lip of S-tube, inside vent scoop.																
616	150	2c	wet	80	15.5	120	7.4	120	7.6	180	6.6			500	8.5	
621	161	2c	wet	90	13.8	90	9.9	140	6.6	190	6.3			510	8.3	

Configuration D.

| | | | | Locations | | | | | | | | | | | Avg. Velocity | | |
| Test No. | Current kA | Flame Wave Arrestor (Fig) | | 1 - 2 | | 2 - 3 | | 3 - 4 | | 4 - 5 | | 5 - 6 | | | | | |
				t msec	v '/sec	t msec	v '/sec	t msec	v '/sec	t msec	v '/sec	t msec	v '/sec	r msec	f '/sec	Remarks
			Reduced propane-air mixture to 3.2% propane (by volume). Electrode positioned in center of vent outlet.													
622	161	2c	wet	140	8.9	200	4.4	270	3.4					610	5.0	
			Propane-air mixture now back to 4.4% propane (by volume).													
704	167	2c	wet			80	27	25	37			10	156	115	40	

- -

Configuration E: 17.5 sq. inch Blowout Area Cut in Surge Tank. This Hole Was Covered with Saran Wrap Prior to Each Test. Flame Arrestor Removed.

Test No.	Current kA	Flame Wave Arrestor (Fig)		1 - 2 t	1 - 2 v	2 - 3 t	2 - 3 v	3 - 4 t	3 - 4 v	4 - 5 t	4 - 5 v	5 - 6 t	5 - 6 v	r	f	Remarks
			Electrode positioned .33" from outside edge of vent opening.													
624	161	2c	out	140	8.9	120	7.4	180	5.1			210	7.4	650	7.1	
			Electrode gap increased to 1.0" from outside edge of vent opening.													
625	161	2c	out	25	50	35	25	20	46			15	104	95	49	
626	161	2c	out	40	31			80	23	40	30			160	27	

Configuration E

Test No.	Current kA	Wave (Fig)	Flame Arrestor	1 - 2		2 - 3		3 - 4		4 - 5		5 - 6		Avg.Velocity		Remarks
				t msec	v '/sec	t msec	v '/sec	t msec	v '/sec	t msec	v '/sec	t msec	v '/sec	t msec	v '/sec	
Electrode positioned 0.5" above lower lip of S-tube, inside of vent.																

Electrode positioned 0.5" above lower lip of S-tube, inside of vent.

Test No.	Current kA	Wave (Fig)	Flame Arrestor	1-2 t msec	1-2 v '/sec	2-3 t msec	2-3 v '/sec	3-4 t msec	3-4 v '/sec	4-5 t msec	4-5 v '/sec	5-6 t msec	5-6 v '/sec	Avg t msec	Avg v '/sec	Remarks
632	161	2c	out	10	124	50	17.8	25	37			25	63	110	42	

Electrode positioned 1.5" above lower lip of S-Tube, inside of vent.

Test No.	Current kA	Wave (Fig)	Flame Arrestor	1-2 t msec	1-2 v '/sec	2-3 t msec	2-3 v '/sec	3-4 t msec	3-4 v '/sec	4-5 t msec	4-5 v '/sec	5-6 t msec	5-6 v '/sec	Avg t msec	Avg v '/sec	Remarks
633	161	2c	out	20	62	60	14.8	30	31			15	104	125	37	
634	161	2c	out	15	83	35	25	25	37			20	78	95	49	Arc occurred from electrode to edge of scoop.

Electrode positioned 0.75" above lower lip of S-tube, inside of vent.

Test No.	Current kA	Wave (Fig)	Flame Arrestor	1-2 t msec	1-2 v '/sec	2-3 t msec	2-3 v '/sec	3-4 t msec	3-4 v '/sec	4-5 t msec	4-5 v '/sec	5-6 t msec	5-6 v '/sec	Avg t msec	Avg v '/sec	Remarks
635	161	2c	out	18	69	34	26	26	35			15	104	93	50	
636	161	3a	out	10	124	25	36	20	46			15	104	70	66	
637	161	3a	out	10	124	18	49	22	42			12	130	62	74	
638	161	3a	out	15	83	35	24	28	33			12	130	80	58	
639	195	3a	out	10	124	25	36	20	46			15	104	70	66	
640	195	3a	out	5	248	30	30	25	37			10	156	70	66	

Configuration E

Test No.	Current kA	Wave (Fig)	Flame Arrestor	Locations 1-2 t msec	v '/sec	2-3 t msec	v '/sec	3-4 t msec	v '/sec	4-5 t msec	v '/sec	5-6 t msec	v '/sec	Avg.Velocity t msec	v '/sec	Remarks
				Vent outlet covered with saran wrap.												
641	195	3a	out	10	124	25	36	20	46			15	104	70	66	
				Vent outlet covered 50% with cloth tape.												
642	195	3a	out	1	1240	24	37	12	77			9	174	46	100	
				Vent outlet covered 90% with cloth tape.												
643	195	3a	out			20	107	15	612			15	104	50	92	
				Vent outlet open. Electrode positioned 1" from outside edge of vent opening.												
644	195	3a	out	3	413	33	27	22	42			14	112	72	64	
645	161	3a	out	10	124	45	20	25	37			10	156	90	51	
				Vent outlet covered 90% with cloth tape.												
646	161	3a	out	3	413	12	74	12	76			11	142	38	121	
				Vent outlet open.												
649	190	3a	out							2	2115	1	375	3	1540	Evidence of multiple ignition at pts.(A,B,C)
651	190	3a	out	11	113	29	31			245	8.6			285	14.8	
657	170	3a	out	10	124	40	22	22	42			20	78	92	50	
661	170	3a	out	10	124	32	28	21	44			10	156	73	63	

Configuration E

Test No.	Current kA Wave (Fig)	Flame Arrestor	Locations										Avg.Velocity		Remarks
			1 – 2		2 – 3		3 – 4		4 – 5		5 – 6				
			t msec	v '/sec	t msec	v '/sec	t msec	v '/sec	t msec	v '/sec	t msec	v '/sec	t msec	v '/sec	
664	38	1a	out	300	4.1	160	5.5	270	3.4					730	4.2	
665	38	1a	out	170	7.3	150	5.9	150	6.1			150	10.4	620	7.5	
666	37	1a	out	200	6.2	230	3.8	170	5.4			200	7.8	800	5.7	
667	58	1a	out	190	6.5	210	4.2	200	4.6			330	4.7	930	5.0	
668	130	3b	out	130	9.5	140	6.3	190	4.8			180	8.7	640	7.2	
670	130	3b	out	100	12.4	65	13.6	135	6.8					300	10.2	
671	130	3b	out	90	13.8	60	14.8	50	18.3			50	31	250	18.4	
672	130	3b	out	70	17.7	55	16.1	65	14.1					190	16.0	
673	130	3b	out	100	12.4	100	8.9	200	4.6			140	11.2	540	8.6	
674	130	3b	out	120	10.3	100	8.9	180	5.1			190	8.2	590	7.8	

Electrode positioned 2" from end of vent outlet.

Test No.	Current kA Wave (Fig)	Flame Arrestor	1 – 2 t msec	v '/sec	2 – 3 t msec	v '/sec	3 – 4 t msec	v '/sec	4 – 5 t msec	v '/sec	5 – 6 t msec	v '/sec	t msec	v '/sec	Remarks
675	130	3b	out	130	9.6	100	8.9	170	5.4			170	9.2	570	8.1	
676	130	3b	out	110	11.3	80	11.0	180	5.1			230	6.8	600	7.7	

Configuration E

| | | | | Locations | | | | | | | | | | | | Avg.Velocity | | |
| | | | | 1 – 2 | | 2 – 3 | | 3 – 4 | | 4 – 5 | | 5 – 6 | | | | | | |
Test No.	Current kA	Wave (Fig)	Flame Arrestor	t msec	v '/sec	t msec	v '/sec	t msec	v '/sec	t msec	v '/sec	t msec	v '/sec	t msec	v '/sec	Remarks
				Electrode positioned 0.75" above lower lip of S-tube, inside of vent.												
677	130	3b	out	90	13.8	130	6.8	150	6.1			170	9.2	640	7.2	
678	126	3b	out	100	12.4	100	8.9	220	4.2			260	14.4	700	6.6	
679	128	3b	out	100	12.4	120	7.4	220	4.6			310	5.1	750	6.2	
680	128	3b	out	110	11.3	125	7.1	245	3.6			300	5.2	780	5.9	
681	128	3b	out	80	15.5	120	7.4	230	4.0			430	3.6	860	5.4	
683	132	3c	out	60	21	80	11.1	60	15.3			50	31	250	18.4	
685	138	3c	out	60	21	65	13.6	35	26			35	45	195	24	
687	150	3c	out	35	35	75	11.8	45	20			45	35	200	23	
688	150	3c	out	35	35	60	15	20	46			20	78	135	34	
689	'150	3c	out	30	41	70	12.7	30	31			40	39	170	27	
690	167	3c	out	20	62	70	12.7	30	31			30	52	150	31	
691	170	3c	out	16	78	84	10.5	30	31			30	52	160	29	
692	170	3c	out	20	62	55	16.1	30	31			20	78	125	37	

Configuration E

| | | | | Locations | | | | | | | | | | Avg.Velocity | | |
| | | | | 1 - 2 | | 2 - 3 | | 3 - 4 | | 4 - 5 | | 5 - 6 | | | | |
Test No.	Current kA Wave (Fig)		Flame Arrestor	t msec	v '/sec	t msec	v '/sec	t msec	v '/sec	t msec	v '/sec	t msec	v '/sec	t msec	v '/sec	Remarks
693	176	3c	out	13	95	42	21	45	20			30	52	130	36	
694	179	3c	out	20	62	65	13.6	35	26			20	78	140	33	
695	172	3c	out	20	62	50	17.7	20	46			15	104	105	44	

Electrode is 8" piece of aluminum foil 0.5" wide extending inside vent to lower lip of S-tube.

Test No.	Current kA	Wave (Fig)	Flame Arrestor	1-2 t	1-2 v	2-3 t	2-3 v	3-4 t	3-4 v	4-5 t	4-5 v	5-6 t	5-6 v	Avg t	Avg v	Remarks
700	155	3c	out			50	43	20	46			20	78	90	51	
703	142	3c	out			85	24	15	61			15	104	115	40	

INTRODUCTION TO TABLE II - IGNITION THRESHOLD TESTS

The following table lists the results of the Ignition Threshold Tests. The materials employed in these tests are as follows:

Titanium – 20, 40, and 60 mil thicknesses
Aluminum – 40 and 60 mil thicknesses
Stainless Steel – 20, 40, and 60 mil thicknesses

This Table is self explanatory; however, the following notes may be helpful:

1)   All tests were performed using a 38kA initial high current spike which lasted a few microseconds.

2)   On most tests, following the initial high current spike, a low amplitude continuing current was applied with both the amplitude and time varied to obtain the desired coulomb transfer. This is often referred to as a two-component discharge.

3)   For a few tests (No. 179 to 181), a three-component waveshape was employed. This consisted of a 38kA spike, a 1380 amp crest 2nd component, lasting 80 microseconds, and the normal low amplitude continuing current lasting up to 1.2 seconds.

4)   High speed photography, which was used to determine ignition time, was not employed on all tests. The cameras were only operated on tests considered to be the most representative of actual lightning strikes. Thus, for many tests no ignition time is given.

TABLE II

IGNITION THRESHOLD TESTS

Test No.	Continuing Current		Charge Transfer (coulombs)	Ignition	Ignition Time (msec)	Hole Formed	Fuel-Air Ratio Fraction of Stoichiometric
	Avg. Amplitude (amps)	Duration (msec)					
			20 mil Titanium				
160	69	960	66.0	no		yes	1.8
161	65	1400	90.0	no		yes	"
163	92	800	73.5	no		yes	"
164	92	1260	116.0	no		yes	"
165	116	1400	148.0	yes	5 sec.	yes	"
166	119	500	59.5	no		yes	"
168	110	1480	163.0	yes	5 sec.	yes	"
179	1380	80	110.0	yes		yes	"
180	1350	80	108.0	yes	5.0	yes	"
181	1380	80	110.0	yes	4.5	yes	"
182	initial spike only		0	no		no	1.5
183	110	240	26.0	yes		no	"
187	105	134	14.0	yes		no	"
188	124	60	7.4	yes		no	"

TABLE II

IGNITION THRESHOLD TESTS

Test No.	Continuing Current Avg. Amplitude (amps)	Duration (msec)	Charge Transfer (coulombs)	Ignition	Ignition Time (msec)	Hole Formed	Fuel-Air Ratio Fraction of Stoichiometric
			20 mil Titanium				
189	initial spike only		0	no		no	1.5
190	92	20	2.0	no		no	"
191	initial spike only		0	no		no	"
192	92	20	2.0	no		no	"
193	92	48	4.0	no		no	"
194	------	-------	6.0	yes		no	"
195	92	56	5.0	no		no	"
196	92	66	6.0	yes		no	"
197	97	60	5.8	yes		no	"
199	92	60	5.5	yes		no	"
200	92	47	4.3	no		no	"
201	92	20	2.0	no		no	"
203	74	108	7.0	no		no	"
205	92	140	12.0	yes		no	"

TABLE II
IGNITION THRESHOLD TESTS

Test No.	Continuing Current Avg. Amplitude (amps)	Duration (msec)	Charge Transfer (coulombs)	Ignition	Ignition Time (msec)	Hole Formed	Fuel-Air Ratio Fraction of Stoichiometric
				20 mil Titanium			
206	92	100	9.2	yes		no	1.5
210	74	60	5.0	yes		no	"
211	74	56	4.0	no		no	"
212	110	36	4.0	no		no	"
213	119	200	24.0	yes		no	"
214	115	200	23.0	yes		no	"
215	92	140	13.0	yes		no	"
245	92	60	5.5	yes		no	"
253	92	46	4.25	no		no	"
254	92	57	5.3	no		no	"
493	39 kA initial spike only		------	no		no	"
494	" " " " "		------	no		no	"
495	58 kA " " "		------	no		no	"
496	86 kA " " "		------	no		no	"

Continued---

TABLE II
IGNITION THRESHOLD TESTS

Test No.	Continuing Current Avg. Amplitude (amps)	Duration (msec)	Charge Transfer (coulombs)	Ignition	Ignition Time (msec)	Hole Formed	Fuel-Air Ratio Fraction of Stoichiometric
			40 mil Titanium				
136	69	360	24.9	no		no	1.8
138	101	260	26.3	no		no	"
139	119	1000	119.5	no		yes	"
140	128	1440	185.0	no		yes	"
141	128	1440	185.0	no		yes	"
216	128	1440	185.0	yes	22	yes	0.75
220	125	126	15.7	no		no	1.5
221	?	?	15.8	no		no	"
224	?	?	46.0	yes	Est.500	no	"
226	138	200	27.6	yes		no	"
229	165	140	23.0	yes		no	"
230	144	100	14.4	yes		no	"
231	165	70	11.5	yes		no	"
232	189	61	11.5	yes		no	"

TABLE II

IGNITION THRESHOLD TESTS

Test No.	Continuing Current Avg. Amplitude (amps)	Duration (msec)	Charge Transfer (coulombs)	Ignition	Ignition Time (msec)	Hole Formed	Fuel-Air Ratio Fraction of Stoichiometric
			20 mil Titanium				
497	88 kA initial spike only		_____	no		no	1.5
518	103	58	6.0	yes	44*	no	"
519	88	56	4.9	no		no	"
520	92	50	4.6	no		no	"
521	191	51	10.0	no		no	"
522	319	69	22.0	yes	13.5	no	"

* Obtained from high level microphone.

TABLE II

IGNITION THRESHOLD TESTS

Test No.	Continuing Current		Charge Transfer (coulombs)	Ignition	Ignition Time (msec)	Hole Formed	Fuel-Air Ratio Fraction of Stoichiometric
	Avg. Amplitude (amps)	Duration (msec)					
			40 mil Titanium				
233	125	60	7.5	yes		no	1.5
234	93	63	5.75	yes		no	"
235	93	63	5.75	yes		no	"
236	60	52	3.0	no		no	"
237	60	52	3.0	no		no	"
238	60	52	3.0	no		no	2.25
239	69	60	4.1	no		no	"
240	55	60	3.5	no		no	"
242	115	52	6.0	no		no	0.75
243	138	68	9.0	no		no	"
346	60	50	3.0	no		no	1.5
327	42	48	2.0	no		no	"
328	?	?	3.5	no		no	"
329	?	?	5.5	no		no	"

TABLE II

IGNITION THRESHOLD TESTS

Test No.	Continuing Current Avg. Amplitude (amps)	Duration (msec)	Charge Transfer (coulombs)	Ignition	Ignition Time (msec)	Hole Formed	Fuel-Air Ratio Fraction of Stoichiometric
			40 mil Titanium				
330	121	57	6.9	yes		no	1.5
331	100	58	5.8	no		no	"
332	129	62	8.0	yes	72*	no	"

* Obtained from high level microphone.

TABLE II

IGNITION THRESHOLD TESTS

Test No.	Continuing Current Avg. Amplitude (amps)	Duration (msec)	Charge Transfer (coulombs)	Ignition	Ignition Time (msec)	Hole Formed	Fuel-Air Ratio Fraction of Stoichiometric
			60 mil Titanium				
255	125	55	6.9	no		no	1.5
258	125	82	10.4	no		no	"
259	125	224	28.0	no		no	"
261	125	296	37.0	no		no	"
263	125	1100	138.0	no		no	"
264	125	1100	138.0	yes		no	"
265	125	1100	138.0	yes		no	"
266	125	960	120.0	no		no	"
268	125	1010	126.0	yes		no	"
269	125	920	115.0	no		no	"
270	125	1150	144.0	yes		no	"
445	733	150	100.0	yes		yes	"
446	733	157	115	yes		yes	"
447	733	314	230	yes		yes	"

TABLE II

IGNITION THRESHOLD TESTS

Test No.	Continuing Current		Charge Transfer (coulombs)	Ignition	Ignition Time (msec)	Hole Formed	Fuel-Air Ratio Fraction of Stoichiometric
	Avg. Amplitude (amps)	Duration (msec)					
			60 mil Titanium				
448	733	75	60	no		no	1.5
449	733	145	106	no		no	"
450	733	145	106	yes		no	"
451	125	1260	157	yes		no	"
483	?	?	99	yes		no	0.75
484	?	?	106	no		no	"
485	147	940	138	yes		no	"
486	129	950	122	no		no	"
487	134	950	127	yes		no	"
488	136	950	129	no		no	1.5
489	113	950	107	yes	900*	yes	"
490	120	440	53	no		no	"
491	126	950	119	yes		yes	"
492	140	950	133	yes		yes	2.25

* Obtained from high level microphone.

TABLE II

IGNITION THRESHOLD TESTS

Test No.	Continuing Current		Charge Transfer (coulombs)	Ignition	Ignition Time (msec)	Hole Formed	Fuel-Air Ratio Fraction of Stoichiometric
	Avg. Amplitude (amps)	Duration (msec)					
			40 mil Aluminum				
208	92	112	10.0	no		no	1.5
209	119	390	46.5	yes		yes	"
317	125	84	10.5	no		no	"
319	125	255	32.0	no		no	"
320	125	300	37.0	yes	100*	yes	"
321	?	?	19.0	yes		yes	"
322	149	138	20.5	no		no	"
323	?	?	23.0	yes		yes	"
324	151	136	20.5	no		no	"
325	169	130	22.0	yes	130*	yes	"

* Obtained from high level microphone.

TABLE II

IGNITION THRESHOLD TESTS

Test No.	Continuing Current		Charge Transfer (coulombs)	Ignition	Ignition Time (msec)	Hole Formed	Fuel-Air Ratio Fraction of Stoichiometric
	Avg. Amplitude (amps)	Duration (msec)					
60 mil Aluminum							
273	125	275	34.5	no		no	1.5
274	111	370	41.0	no		no	"
275	138	210	29.0	no		no	"
277	115	700	80.5	no		no	"
278	264	440	116.0	yes		yes	"
288	?	?	93.0	yes		yes	"
289	150	575	86.0	yes		yes	"
290	141	370	52.0	yes		yes	"
291	129	310	40.0	no		no	"
292	158	292	46.0	yes		yes	"
293	140	350	49.0	yes		yes	"
294	140	215	30.0	no		no	"
295	148	280	41.5	no		no	"
296	154	270	41.5	no		no	"

TABLE II

IGNITION THRESHOLD TESTS

Test No.	Continuing Current		Charge Transfer (coulombs)	Ignition	Ignition Time (msec)	Hole Formed	Fuel-Air Ratio Fraction of Stoichiometric
	Avg. Amplitude (amps)	Duration (msec)					
60 mil Aluminum							
297	?	?	53.0	yes		yes	1.5
298	146	333	48.5	no		no	"
299	162	340	55.0	yes		yes	"

TABLE II

IGNITION THRESHOLD TESTS

Test No.	Continuing Current Avg. Amplitude (amps)	Duration (msec)	Charge Transfer (coulombs)	Ignition	Ignition Time (msec)	Hole Formed	Fuel-Air Ratio Fraction of Stoichiometric
			20 mil Stainless Steel				
302	65	54	3.5	no		no	1.5
303	79	58	4.6	yes		no	"
304	56	57	3.2	no		no	"
305	60	47	2.8	no		no	"
306	?	?	4.5	no		no	"
307	84	56	4.7	no		no	"
308	82	57	4.7	no		no	"
309	?	?	6.0	no		no	"
310	96	55	5.3	no		no	"
311	109	55	6.0	no		no	"
312	125	55	6.9	no		no	"
313	128	58	8.0	no		no	"
314	115	58	6.7	no		no	"
315	121	58	7.0	no		no	"

TABLE II
IGNITION THRESHOLD TESTS

Test No.	Continuing Current Avg. Amplitude (amps)	Duration (msec)	Charge Transfer (coulombs)	Ignition	Ignition Time (msec)	Hole Formed	Fuel-Air Ratio Fraction of Stoichiometric
			20 mil Stainless Steel				
316	145	55	8.0	yes	105*	no	1.5
334	91	48	4.4	yes	125*	no	"
335	70	53	3.7	no		no	"
336	70	53	3.7	no		no	"
337	66	53	3.5	no		no	"
338	79	51	4.0	no		no	"
339	96	54	5.2	no		no	"
340	75	53	4.0	no		no	"
341	96	54	5.2	no		no	"
342	115	57	6.6	yes		yes	"

* Obtained from high level microphone.

123

TABLE II

IGNITION THRESHOLD TESTS

Test No.	Continuing Current		Charge Transfer (coulombs)	Ignition	Ignition Time (msec)	Hole Formed	Fuel-Air Ratio Fraction of Stoichiometric
	Avg. Amplitude (amps)	Duration (msec)					
			40 mil Stainless Steel				
279	138	290	40.0	yes		no	1.5
280	153	209	32.0	no		no	"
282	127	291	37.0	yes		no	"
284	187	222	41.5	yes		no	"
285	152	69	10.5	no		no	"
286	72	160	11.5	no		no	"
287	?	?	25.2	yes		yes	"
300	205	61	12.5	no		no	"
301	197	61	12.0	yes		no	"

TABLE II

IGNITION THRESHOLD TESTS

Test No.	Continuing Current Avg. Amplitude (amps)	Duration (msec)	Charge Transfer (coulombs)	Ignition	Ignition Time (msec)	Hole Formed	Fuel-Air Ratio Fraction of Stoichiometric
			60 mil Stainless Steel				
343	156	59	9.2	no		no	1.5
344	?	?	11.0	no		no	"
345	?	?	33.0	no		no	"
346	?	?	41.0	yes		no	"
347	?	?	45.0	yes		no	"
348	?	?	30.0	no		no	"
349	?	?	32.5	no		no	"
350	?	?	36.5	no		no	"
351	?	?	36.0	no		no	"
352	?	?	46.0	yes		no	"